

UNIVERSITY OF CALIFORNIA
SANTA CRUZ

**Biosynthetic and Inhibitory Investigations of Human Lipoxygenase Isozymes
and Their Oligomers: Deciphering the Resolution of Inflammation through
Drug Design, Mutagenesis and Lipidomics**

A dissertation submitted in partial satisfaction
of the requirements for the degree of
DOCTOR OF PHILOSOPHY

in

Chemistry & Biochemistry

by

Wan-Chen Carissa Tsai

March 2021

The Dissertation of Wan-Chen Carissa Tsai
is approved by:

Professor Ted Holman, chair

Professor Seth Rubin

Professor Michael Stone

Quentin Williams
Acting Vice Provost and Dean of Graduate Studies

Copyright © by

Wan-Chen Carissa Tsai

2021

Table of Contents

List of Figures.....	iv
List of Tables.....	vi
List of Schemes.....	viii
Abstract.....	ix
Aknowledgements.....	xi
Chapter 1 Introductions.....	1
Chapter 2 Probing the Electrostatic and Steric Requirements for Substrate Binding in Human Platelet-Type 12-Lipoxygenase.....	20
Chapter 3 In Vitro Biosynthetic Pathway Investigations of Neuroprotectin D1 (NPD1) and Protectin DX (PDX) by Human 12-Lipoxygenase, 15-Lipoxygenase-1 and 15-Lipoxygenase-2.....	67
Chapter 4 Mutagenesis, Hydrogen-Deuterium Exchange, and Molecular Dynamic Investigations Establish the Dimeric Interface of Human Platelet-type 12-Lipoxygenase.....	136
Chapter 5 Docking and Mutagenesis Studies Lead to Improved Inhibitor Development of ML355 for Human Platelet 12-lipoxygenase.....	190
Chapter 6 Kinetic and Structural Investigations of Novel Inhibitors of Human Epithelial 15-Lipoxygenase-2.....	234

List of Figures

Chapter 1

Figure 1.1.....	3
Figure 1.2.....	6
Figure 1.3.....	12

Chapter 2

Figure 2.1.....	37
Figure 2.2.....	53
Figure 2.3.....	56
Figure 2.4.....	58

Chapter 3

Figure 3.1.....	75
Figure 3.2.....	107
Figure 3.3.....	111
Figure 3.4.....	116

Chapter 4

Figure 4.1.....	142
Figure 4.2.....	158
Figure 4.3.....	160
Figure 4.4.....	162
Figure 4.5.....	166
Figure 4.6.....	169
Figure 4.7.....	171
Figure 4.8.....	173

Chapter 5

Figure 5.1.....	210
Figure 5.2.....	211
Figure 5.3.....	213
Figure 5.4.....	217

Figure 5.5.....	217
Figure 5.6.....	218
Figure 5.7.....	221
Figure 5.8.....	223
Figure 5.9.....	225
Chapter 6	
Figure 6.1.....	239
Figure 6.2.....	274
Figure 6.3.....	278
Figure 6.4.....	280

List of Tables

Chapter 1

Table 1.1.....	6
----------------	---

Chapter 2

Table 2.1.....	41
----------------	----

Table 2.2.....	44
----------------	----

Table 2.3.....	44
----------------	----

Table 2.4.....	49
----------------	----

Table 2.5.....	49
----------------	----

Table 2.6.....	53
----------------	----

Chapter 3

Table 3.1.....	91
----------------	----

Table 3.2.....	91
----------------	----

Table 3.3.....	95
----------------	----

Table 3.4.....	97
----------------	----

Table 3.5.....	100
----------------	-----

Table 3.6.....	101
----------------	-----

Table 3.7.....	106
----------------	-----

Table 3.8.....	106
----------------	-----

Chapter 4

Table 4.1.....	164
----------------	-----

Chapter 5

Table 5.1.....	207
----------------	-----

Table 5.2.....	212
----------------	-----

Table 5.3.....	213
----------------	-----

Table 5.4.....	219
----------------	-----

Table 5.5.....	219
----------------	-----

Table 5.6.....	222
----------------	-----

Table 5.7.....	223
----------------	-----

Chapter 6

Table 6.1.....	266
Table 6.2.....	268
Table 6.3.....	269
Table 6.4.....	273
Table 6.5.....	288

List of Schemes

Chapter 3	
Scheme 3.1.....	123
Chapter 5	
Scheme 5.1.....	205
Chapter 6	
Scheme 6.1.....	242

Abstract

Biosynthetic and Inhibitory Investigations of Human Lipoxygenase Isozymes and Their Oligomers: Deciphering the Resolution of Inflammation through Drug Design, Mutagenesis and Lipidomics

Wan-Chen Carissa Tsai

Research has shown that chronic inflammation is associated with many diseases such as cardiovascular disease, diabetes, cancer, and asthma. This chronic inflammation is caused by the failure of proper resolution of the inflammation overtime. Therefore, this dissertation explores the biosynthesis of lipoxygenase-derived products from DHA, drug discovery, and site-directed mutagenesis to determine the substrate and inhibitors binding to the lipoxygenase active site in order to understand how these pro-resolving molecules are made and help to guide for chronic disease therapy. The first chapter probes the electrostatic and steric requirements for substrate binding in human 12-LOX. The second chapter investigates the biosynthetic pathway of NPD1 and PDX by human lipoxygenase isozymes. The third chapter determines the dimeric interface of human 12-LOX by

site-directed mutagenesis. The fourth and fifth chapters discover potent and selective inhibitors against human 12-LOX and 15-LOX-2 for thrombosis and atherosclerosis therapy.

Acknowledgements

First of all, I'd like to express how thankful I am to my PI, Ted Holman. He is an awesome scientist and mentor that is very supportive to all his graduate students not just in research but also our life. During this time in graduate school, I was trained to be an independent researcher and how to think scientifically. I also so appreciate he gave me an opportunity to join his lab since I didn't have any background in biochemistry. I can't thank him enough for what he has done for me to make me what I am today.

Next, I'd like to thank to all of my committee, Professor Seth Rubin and Professor Michael Stone. It's my honor to have you on my committee to give me suggestions on my projects and the thesis. Without your help, my entire PhD journey won't be that smoothly.

I'd also like to thank everyone in Ted Holman's lab. It's my pleasure to work with all of you and definitely I couldn't accomplish my study in 5 years without your help.

I would also thank all of my collaborators from University of Michigan, UCSF, and East Carolina University, etc.... I was lucky to be able to collaborate with Michael Holinstat's lab from Univ. Michigan for platelet experiments, Matt Jacobson and CK from UCSF for molecular modeling, and Adam Offenbacher from East Carolina University for HDX-MS experiments.

Chapter 1

INTRODUCTION

1.1 n-3 and n-6 Polyunsaturated Fatty Acids (PUFAs)

Polyunsaturated fatty acids (PUFAs) are fatty acids that have more than one unsaturated carbon bond in the lipid chain. Instead of being solid at room temperature like saturated fatty acids, PUFAs are typically liquid at room temperature due to their double bonds in the molecule. PUFAs are classified as n-3 and n-6 on the basis of the location of the last double bond relative to the terminal methyl end of the molecule. In westernized diets, linoleic acid (LA, 18:2, n-6) is the primary PUFA followed by α -linoleic acid (ALA, 18:3, n-3) and since these two fatty acids cannot be synthesized in mammals, they are defined as essential fatty acids¹. From these two essential fatty acids, all of the other needed PUFAs can be produced within mammalian cells through the actions of a series of human desaturase and elongase enzymatic reactions² (**Figure 1**). By these enzymes, LA (18:2 n-6) is first desaturated to γ -linolenic acid (GLA, 18:3, n-6) and then elongated to dihomo- γ -linolenic acid (DGLA, 20:3, n-6). With another desaturase enzyme, DGLA can be converted to arachidonic acid (AA,

20:4, n-6), which is highly concentrated in red meat. ALA can be converted to a series of n-3 fatty acids in a similar manner, such as eicosapentaenoic acid (EPA, 20:5, n-3), n-3 docosapentaenoic acid (DPA_{n-3}, 22:5, n.3), and docosahexaenoic acid (DHA, 22:6, n-3). As it was shown in **Figure 1**, conversion of both n-3 and n-6 fatty acids share the same series of enzymes. Therefore, the production of n-3 PUFAs can act as competitive substrates to n-6 PUFAs (*vice versa*)³.

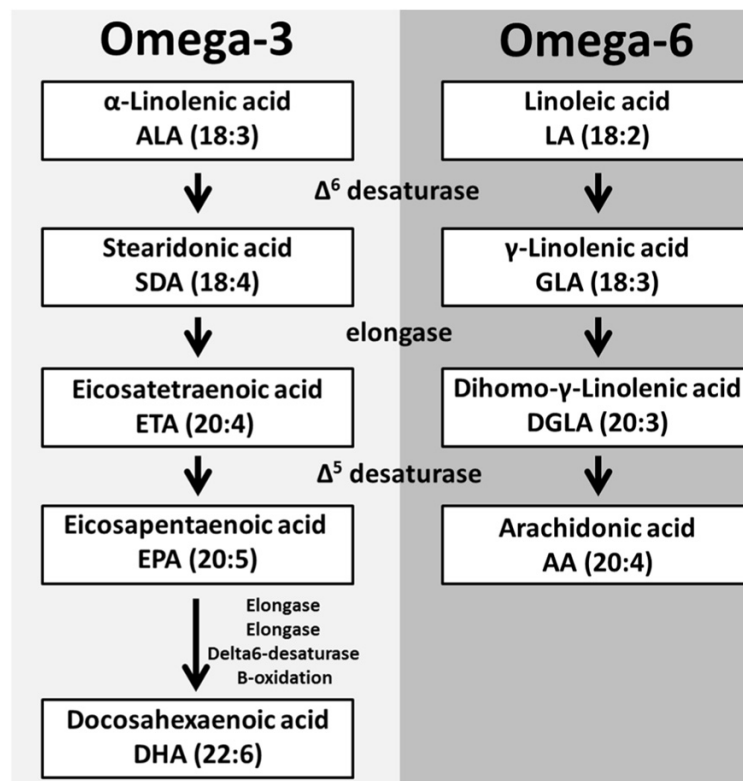


Figure 1. Metabolism of n-3 and n-6 fatty acids

1.2 Lipoxygenase (LOX)

Lipoxygenases (LOXs) are a family of non-heme iron-containing enzymes that can catalyze the dioxygenation of PUFAs containing a cis, cis-1, 4- pentadiene into cell signaling agents. Lipoxygenase (LOX) structures consist of a single polypeptide chain with a molecular mass of ~75-80 kDa in animals and ~94-104 kDa in plants. The enzymes have an N-terminal β -barrel domain and a larger C-terminal catalytic domain containing a single non-heme iron atom, which is chelated by 4 histidines and the C-terminus⁴. Lipoxygenases (LOX) are found abundantly in many tissues of the plant and animal kingdoms, but rarely in some bacteria⁵. In humans, there are six lipoxygenase isozymes including h5-LOX, h15-LOX-1, h15-LOX-2, h12-LOX, h12R-LOX, and eLOX3 (**Table 1**), with the naming of LOXs depending on which carbon atom of arachidonic acid (AA) is oxidized. For example, h12-LOX metabolizes AA to 12-hydroperoxyeicosatetraenoic acid (12-HpETE), and h15-LOX-2 metabolizes AA to 15-hydroperoxyeicosatetraenoic acid (15-HpETE). The detailed mechanism of the LOX-reaction consists of four consecutive elementary reactions, of

which the stereochemistry is tightly controlled (**Figure 2**). (i). Hydrogen atom abstraction: the proton is abstracted from a cis, cis-1, 4- pentadiene methylene by ferric-hydroxide and the electron is abstracted by the ferric-iron, being reduced to the ferrous form. (ii). Radical re-arrangement: the radical electron is relocated in the direction of the methyl end of the fatty acid [+2] or in the direction of the carboxylate [-2]. (iii). Dioxygen insertion: O₂ is introduced antarafacially related to hydrogen abstraction generating a peroxy-radical. (iv). Peroxy-radical reduction: The peroxy-radical is reduced by the hydrogen atom from the ferrous-water intermediate, converting the radical to the corresponding hydroperoxide product and the iron is reoxidized to its ferric form⁶. It is now recognized that LOX isozymes involve in the production of both pro-inflammatory and pro-resolving molecules during inflammation^{7, 8}. Therefore, investigation of the biosynthetic pathways of these oxylipin mediators and the active sites of LOX isozymes will surely allow for better therapeutic intervention into a number of inflammatory diseases.

Gene	Enzyme	Major Expression Site
ALOXE3	eLOX3	Skin
ALOX5	h5-LOX	Neutrophils/Dendritic cells
ALOX12	h12-LOX	Platelets
ALOX12B	h12R-LOX	Skin
ALOX15	h15-LOX-1	Eosinophils/Macrophages
ALOX15B	h15-LOX-2	Skin/Hair roots

Table 1. LOX isozyme gene name, common name, and major expression site⁹

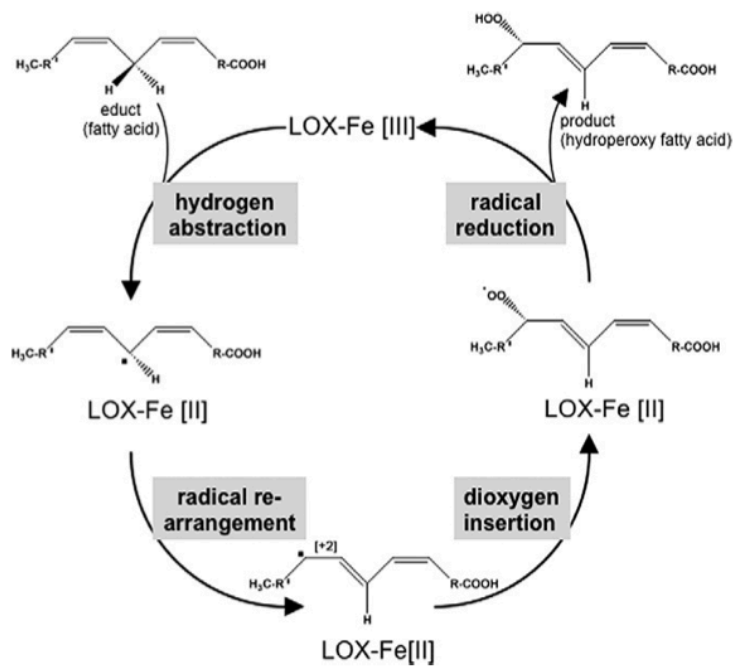


Figure 2. Mechanism of the LOX-reaction⁶

1.3 The Protectin Family and the Resolution of Inflammation

Acute inflammation is the initial response of the body to injury and infection and is initiated by neutrophils, eosinophils, and M1-polarized macrophages, which are activated by bioactive molecules, such as prostaglandins and leukotrienes¹⁰. However, an uncontrolled inflammatory response promotes chronic inflammation and unresolved tissue damage^{11, 12}. At the peak of the acute inflammatory response, the immune cells undergo a temporal lipid mediator class switch and start producing specialized pro-resolving mediators (SPMs)^{8, 13}. To date, there are more than 20 different SPMs that have been identified, which can be subdivided into six main classes: AA-derived lipoxins (LXs), EPA-derived E-series resolvins (RvEs), DHA-derived D-series resolvins (RvDs), neuroprotectins (i.e. NPD1, also known as protectin-1 (PD1)) and their conjugates (PCTRs), maresins (Mar1) and their conjugates (MCTRs), and DPA-derived 13-series resolvins (RvTs)¹². Neuroprotectin D1 (NPD1) was the first identified neuro-protective mediator of docosahexaenoic

acid (DHA) belonging to the SPMs and was fully assigned by matching the biological sample with stereo-chemically pure and enantio-enriched isomers obtained by total synthesis¹⁴. The name “neuroprotectin D1” was derived by its neuroprotective bioactivity in brain ischemia reperfusion (BIR) and oxidatively stressed retina pigment epithelial (RPE) cells, as well as its ability to protect cells from oxidative stress-induced apoptosis^{15, 16}. It can also up-regulate the stimulation of the anti-apoptotic protein, Bcl-2, and decrease the pro-apoptotic protein, Bax, in ARPE-19 cells during oxidative stress¹⁵. Protectin DX (PDX), another SPM and stereoisomer of NPD1, was first obtained enzymatically by Serhan et al. *in vitro* then its structure was re-examined later by Butovich et al. to confirm the geometry of the double bonds of the conjugated triene unit and the stereo-configuration at carbon 10¹⁷⁻¹⁹. The bioactivity of PDX revealed that it can inhibit inflammation associated with cyclooxygenase (COX) activities, reactive oxygen species (ROS) formation and influenza virus replication²⁰. The biosynthesis of NPD1 and PDX are both proposed to be catalyzed by LOX isozymes, however, the specific LOX isozymes involved and

the detailed biosynthetic pathway are not well characterized. In order to extrapolate their *in vivo* biosynthetic pathways, understanding which LOX enzyme is involved in the *in vitro* biosynthesis of NPD1 and PDX could help predict the cellular consequences of specific LOX inhibition in the treatment of human disease.

1.4 Investigations of Inhibitor Binding to Human Platelet 12-LOX (h12-LOX)

Although human platelet 12-LOX (h12-LOX) expression is predominantly restricted to platelets (~14,000 molecules per platelet), it is also expressed in some hematopoietic and solid tumors^{21, 22}. Human 12-LOX has garnered the majority of scientific attention because of its implication in a variety of human diseases, such as skin inflammation, certain cancers (i.e., breast, pancreatic, and prostate), blood coagulation, platelet activation, and diabetes²³. Its activity is crucial for a number of platelet functions, including granule secretion, platelet aggregation, and normal adhesion through specific agonist-mediated pathways, such as collagen and the

thrombin receptor, PAR4²⁴. Normal platelet activation plays a central role in the regulation of hemostasis, but uncontrolled activation can lead to pathologic thrombotic events, such as ischemic coronary heart disease²⁵. Although currently approved antiplatelet drugs, such as Ticlopidine , Clopidogrel, Prasugrel , Abciximab , Eptifibatide , Tirofiban and Dipyridamole have significantly decreased the morbidity and mortality of ischemic heart disease, their efficacy is limited by the subsequent increased risk of severe bleeding²⁶. This limitation has motivated the development of new approaches for limiting platelet activation, and a number of new platelet targets are currently being investigated for their potential to limit clot formation, including antagonists for the thrombin receptor (PAR1), newer α IIb β 3 antagonists, and GPVI antagonists²⁶. We propose that targeting 12-LOX, as one of the key pro-thrombotic enzymes within the platelet, may be an effective approach to anti-platelet therapy^{24, 27,}

28

1.5 Study of Dimeric Interface of Human Platelet 12-LOX (h12-LOX)

Previously, Shang and co-workers used a combination of thermodynamic calculations, concerning the stability of molecular assemblies, thermal motion analysis [TLSMD (translation, vibration, and screw rotation motion detection based on crystallographic temperature factor)], and results of small angle X-ray analysis (SAXS) to propose a dimeric structure of h12-LOX connected in a TOP-to-TOP fashion (**Figure 3**), defined by interactions between their $\alpha 2$ helices²⁹. The assembly of dimers via the $\alpha 2$ helices, running in opposite directions (anti-symmetric), has been tested in r15-LOX-1 by site-directed mutagenesis and SAXS, supporting a model that such dimers, as found in its crystal structure³⁰, are stabilized by a leucine zipper motif formed by L179A:L192B and L183A:L188B³¹. However, dimerization in coral 11R-LOX was studied by SAXS, and tested by chemical cross-linking and site-directed mutagenesis to reveal that its dimerization interaction is through its PDZ-like domain³². Although a similar PDZ-like domain interaction for h12-LOX was predicted by thermodynamic stability calculations, a model of dimerization

through this domain was inconsistent with SAXS analysis^{29, 33} and thus was rejected as a possible dimer structure model. Currently, the main effort in the search for inhibitors targeting lipoxygenases has been directed to the active site, blocking the direct enzymatic activity of fatty acid peroxidation. However, allosteric inhibition with respect to the dimerization state of h12-LOX may also be relevant, as seen for cyclooxygenase (COX)^{34, 35}.

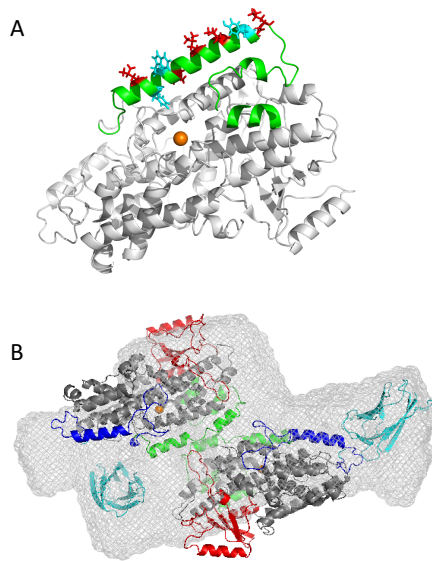


Figure 3. A: Homology model of wt-h12-LOX catalytic domain with TOP region (163-222) depicted in green. Leucines in this region are depicted in red, aromatic amino acids in cyan. B: TOP-to-TOP model (from our earlier publication³³).

1.6 Discovery of Novel Inhibitors of Human Epithelial 15-Lipoxygenase-2

h15-LOX-2 is expressed in macrophages, neutrophils, skin, hair roots and prostate^{36, 37}. It is also highly expressed in atherosclerotic plaques and linked to the progression of macrophages to foam cells, which are present in atherosclerotic plaques. Additionally, h15-LOX-2 has been shown to play a central role in the “ class switch “ of eicosanoid mediator biosynthesis from leukotrienes (LTs) to lipoxins (LXs) in the airways. The Urbach lab observed that the reduced expression level of h15-LOX-2 in the lower airways was associated with a depressed of LXA₄/LTB₄ ratio which contributed to cystic fibrosis (CF) lung disease in children³⁸. Furthermore, the h15-LOX-2/PEBP1 complex has been demonstrated to be a regulator of ferroptosis, with PEBP1 acting as a rheostat by changing h15-LOX-2 substrate specificity from free PUFA to PUFA-PE, leading to the generation of HpETE-PEs³⁹. Accumulation of these hydroperoxy membrane phospholipids has been shown to cause ferroptotic cell death, which implicates h15-LOX-2 in neurodegenerative diseases, such as

Alzheimer's, Parkinson's and Huntington's diseases⁴⁰. Therefore, the role of h15-LOX-2 in atherosclerosis, cystic fibrosis (CF) lung disease and ferroptosis implicates h15-LOX-2 as a potential therapeutic target for drug discovery.

Reference

1. Schmitz, G.; Ecker, J., The opposing effects of n-3 and n-6 fatty acids. *Prog Lipid Res* **2008**, *47* (2), 147-55.
2. Calder, P. C., Omega-3 polyunsaturated fatty acids and inflammatory processes: nutrition or pharmacology? *Br J Clin Pharmacol* **2013**, *75* (3), 645-62.
3. Wijendran, V.; Hayes, K. C., Dietary n-6 and n-3 fatty acid balance and cardiovascular health. *Annu Rev Nutr* **2004**, *24*, 597-615.
4. Boyington, J. C.; Gaffney, B. J.; Amzel, L. M.
5. Baysal, T.; Demirdöven, A.
6. Ivanov, I.; Heydeck, D.; Hofheinz, K.; Roffeis, J.; O'Donnell, V. B.; Kuhn, H.; Walther, M., Molecular enzymology of lipoxygenases. *Arch Biochem Biophys* **2010**, *503* (2), 161-74.
7. Wisastra, R.; Dekker, F. J., Inflammation, Cancer and Oxidative Lipoxygenase Activity are Intimately Linked. *Cancers (Basel)* **2014**, *6* (3), 1500-21.
8. Serhan, C. N.; Chiang, N.; Van Dyke, T. E., Resolving inflammation: dual anti-inflammatory and pro-resolution lipid mediators. *Nat Rev Immunol* **2008**, *8* (5), 349-61.
9. Kuhn, H.; Banthiya, S.; van Leyen, K., Mammalian lipoxygenases and their biological relevance. *Biochim Biophys Acta* **2015**, *1851* (4), 308-30.
10. Chen, L.; Deng, H.; Cui, H.; Fang, J.; Zuo, Z.; Deng, J.; Li, Y.; Wang, X.; Zhao, L., Inflammatory responses and inflammation-associated diseases in organs. *Oncotarget* **2018**, *9* (6), 7204-7218.
11. Tabas, I.; Glass, C. K., Anti-inflammatory therapy in chronic disease: challenges

and opportunities. *Science* **2013**, 339 (6116), 166-72.

12. Chiurchiù, V.; Leuti, A.; Maccarrone, M., Bioactive Lipids and Chronic Inflammation: Managing the Fire Within. *Front Immunol* **2018**, 9, 38.

13. Wongrakpanich, S.; Wongrakpanich, A.; Melhado, K.; Rangaswami, J., A Comprehensive Review of Non-Steroidal Anti-Inflammatory Drug Use in The Elderly. *Aging Dis* **2018**, 9 (1), 143-150.

14. Serhan, C. N.; Gotlinger, K.; Hong, S.; Lu, Y.; Siegelman, J.; Baer, T.; Yang, R.; Colgan, S. P.; Petasis, N. A., Anti-inflammatory actions of neuroprotectin D1/protectin D1 and its natural stereoisomers: assignments of dihydroxy-containing docosatrienes. *J Immunol* **2006**, 176 (3), 1848-59.

15. Bazan, N. G., Neuroprotectin D1 (NPD1): a DHA-derived mediator that protects brain and retina against cell injury-induced oxidative stress. *Brain Pathol* **2005**, 15 (2), 159-66.

16. Bazan, N. G., Neuroprotectin D1-mediated anti-inflammatory and survival signaling in stroke, retinal degenerations, and Alzheimer's disease. *J Lipid Res* **2009**, 50 Suppl (Suppl), S400-5.

17. Butovich, I. A., On the structure and synthesis of neuroprotectin D1, a novel anti-inflammatory compound of the docosahexaenoic acid family. *J Lipid Res* **2005**, 46 (11), 2311-4.

18. Chen, P.; Fenet, B.; Michaud, S.; Tomczyk, N.; Vericel, E.; Lagarde, M.; Guichardant, M., Full characterization of PDX, a neuroprotectin/protectin D1 isomer, which inhibits blood platelet aggregation. *FEBS Lett* **2009**, 583 (21), 3478-84.

19. Hong, S.; Gronert, K.; Devchand, P. R.; Moussignac, R. L.; Serhan, C. N., Novel docosatrienes and 17S-resolvins generated from docosahexaenoic acid in

murine brain, human blood, and glial cells. Autacoids in anti-inflammation. *J Biol Chem* **2003**, *278* (17), 14677-87.

20. Lagarde, M.; Guichardant, M.; Bernoud-Hubac, N., Anti-inflammatory and anti-virus potential of poxytrins, especially protectin DX. *Biochimie* **2020**.

21. Pidgeon, G. P.; Lysaght, J.; Krishnamoorthy, S.; Reynolds, J. V.; O'Byrne, K.; Nie, D.; Honn, K. V., Lipoxygenase metabolism: roles in tumor progression and survival. *Cancer Metastasis Rev* **2007**, *26* (3-4), 503-24.

22. Burkhart, J. M.; Vaudel, M.; Gambaryan, S.; Radau, S.; Walter, U.; Martens, L.; Geiger, J.; Sickmann, A.; Zahedi, R. P., The first comprehensive and quantitative analysis of human platelet protein composition allows the comparative analysis of structural and functional pathways. *Blood* **2012**, *120* (15), e73-82.

23. Aleem, A. M.; Tsai, W. C.; Tena, J.; Alvarez, G.; Deschamps, J.; Kalyanaraman, C.; Jacobson, M. P.; Holman, T., Probing the Electrostatic and Steric Requirements for Substrate Binding in Human Platelet-Type 12-Lipoxygenase. *Biochemistry* **2019**, *58* (6), 848-857.

24. Yeung, J.; Apopa, P. L.; Vesci, J.; Stolla, M.; Rai, G.; Simeonov, A.; Jadhav, A.; Fernandez-Perez, P.; Maloney, D. J.; Boutaud, O.; Holman, T. R.; Holinstat, M., 12-lipoxygenase activity plays an important role in PAR4 and GPVI-mediated platelet reactivity. *Thromb Haemost* **2013**, *110* (3), 569-81.

25. Elwood, P. C.; Renaud, S.; Sharp, D. S.; Beswick, A. D.; O'Brien, J. R.; Yarnell, J. W., Ischemic heart disease and platelet aggregation. The Caerphilly Collaborative Heart Disease Study. *Circulation* **1991**, *83* (1), 38-44.

26. Yeung, J.; Holinstat, M., Newer agents in antiplatelet therapy: a review. *J Blood Med* **2012**, *3*, 33-42.

27. McMahon, G. S.; Jones, C. I.; Hayes, P. D.; Naylor, A. R.; Goodall, A. H.,

Transient heparin-induced platelet activation linked to generation of platelet 12-lipoxygenase. Findings from a randomised controlled trial. *Thromb Haemost* **2013**, *109* (6), 1099-107.

28. Svensson Holm, A. C.; Grenegard, M.; Ollinger, K.; Lindstrom, E. G., Inhibition of 12-lipoxygenase reduces platelet activation and prevents their mitogenic function. *Platelets* **2014**, *25* (2), 111-7.

29. Shang, W.; Ivanov, I.; Svergun, D. I.; Borbulevych, O. Y.; Aleem, A. M.; Stehling, S.; Jankun, J.; Kühn, H.; Skrzypczak-Jankun, E., Probing dimerization and structural flexibility of mammalian lipoxygenases by small-angle X-ray scattering. *J Mol Biol* **2011**, *409* (4), 654-68.

30. Choi, J.; Chon, J. K.; Kim, S.; Shin, W., Conformational flexibility in mammalian 15S-lipoxygenase: Reinterpretation of the crystallographic data. *Proteins* **2008**, *70* (3), 1023-32.

31. Ivanov, I.; Shang, W.; Toledo, L.; Masgrau, L.; Svergun, D. I.; Stehling, S.; Gómez, H.; Di Venere, A.; Mei, G.; Lluch, J. M.; Skrzypczak-Jankun, E.; González-Lafont, À.; Kühn, H., Ligand-induced formation of transient dimers of mammalian 12/15-lipoxygenase: A key to allosteric behavior of this class of enzymes? *Proteins: Structure, Function, and Bioinformatics* **2012**, *80* (3), 703-712.

32. Eek, P.; Poldemaa, K.; Kasvandik, S.; Jarving, I.; Samel, N., A PDZ-like domain mediates the dimerization of 11R-lipoxygenase. *Biochim Biophys Acta Mol Cell Biol Lipids* **2017**, *1862* (10 Pt A), 1121-1128.

33. Aleem, A. M.; Jankun, J.; Dignam, J. D.; Walther, M.; Kühn, H.; Svergun, D. I.; Skrzypczak-Jankun, E., Human platelet 12-lipoxygenase, new findings about its activity, membrane binding and low-resolution structure. *J Mol Biol* **2008**, *376* (1), 193-209.

34. Sidhu, R. S.; Lee, J. Y.; Yuan, C.; Smith, W. L., Comparison of

cyclooxygenase-1 crystal structures: cross-talk between monomers comprising cyclooxygenase-1 homodimers. *Biochemistry* **2010**, *49* (33), 7069-79.

35. Dong, L.; Vecchio, A. J.; Sharma, N. P.; Jurban, B. J.; Malkowski, M. G.; Smith, W. L., Human cyclooxygenase-2 is a sequence homodimer that functions as a conformational heterodimer. *J Biol Chem* **2011**, *286* (21), 19035-46.

36. Brash, A. R.; Boeglin, W. E.; Chang, M. S., Discovery of a second 15S-lipoxygenase in humans. *Proc Natl Acad Sci U S A* **1997**, *94* (12), 6148-52.

37. Hultén, L. M.; Olson, F. J.; Aberg, H.; Carlsson, J.; Karlström, L.; Borén, J.; Fagerberg, B.; Wiklund, O., 15-Lipoxygenase-2 is expressed in macrophages in human carotid plaques and regulated by hypoxia-inducible factor-1alpha. *Eur J Clin Invest* **2010**, *40* (1), 11-7.

38. Ringholz, F. C.; Buchanan, P. J.; Clarke, D. T.; Millar, R. G.; McDermott, M.; Linnane, B.; Harvey, B. J.; McNally, P.; Urbach, V., Reduced 15-lipoxygenase 2 and lipoxin A4/leukotriene B4 ratio in children with cystic fibrosis. *Eur Respir J* **2014**, *44* (2), 394-404.

39. Wenzel, S. E.; Tyurina, Y. Y.; Zhao, J.; St Croix, C. M.; Dar, H. H.; Mao, G.; Tyurin, V. A.; Anthonymuthu, T. S.; Kapralov, A. A.; Amoscato, A. A.; Mikulska-Ruminska, K.; Shrivastava, I. H.; Kenny, E. M.; Yang, Q.; Rosenbaum, J. C.; Sparvero, L. J.; Emlet, D. R.; Wen, X.; Minami, Y.; Qu, F.; Watkins, S. C.; Holman, T. R.; VanDemark, A. P.; Kellum, J. A.; Bahar, I.; Bayır, H.; Kagan, V. E., PEBP1 Wardens Ferroptosis by Enabling Lipoxygenase Generation of Lipid Death Signals. *Cell* **2017**, *171* (3), 628-641.e26.

40. Reichert, C. O.; de Freitas, F. A.; Sampaio-Silva, J.; Rokita-Rosa, L.; Barros, P. L.; Levy, D.; Bydlowski, S. P., Ferroptosis Mechanisms Involved in Neurodegenerative Diseases. *Int J Mol Sci* **2020**, *21* (22).

Chapter 2

Probing the Electrostatic and Steric Requirements for Substrate Binding in

Human Platelet-Type 12-Lipoxygenase

2.1 Abstract

Human platelet ALOX12 (hALOX12 or h12-LOX) has been implicated in a variety of human diseases. The present study investigates the active site of hALOX12 to more thoroughly understand how it positions the substrate and achieves nearly perfect regio- and stereospecificities (i.e., $100 \pm 5\%$ of the 12(S)-hydroperoxide product), utilizing site-directed mutagenesis. Specifically, we have determined that Arg402 is not as important in substrate binding as previously seen for hALOX15 but that His596 may play a role in anchoring the carboxy terminal of the arachidonic acid during catalysis. In addition, Phe414 creates a π -stacking interaction with a double bond of arachidonic acid (Δ^{11}), and Ala417/Val418 define the bottom of the cavity. However, the influence of Ala417/Val418 on the profile is markedly less for hALOX12 than that seen in hALOX15. Mutating these two residues to larger amino acids (Ala417Ile/Val418Met) only increased the generation of 15- HpETE by $24 \pm 2\%$, but conversely, smaller residues at these positions converted hALOX15 to almost

100% hALOX12 reactivity [Gan et al. (1996) J. Biol. Chem. 271, 25412–25418].

However, we were able to increase 15-HpETE to $46 \pm 3\%$ by restricting the width of the active site with the Ala417Ile/Val418Met/Ser594Thr mutation, indicating both depth and width of the active site are important. Finally, residue Leu407 is shown to play a critical role in positioning the substrate correctly, as seen by the increase of 15-HpETE to $21 \pm 1\%$ for the single Leu407Gly mutant. These results outline critical differences between the active site requirements of hALOX12 relative to hALOX15 and explain both their product specificity and inhibitory differences.

2.2 Introduction

Lipoxygenases (LOXs)¹ are ubiquitous nonheme iron- containing dioxygenases that catalyze the oxidation of polyunsaturated fatty acids (PUFAs) with a cis,cis-1,4-pentadiene moiety.^{2,3} Human LOXs are classified into three major categories, 5-LOX,⁴ 12-LOX,⁵ and 15-LOX,⁶ designat- ing which carbon in arachidonic acid (AA) is oxygenated to produce their respective hydroperoxyeicosatetraenoic acid (HpETE) product. The enzymes can be further classified on the basis of the chirality of oxygen insertion, i.e., “R” or “S” LOXs. The HpETE products are subsequently reduced by glutathione peroxidase to form the hydroxyeicosatetraenoic acid (HETE).⁷⁻¹² Accordingly, 12-lipoxygenase catalyzes the transformation of arachidonic acid into 12-HpETE. In humans, two 12-lipoxygenase isozymes are expressed, platelet-type 12(S)-lipoxygenase (hALOX12 or h12-LOX) and epithelial- type 12(R)-lipoxygenase (hALOX12B or 12R-LOX).^{13,14} hALOX12 makes the S-product and is primarily expressed in platelets, whereas hALOX12B is primarily expressed in epithelial tissue

and makes the R-product. hALOX12 has garnered the majority of scientific attention because of its implication in a variety of human diseases, such as skin inflammation,¹⁵ certain cancers (i.e., breast,^{16,17} pancreatic,¹⁸ and prostate¹⁹), blood coagulation,²⁰ platelet activation,^{21,22} and diabetes.²³

One of the critical properties of LOXs is their ability to oxygenate fatty acids both regio- and stereospecifically. The structural basis for this product specificity has been investigated extensively for human reticulocyte 15-lipoxygenase-1 (hALOX15 or h15-LOX-1). Sigal and co-workers determined that F414 formed a π - π stacking interaction with the Δ^{11} double bond of AA, while I417/M418 defined the bottom of the active site cavity for hALOX15, which positions the appropriate carbon for oxygenation.^{24,25} This work was expanded by Kühn and co-workers, who established that F353 in rabbit reticulocyte ALOX15 (rALOX15 or r15-LOX-1) also played a critical role in defining the overall size and shape of the active site and thus the specificity for C-15 versus C-12 oxidation of AA (F352 in hALOX15).^{26,27} These data led to the “triad” concept for rALOX15, wherein F353, I418, and I593,

positioned in the deepest portion of the substrate-binding pocket, were critical for positional specificity (F352, I417, and I592 in hALOX15).²⁸ Vogel et al. concluded that this hypothesis could explain the positional specificity of several mammalian ALOX15 enzymes, specifically those from rabbit, human, *M. mulatta*, *P. pygmaeus*, and mouse.²⁸ However, the specificity of hALOX12 was only partially explained by the triad hypothesis, and for human epithelial ALOX15B (hALOX15B or h15-LOX-2) and hALOX12B, the triad hypothesis did not apply.²⁸ It has also been hypothesized that proper alignment of the substrates in LOX active sites additionally requires specific interactions with the carboxylate of the fatty acid. R402 has been proposed to play this role in hALOX15,²⁵ but the effect of mutating this amino acid on enzyme kinetics could also be partially explained by destabilization of the tertiary structure.²⁹

Overall, a three-point interaction mechanism is proposed for hALOX15 to align the substrate in the active site so that the iron abstracts a hydrogen from the appropriate bis-allylic carbon: (i) hydrophobic interaction of the methyl end of the substrate with the hydrophobic side chains of the bottom of the active site pocket, F352, I417,

and I592; (ii) ionic interaction of the carboxylate end of the fatty acid with R402;²⁵
and (iii) π - π interaction between the fatty acid double bond (Δ^{11}) and F414.²⁵

The structural basis for product selectivity in hALOX12 has been less extensively studied, and previous mutagenesis studies indicate the positional specificity is more complicated than for human/rabbit ALOX15. For porcine leukocyte ALOX15 (pALOX15 or p12-LOX), a double mutation, V418I/ V419M, was sufficient to produce 85% 15-HpETE, versus 10% for the wild-type enzyme.³⁰

However, pALOX15 is more closely related to hALOX15 than hALOX12. For hALOX12, the factors governing positional specificity are not as straightforward. In particular, hALOX12 generates insignificant quantities of 15-HpETE, and the double mutant, A417I/V418 M (I417/M418 for hALOX15 and V418/V419 for pALOX15) increased the 15-HpETE percentages to only 14%.²⁸ K416 was also proposed to be a specificity determinant, but the triple mutant K416Q/A417I/V418M only increased 15-HpETE to 20% of the total.³¹ The substitution of the remaining amino acid variants between positions 398–429 in hALOX12 to the corresponding hALOX15

amino acids (T401V/Q406G/ I408V/G411M/K416Q/A417I/V418M) increased 15-HpETE to 66%; however, the enzyme activity was reduced to 25% of the wt-hALOX12 activity, indicating extensive structural changes.³¹ Other aspects of the three-point interaction hypothesis, including the positioning of the carboxylate (R402) and possible π - π interactions (F414), were not previously tested for hALOX12.

In the current work, we expand our investigations of the size and shape of the active site of hALOX12 and probe the role of R402 and F414. This work refines the multipoint interaction properties between AA and hALOX12 and determines that the hALOX12-substrate interactions are similar but not analogous to the previously described interactions observed in hALOX15.

2.3 Material and Methods

Chemicals. All the fatty acids used in this study were purchased from Nu-Chek Prep, Inc. (MN, U.S.). All other solvents and chemicals were of reagent grade or better and were used as purchased without further purification.

Homology Model of hALOX12 and Docking of Arachidonic Acid. A crystal structure of human ALOX12 is available in the Protein Data Bank (PDB ID: 3d3l; resolution 2.6 Å); however, this structure is not suitable for the present modeling because of several missing residues. For instance, helix $\alpha 11$, located at the entrance of the active site in rabbit ALOX15 and porcine ALOX15 structures, is missing in the hALOX12 structure. Also, helix $\alpha 2$, positioned parallel to the helix $\alpha 11$ in rabbit ALOX15 and porcine ALOX15 structures, is reoriented horizontally above the active site entrance in the hALOX12 structure (structural superposition is shown in Figure S1 of the Supporting Information). Therefore, the active site is fully exposed to the

solvent. Further, the C- terminal residue, I663, whose carboxylate coordinates to the active site ferric ion, is missing in the hALOX12 structure. Finally, McGovern et al. have shown that structure-based virtual screening calculations performed better if the structure had a ligand bound in the active site,³² but the hALOX12 structure does not contain a ligand in the active site. However, the structure of porcine leukocyte ALOX15, a close homologue of hALOX12 (PDB ID: 3RDE, 66% sequence identity), contains a substrate-mimetic, inhibitor bound in the active site. In addition, its crystal structure resolution is 1.9 Å, better than that of the hALOX12 structure. Therefore, we decided to build a homology model of hALOX12 based on the porcine hALOX15 structure. The homology model of hALOX12 (Uniprot accession P18054) was built using the software PRIME (v4.7, Schrödinger Inc.). During homology modeling we retained the metal ion (Fe^{3+}); a hydroxide ion coordinated to the metal ion; and the cocrystallized ligand, 3-(4-[(tridec-2-yn-1-yloxy) methyl]phenyl)propanoic acid, from the porcine ALOX15 structure. The hALOX12 model was subsequently energy-minimized using Protein Preparation Wizard (Schrödinger Inc.). During the

protein preparation step, hydrogen atoms were optimized to make better hydrogen-bonding interactions and all heavy atoms were relaxed such that they did not move beyond 0.3 Å from their starting position. After the protein preparation step, we deleted the cocrystallized ligand from the template structure but retained the metal (Fe^{3+}) and hydroxide ion.

The AA substrate and a C10-carbanion reaction intermediate were prepared using the Edit/Build panel (Maestro v11.1.012, Schrödinger Inc.) and then energy minimized using LigPrep (v41012, Schrödinger Inc.). We set OPLS-2005 atom-type parameters for the reaction intermediate during LigPrep energy minimization. We subsequently used Glide (v7.4, Schrödinger Inc.) to dock both compounds using flexible ligand sampling and extra precision (XP) scoring function options. Glide docking consisted of a grid preparation step and a docking step. We used the centroid of the cocrystallized ligand from the template structure to define the binding site.

Site-Directed Mutagenesis. Guided by the model of hALOX12 and the predicted binding model of the arachidonic acid C10 carbanion reaction intermediate, we chose

the following amino acid mutations to test their importance for substrate positioning: R402L, L407G, L407A, F414L, F414W, A417I, V418M, A417I/V418M, A417I/V418M/S594T, and H596L. The numbering in the text refers to UniProt accession number P18054 for the hALOX12 sequence without 6XHis-tag and with the N-terminal methionine assigned as amino acid number one. Online QuikChange Primer Design tool (<http://www.genomics.agilent.com/primerDesignProgram.jsp>) from Agilent Technologies (CA, U.S.) was used to design the primers for all the mutants of hALOX12. The mutations were introduced using a QuikChangeII XL site-directed mutagenesis kit from Agilent Technologies using the provided protocol. The mutations were confirmed by sequencing the hALOX12 insert in the pFastBac1 shuttle vector (Eurofins Genomics, KY, U.S.).

Protein Expression and Purification. The expression and purification of hALOX12 and all mutant enzymes used in this study were performed as previously described.³³ The wild- type hALOX12 (wt-hALOX12) enzyme and its mutants were expressed as fusion proteins with a 6-His tag on the N- terminus and were purified by affinity

nickel-iminodiacetic acid agarose using a FPLC (Biorad). The entire purification process was performed at 4 °C. The purity of all proteins was greater than 90%, as determined by SDS-PAGE analysis and the oligomeric state similar to wt-hALOX12, as determined by SEC.

Determination of Iron Content Using ICP-MS. The iron content of wt-hALOX12 and all the mutant enzymes was determined on a Thermo Element XR inductively coupled plasma mass spectrometry (ICP-MS) instrument. Cobalt (EDTA) was used as an internal standard. Iron concentrations were compared with standardized iron solutions, and all the kinetic data were normalized to the iron content. Protein concentrations were determined by a Bradford assay, with bovine serum albumin (BSA) as protein standard.

Steady-State Kinetics. hALOX12 and all the mutant protein enzymatic rates were determined by following the formation of the conjugated diene product, 12(S)-HpETE ($\epsilon = 27\,000\text{ M}^{-1}\text{ cm}^{-1}$), at 234 nm with a PerkinElmer Lambda 40 UV/vis spectrophotometer. The reactions were done in triplicate and started by

adding approximately 40 nM enzyme to a 2 mL reaction mixture containing 1–20 μM AA, in 25 mM HEPES buffer (pH 8.00), at room temperature (23 °C), with constant stirring. Triton X-100 (0.01% by wt) was added to reduce substrate inhibition, of which minimal inhibition was observed up to 20 μM AA. Kinetic data were obtained by recording initial enzymatic rates at each substrate concentration and then fitting them to the Michaelis–Menten equation using the KaleidaGraph (Synergy) program to determine k_{cat} and $k_{\text{cat}}/K_{\text{M}}$ values.

LC-MS Analysis of Enzymatic Products. To determine the products formed, wt-hALOX12 and the mutant enzymes were added to a solution of 25 mM HEPES buffer (pH 7.5) and 10 μM of a fatty acid substrate (arachidonic acid, docosahexaenoic acid, eicosadienoic acid, gamma linoleic acid, linoleic acid) for 10 min, in triplicate. The reactions were quenched with 1% glacial acetic acid and extracted three times with dichloromethane (DCM). The products were then reduced with trimethylphosphite and evaporated under a stream of N_2 gas. The reaction products were reconstituted in methanol and analyzed via LC-MS/MS.

Chromatographic separation was performed using a C18 Synergi (4 μ M) Hydro-RP 80 Å LC column (150 × 2 mm). The injection volume was 20 μ L. The chromatography system was coupled to a Thermo- Electron LTQ LC-MS/MS for mass analysis. All analyses were performed in negative ionization mode at the normal resolution setting. The two mobile phases (A and B) consisted of water with 0.1% (v/v) formic acid and acetonitrile with 0.1% formic acid, respectively. The protocol ran 60% mobile phase A and 40% mobile phase B initially; at 30 min, the protocol decreased mobile phase A to 55% and increased mobile phase B to 45%; finally, the protocol gradually decreased the percentage of mobile phase A and increased the percentage of mobile phase B until it reached 25% mobile phase A and 75% mobile phase B at 60 min. The flow rate was 200 μ L/min. The products were ionized by electrospray ionization. MS2 was performed in a targeted manner with a mass of 319.5 (for HETE detection). Thermo PDA Plus UV detectors were used. Products were identified by matching retention times, fragmentation, and UV spectra to known standards.

2.4 Results and Discussion

Model of hALOX12 with Substrate and Reaction Intermediate. To guide the design and interpretation of the mutagenesis studies, we created a homology model of hALOX12 and then used computational docking to predict the binding mode of arachidonic acid (substrate) and a carbanion reaction intermediate (an approximation of the arachidonyl radical). The LOX reaction mechanism involves the abstraction of a hydrogen atom from the bisallylic methylene, thereby producing a free radical at the methylene carbon (i.e., C10). Unfortunately, the force-field used in molecular docking calculations does not support free radical atom-type. Therefore, we modeled the lone-pair electron on C10 as a carbanion for docking purposes. Results using the intermediate were more consistent with available experimental data, similar to earlier work by Hermann et al., who showed that docking high-energy reaction intermediates of substrate molecules was better in identifying substrates than docking ground-state

substrate molecules alone in a large metabolite library docking study.³⁴ An extra-precision (XP) docking score of -4.2 was obtained, and its docking pose is shown in **Figure 1**. The carbanion locks the substrate into a position consistent with the characterized enzyme mechanism, in which the ferric-hydroxide abstracts the hydrogen atom from C10, generating a pentadienyl radical. Specifically, the carbanion on C10 is 4.9 \AA from the metal ion (Fe^{3+}) and 3.0 \AA to the hydrogen atom of the hydroxide ion. As expected, the hydrophobic C20 terminal methyl of AA binds deeply in the hydrophobic pocket created by F352, F414, V418, C559, and L589. The distances between the carbanion intermediate and the side chains of residues that interact with the intermediate are given in the Supporting Information (**Table S1**). The predicted docking score for AA was -2.3 , and it bound outside the catalytic site.

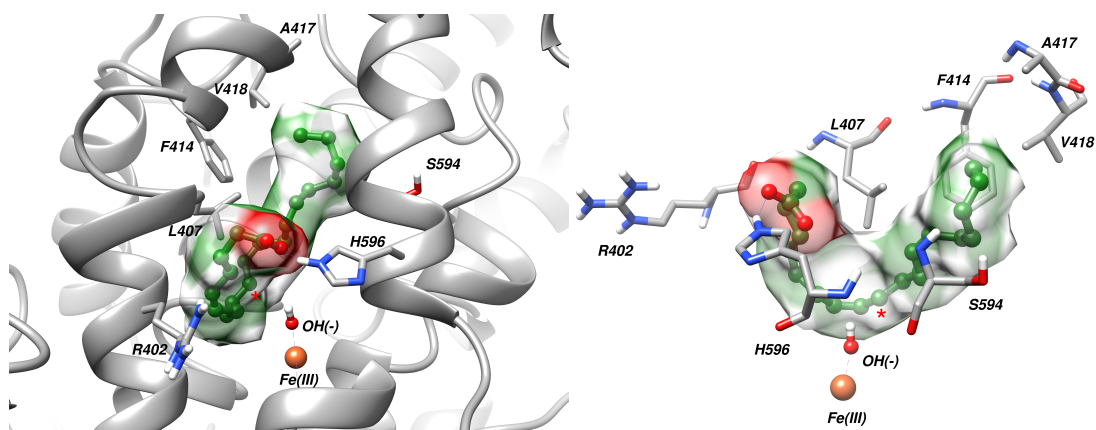


Figure 1. Two representations of the predicted binding mode of the AA C-10 carbanion intermediate in the 12-LOX wild-type enzyme active site. The negatively charged carbanion C10 is identified with a star (*). H596 is predicted to form a hydrogen bond to the carboxylate group of the fatty acid. The AA carbanion intermediate is shown in a ball-and-stick and surface representations. The hydroxide ion is shown in a ball-and-stick representation while the key residues that are mutated in this study are shown in a stick representation. Carbon atoms of AA and the protein are shown in grey and green, respectively. Iron is depicted as an orange sphere. Nitrogen, oxygen atom hydrogen atoms are shown in blue, red and white colors, respectively.

Binding Interactions with the Carboxylate Moiety of Arachidonic Acid.

Previously, Gan et al. demonstrated that R402 in hALOX15 interacted with the carboxylate moiety of the fatty acid substrate, positioning the substrate in the active site relative to the catalytic iron for hydrogen atom abstraction.²⁵ R402 is conserved in both hALOX15 and hALOX12 (R402), suggesting that it might play a similar role for fatty acid binding in hALOX12. However, the model of hALOX12 with the

reaction intermediate predicts that the carboxylic acid of AA makes a hydrogen-bonding interaction with H596 (Q595 in hALOX15) and not R402. We therefore mutated both R402 and H596 to test these competing hypotheses.

To interrogate the role of R402, we replaced it with a nonpolar leucine to disrupt the proposed hydrogen bond interaction with the substrate. This hALOX12 mutant, R402L, demonstrated only a 2-fold decrease in $k_{\text{cat}}/K_{\text{M}}$ when compared to wt-hALOX12, 6.3 ± 0.5 and $14 \pm 0.9 \mu\text{M}^{-1} \text{s}^{-1}$, respectively (**Table 1**). There was also no significant change in the K_{M} value of AA, which was $0.89 \pm 0.09 \mu\text{M}$ for R402L and $1.9 \pm 0.2 \mu\text{M}$ for wt-hALOX12. R402L therefore has an effect on catalysis, but it is not nearly as dramatic as that seen for hALOX15, where $k_{\text{cat}}/K_{\text{M}}$ decreased by 136-fold with the analogous mutation. The R402L mutation also did not significantly impact the positional specificity of hALOX12, as both wt-hALOX12 and R402L yielded approximately 100% 12-HETE (**Table 1**), in contrast to previous results on hALOX15, which showed a larger change in product profile. Both the kinetic and specificity results suggest that R402 of hALOX12 does not interact with

AA as significantly as it does in hALOX15. It should be noted that in *Plexaura homomalla* (black sea whip coral) 8R-LOX (cALOX8),³⁵ they observe R182 directly interacting with the carboxylate of AA, but the R182L mutant only manifests a 2-fold decrease in k_{cat}/K_M , similar to hALOX12. However, they also observe significant substrate inhibition with the R182L mutant, which we do not observe for the hALOX12 R402L mutant. Considering that cALOX8 shares only 30% sequence identity with hALOX12, it is difficult to compare these two LOX isozymes with respect to this mechanistic detail, but we still cannot completely rule out a substrate binding role for R402 in hALOX12 based on the cALOX8 result.

hALOX12 also accepts docosahexaenoic acid (DHA) as a substrate, with reaction kinetics similar to that of AA (**Table 1**), and because DHA is 2 carbons longer than AA, it is possible DHA could interact with R402. We therefore tested if R402 might coordinate the carboxylate of DHA; however, no significant change in the activity was observed with DHA between wt-hALOX12 and R402L, further supporting our hypothesis that R402 in hALOX12 does not interact with the

carboxylate group of its fatty acid substrates significantly. A minor change was observed in the product distribution, which also supports a minimal effect of R402 on catalysis. It should be noted that the percent of 11-HDHA:14-HDHA is larger than reported previously with hALOX12 from *E. coli.*,³⁶ which is possibly because the current work expresses hALOX12 in SF9 cells. We are currently investigating this further.

To test the alternate hypothesis suggested by the computational model, H596 was replaced with a nonpolar leucine (H596L) to disrupt H-bonding with the substrate, but only a relatively small decrease in enzyme activity was observed. Kinetic characterization of H596L under steady-state conditions showed a 2-fold decrease in k_{cat}/K_M relative to wt- hALOX12, 6.3 ± 0.4 and $14 \pm 0.9 \mu\text{M}^{-1} \text{s}^{-1}$, respectively, and 3-fold decrease in k_{cat} ($8.6 \pm 0.7 \text{s}^{-1}$) relative to wt-hALOX12 ($28 \pm 0.9 \text{s}^{-1}$) (**Table 1**). However, more significant changes were observed in positional specificity, with H596L producing both 12-HETE and 15-HETE, in a ratio of $\sim 3:1$, along with a small amount of 11-HETE ($5 \pm 1\%$), while wt-hALOX12 produced 100

$\pm 5\%$ 12-HETE. We hypothesize that in H596L, the carboxylate group of AA now interacts with R402, which could explain the production of 15-HETE upon H596L mutation. In order to test this hypothesis, we docked C13-carbanion intermediate of AA to hALOX12 with H596L mutation, and the carboxylate group can indeed hydrogen bond to R402, positioning the reactive carbon atom, C13, 5.0 Å from the metal ion (please see the Supporting Information, **Figure S2**). These results suggest that H596 in wt-hALOX12 may contribute to properly positioning AA for catalysis, possibly through its interaction with the carboxylate moiety of AA.

Substrate	Arachidonic acid			Docosahexaenoic acid		
	Enzymes	wt-12-LOX	H596L	R402L	wt-12-LOX	R402L
K_M (μM)		1.9 ± 0.2	1.3 ± 0.4	0.89 ± 0.09	0.59 ± 0.1	1.5 ± 0.5
K_{cat} (s^{-1})		28 ± 0.9	8.6 ± 0.7	5.6 ± 0.1	4.5 ± 0.1	5.6 ± 0.5
K_{cat}/K_M ($\mu\text{M})^{-1}\text{s}^{-1}$		14 ± 0.9	6.3 ± 0.4	6.3 ± 0.5	7.6 ± 1.5	3.8 ± 1
Product profile (12-HETE:15-HETE:11-HETE)		100:0:0	73:22:5	100:0:0	-	-

Table 1. Mutagenesis experiments to interrogate binding of the carboxylate end of fatty acid substrates with 12-LOX. Steady state kinetics measurements with AA and DHA reveal only relatively small differences in the catalytic efficiency among wt and the 2 mutants. Major changes in the positional specificity are observed for H596L but not R402L, with AA.

π - π Interactions of AA Double Bonds with Aromatic Amino Acids of hALOX12.

On the basis of their model of substrate binding in hALOX15, Gan et al. identified F414 as an important substrate binding determinant,²⁵ proposing that the Δ^{11} double bond of AA participated in a π - π interaction with the aromatic side chain. We mutated the corresponding amino acid in hALOX12, F414L, resulting in a 12-fold decrease in the $k_{\text{cat}}/K_{\text{M}}$ and a 16-fold decrease in k_{cat} (**Table 2**). In contrast, F414W resulted in a more modest reduction in catalytic activity, manifesting a 3.5-fold decrease in $k_{\text{cat}}/K_{\text{M}}$ and a 1.8-fold decrease in k_{cat} , relative to wild-type. These data suggest that the side-chain aromaticity at position 414 is important for binding, consistent with F414 forming a π - π interaction with AA.

Having established the importance of F414, we investigated which specific double bond in AA interacted with F414. The docking model predicted F414 interacted with either Δ^{11} or Δ^{14} , so we measured the catalytic rates of mead acid (5Z,8Z,11Z-eicosatrienoic acid) with wt-hALOX12 and the two mutant hALOX12s, F414L and F414W. Mead acid has the same 20-carbon length as AA but has only

three double bonds, missing the last Δ^{14} double bond. It is hypothesized that if F414 interacts with the Δ^{14} double bond, then wt-hALOX12, F414L, and F414W would all show a decreased activity with mead acid. However, if the interaction was with the Δ^{11} double bond, then the activity of these three LOXs would show the same pattern as seen with AA. As seen in **Table 3**, the catalytic activity with mead acid follows the same pattern as seen with AA, except that the catalytic efficiency actually increases in F414W relative to wt-hALOX12. We therefore conclude that the docking model and the AA and mead acid kinetic data are consistent with a model in which the aromatic side chain of F414 in hALOX12 π - π stacks with the Δ^{11} double bond of AA, similar to that seen for hALOX15. This interaction could facilitate the formation of an allyl radical by delocalizing the π - electrons, as suggested by earlier studies on hALOX15 and soybean LOX-1.^{25,37} It should be noted that removal of Δ^{11} from the substrate eliminates all activity of hALOX12 because the activated methylene is lost.

Enzymes	K_M (μM)	k_{cat} (s^{-1})	k_{cat}/K_M (μM) $^{-1}\text{s}^{-1}$	Products (%)	
				12-HETE	15-HETE
wt-12-LOX	1.9 ± 0.2	28 ± 0.9	14 ± 0.9	100 ± 5	0
F414L	1.4 ± 0.2	1.7 ± 0.06	1.2 ± 0.1	97 ± 4	3 ± 1
F414W	4.0 ± 0.3	16 ± 0.6	4.0 ± 0.2	100 ± 5	0

Table 2. Steady state kinetics and product profile of wt-12-LOX and its mutants with arachidonic acids to test the aromatic interactions between these residues and the substrate.

Enzymes	K_M (μM)	k_{cat} (s^{-1})	k_{cat}/K_M (μM) $^{-1}\text{s}^{-1}$	Products (%)	
				12-product	15-product
Wt-12 LOX	1.3 ± 0.09	1.5 ± 0.03	1.2 ± 0.06	100 ± 5	0
F414L	1.8 ± 0.5	0.60 ± 0.05	0.33 ± 0.07	100 ± 5	0
F414W	1.9 ± 0.2	8.5 ± 0.2	4.5 ± 0.3	100 ± 5	0

Table 3. Steady state kinetics and product profile of wt-12-LOX and its mutants with Mead acid to examine the interacting double bond of the substrate with F414.

Interaction of the Fatty Acid Tail with the Hydrophobic Bottom of the Active

Site. The importance of the volume of the hydrophobic binding site for the lipid tail

has been well established as an important factor in determining the remarkable

specificity of lipoxygenases for fatty acid oxygenation.³⁸ Mutagenesis studies on

various ALOX15 isoforms led to the development of a hypothesis to explain its

product specificity,^{26,27,39} which postulates that F352, I417, M418, and I592

(hALOX15 numbering), which lie at the bottom of the catalytic cavity, regulate the

depth of fatty acid penetration and thus the proper positioning of the substrate for catalysis. Similar studies for hALOX12, focusing on A417 and V418 at the bottom of the hydrophobic pocket (corresponding to the larger amino acids I417 and M418 in hALOX15), have been less conclusive. V418M resulted in no significant change in positional specificity,^{28,31} while A417I and the double mutant A417I/V418M altered the positional specificity only slightly for hALOX12, with ~15% of 15-HpETE being produced. In the current work, we observed somewhat larger changes in product distribution for the double mutant, A417I/V418M, resulting in $24 \pm 2\%$ 15-HpETE and a small amount of 11- HpETE ($0.5 \pm 0.1\%$), as shown in **Table 4**. Nonetheless, the overall percent change in positional specificity of these hALOX12 mutants is lower than that seen for mutations in analogous positions for ALOX15s. For example, a single mutation of hALOX15 (I418A) increased the yield of 12- HETE from 14% for wt-hALOX15 to 94% ²⁸ for the I418A mutant.

We therefore postulated that the hALOX12 active site was wider than that in hALOX15 and thus could allow for additional space for substrate positioning. The

residue, S594, was selected for mutation because its corresponding position in hALOX15 is occupied by a slightly bulkier residue threonine, which would make the active site more narrow in hALOX15. We investigated this possibility by creating a triple mutant (A417I/V418M/S594T) that makes the base of the cavity not only smaller and shallower (A417I and V418M) but also narrower (S594T), as seen in Figure 1. This change results in an increase in 15-HpETE generated to $46 \pm 3\%$ for A417I/V418M/S594T, as compared to $23 \pm 1\%$ for A417I/V418M.

Considering that A417I/V418M affected the product ratio of AA catalysis, we subsequently investigated the effect these mutations would have on fatty acids with varied length and unsaturation. The substrates utilized were the C-20 fatty acid; 11Z,14Z-eicosadienoic acid (EDA); and the C-18 fatty acids, 9Z,12Z-linoleic acid (LA) and gamma 6Z,9Z,12Z-linolenic acid (GLA). Previous studies in our lab have shown that EDA and LA are poor substrates for hALOX12 because the bis-allylic hydrogen is not positioned properly for hydrogen atom abstraction (**Table 5**).⁴⁰ However, the mutant, A417I/V418M, reacts with both EDA and LA, effectively

shifting the substrate backward into the active site so that the bis-allylic carbon, C-13 for EDA and C-11 for LA, are positioned so the catalytic ferric- hydroxide abstracts the proper hydrogen atom. The products generated were as expected, 100% 15-HpEDA with EDA and 100% 13-HpODE for LA (**Table 5**). It should be noted that GLA is a substrate for wt-hALOX12, but its k_{cat}/K_M is very low ($k_{\text{cat}}/K_M = 0.08 \pm 0.01 \mu\text{M}^{-1} \text{s}^{-1}$) and two products are generated, $30 \pm 2\%$ 10-HpOTrE and $70 \pm 4\%$ 13-HpOTrE (**Table 5**). However, the reactivity of GLA with A417I/V418M increases 32-fold ($k_{\text{cat}}/K_M = 2.6 \pm 0.10 \mu\text{M}^{-1} \text{s}^{-1}$) relative to the wt-hALOX12 and it produces entirely 13-HpOTrE, as shown in the **Table 5**. It should be noted that the wt-hALOX12 result does not follow the classical interpretation of LOX product formation. One would predict that the main product of wt-hALOX12 from GLA would be 10-HpOTrE, because of the positioning of C9 near the active site iron; however, 13-HpOTrE is the major product. It appears that the shorter length of GLA relative to AA not only lowers the catalytic efficiency but also affects substrate positioning by increasing the formation of 13-HpOTrE relative to 10- HpOTrE. For

all three of these fatty acids, the increase in enzyme activity of the A417I/V418M mutant relative to wt- hALOX12 appears to be due to a repositioning of the fatty acid by restricting the depth of the active site, such that the bis- allylic hydrogen is now positioned properly for abstraction. While this effect is dramatic for these three fatty acids because there is little or no activity with wt-hALOX12, it is comparable to the change in reactivity of wt-hALOX12 and A417I/V418M with AA. A417I/V418 M produces $24 \pm 2\%$ 15-HpETE from AA, and given that its $k_{\text{cat}}/K_{\text{M}}$ is $59 \mu\text{M}^{-1} \text{s}^{-1}$, this translates to an approximate $k_{\text{cat}}/K_{\text{M}}$ of $14 \mu\text{M}^{-1} \text{s}^{-1}$ for producing 15-HpETE, which is of comparable magnitude to the $k_{\text{cat}}/K_{\text{M}}$ values of A417I/V418M with LA, EDA, and GLA.

Enzymes	wt-12-LOX	A417I	V418M	A417I/V418M	A417I/V418M/ S594T
K_{M} (μM)	1.9 ± 0.2	0.86 ± 0.1	3.2 ± 0.6	0.56 ± 0.1	0.52 ± 0.1
k_{cat} (s^{-1})	28 ± 0.9	15 ± 0.4	20 ± 2	34 ± 1	2.7 ± 0.09
$k_{\text{cat}}/K_{\text{M}}$ ($\mu\text{M}^{-1}\text{s}^{-1}$)	14 ± 0.9	18 ± 2	6.3 ± 0.7	59 ± 10	5.1 ± 0.9
Product profile					
(12-HETE:15-HE TE:11-HETE)	100:0:0	85:15:0	100:0:0	75.5:24:0.5	56:46:0

Table 4. Steady state kinetics of mutant enzymes with shallower and narrower cavity.

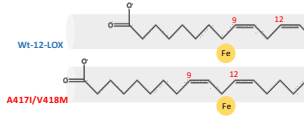
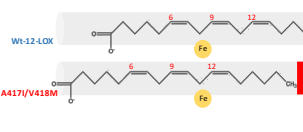
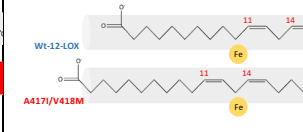
						
Substrate	LA		GLA		EDA	
Enzymes	wt-12-LOX	A417I/V418M	wt-12-LOX	A417I/V418M	wt-12-LOX	A417I/V418M
K_M (μM)	NA	2.8 ± 0.5	4.1 ± 0.9	4.7 ± 0.2	NA	1.7 ± 0.6
K_{cat} (s^{-1})	NA	3.8 ± 0.3	0.34 ± 0.03	12 ± 0.3	NA	2.5 ± 0.4
K_{cat}/K_M (μM) $^{-1}$ s^{-1}	NA	1.4 ± 0.2	0.08 ± 0.01	2.6 ± 0.1	NA	1.4 ± 0.3
Major Product	NA	13HODE	13HOTrE	13HOTrE	NA	15HEDA

Table 5. Steady-state kinetics of the wt-12-LOX and A417I/V418M mutant enzyme with linoleic acid (LA), gamma linoleic acid (GLA), and eicosadienoic acid (EDA). The cartoons in the table are depicting how the double mutant restricts the depth of the substrate by two carbons. (NA = No activity above the detection limit).

Critical Role of L407 in Substrate Positioning. The model of wt-hALOX12 with AA bound suggests that the bulky hydrophobic side chain of L407 plays a critical role in defining the “U” shape of the binding site and thus properly positioning AA for catalysis. Because L407 is conserved in all lipoxygenases²⁵ and is observed at the base of the U-shaped AA in the cALOX8 (8R-LOX) costructure,³⁵ we hypothesized that mutations of L407 would affect catalytic efficiency and possibly positional specificity. Specifically, replacing L407 with the much smaller amino acids alanine (L407A) and glycine (L407G) was predicted to greatly widen the binding site near the iron, essentially eliminating the characteristic “U” shape (**Figure 2**). Consistent with this hypothesis, we observed a ~100-fold decrease in both k_{cat} and k_{cat}/K_M for both of these mutants, when compared to wt-hALOX12 (**Table 6**), confirming its important role in catalysis. For comparison, we previously mutated this residue in hALOX15 (L407A) and demonstrated a 5-fold decrease in k_{cat} and a 3-fold decrease in k_{cat}/K_M .⁴¹ These effects are less than that seen for hALOX12, indicating a reduced effect of L407 in hALOX15.

In addition, widening the active site cavity with L407A caused a slight decrease in positional specificity, with $3 \pm 1\%$ 15-HpETE and $6 \pm 1\%$ 11-HpETE generation. This change in positional specificity increased when the cavity was made even larger with the L407G mutant enzyme, with the percentages of the 15-HpETE and 11-HpETE increasing to $21 \pm 2\%$ and $19 \pm 2\%$, respectively (**Table 6**). These results imply that L407 is partly responsible for positioning the C10 for abstraction, with a smaller residue at position 407 possibly leading to a “looser” substrate binding mode, thus affecting the percent of 15- HpETE product synthesized. The triple mutant, L407G/ A417I/V418M, increases the percent of 15-HETE even further to $31 \pm 2\%$, which is consistent with this hypothesis, because A417I/V418M reduces the length of the cavity and adjusts the substrate positioning further, aligning C13 for hydrogen atom abstraction. Previously, the homologous mutation, L546A, in soybean LOX-1 was shown to affect catalysis significantly, similar to what we observe for L407A.⁴² Klinman and co-workers determined that the decreased rate of L546A was due to an increased cavity size across from the ferric-hydroxide moiety, which altered

heavy-atom motions and led to an increase in the energy of activation for hydrogen atom abstraction. They did not investigate if L546A demonstrated altered product reactivity, but given our results, it would be a likely result. It should be noted that the percentage of 11- HETE increases as the cavity increases in size (L407A vs L407G) but then decreases as the cavity shrinks with the triple mutant (L407G/A417I/V418M), suggesting that the 11- HETE product correlates with a larger cavity. Finally, we generated the 4-residue mutant, A407G/A417I/V418M/S594T, to increase the 15-HETE percentage even further, but it was inactive, suggesting these four mutations make the enzyme incapable of positioning the hydrogen atom for abstraction. We are currently investigating this result in more detail to understand the substrate binding determinants in more detail.

Protein	K_M (uM) (AA)	k_{cat} (s^{-1}) (AA)	k_{cat}/K_M (μM) $^{-1}s^{-1}$ (AA)	Products with AA (%)		
				12HETE	11HETE	15HETE
Wt-12 LOX	1.9 ± 0.2	28 ± 0.9	14 ± 0.9	100 ± 5	0	0
L407A	2.4 ± 0.2	0.28 ± 0.01	0.12 ± 0.01	91 ± 4	6 ± 1	3 ± 1
L407G	1.8 ± 0.3	0.22 ± 0.01	0.12 ± 0.02	60 ± 3	19 ± 2	21 ± 2
L407G/A417I/V418M	1.5 ± 0.3	0.19 ± 0.01	0.13 ± 0.02	66 ± 3	3 ± 1	31 ± 2

Table 6. Steady - state kinetics parameters of wt-12-LOX and the mutants that makes the binding cavity wider (L407A, L407G) and wider as well as smaller (L407G/A417I/V418M).

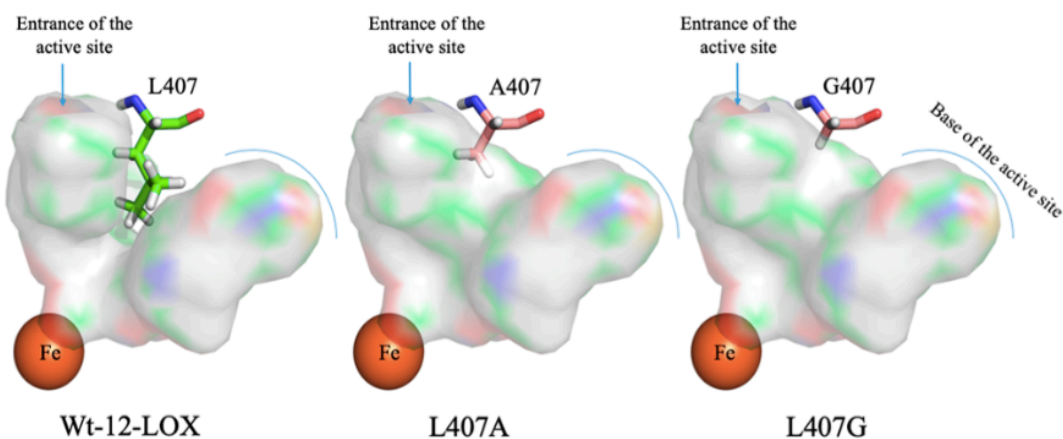


Figure 2. Relative cavity shapes and sizes of wt-hALOX12, L407A, and L407G. Pymol was used in the generation of this figure.

Substrate Positioning in hALOX12 and Other Lipoxygenases. The remarkable product specificity achieved by LOX enzymes can be traced to proper positioning of substrates in the active site, specifically, (1) how the carboxylate group of the fatty

acid is anchored as the substrate binds in the active site and (2) the depth of the active site. Here we compare residues that coordinate to the carboxylate group of AA in hALOX12 to other LOX enzymes. The available crystal structure of rALOX15 does not have a substrate or substrate analogue bound in the active site. However, a mutational study showed that R402 from helix α 11 in hALOX15 (equivalent to R403 in rALOX15) anchored the carboxylate group of AA and LA.¹⁵ Structural and mutational studies of cALOX8 (8R-LOX) showed that R182 from helix α 2 hydrogen bonds to the carboxylate group of AA.^{35,43} The pALOX15 crystal structure showed that Q596 from helix α 21 interacted with the carboxylate group of the cocrystallized substrate-analogue inhibitor.⁴⁴ Finally, the results of this study demonstrate that H596 from helix α 21 plays the role of anchoring the carboxylate group of AA in hALOX12.

In **Figure 3**, we structurally superimpose these three structures and one model, highlighting the carboxylate group anchoring residues. In all cases, the substrate binds in a head- to-tail orientation, with the head (i.e., the carboxylate group) binding

at the entrance of the active site and the hydrophobic tail binding at the interior of the protein. However, the side chains coordinating the carboxylate are located on three different helices: helix $\alpha 11$ for rALOX15 and hALOX12, helix $\alpha 21$ for pALOX15, and helix $\alpha 2$ for cALOX8 (8R-LOX). These observations, therefore, support the hypothesis that LOX enzymes may have evolved to achieve different regio- and stereospecificities by selectively positioning the polar residues on different helices near the entrance of the active site.

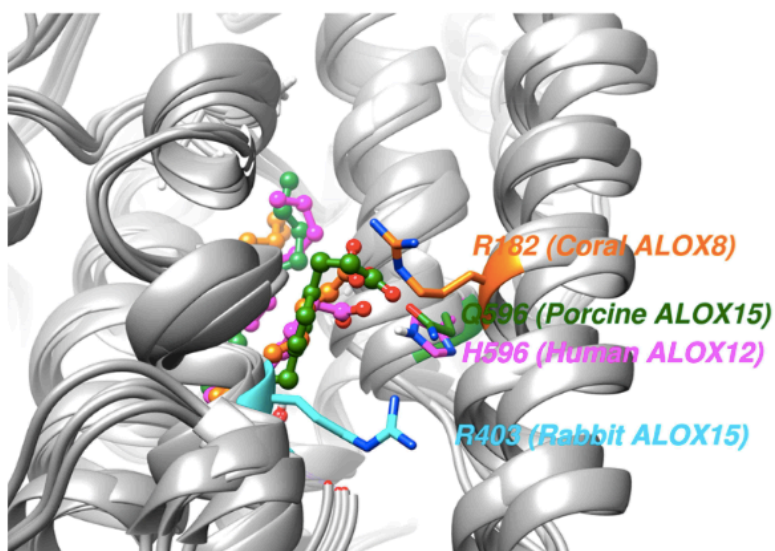


Figure 3. Superimposed crystal structures of lipoygenases with differing product specificity: cALOX8 (PDB ID: 4qwt) cocrystallized with AA (orange), rALOX15 (PDB ID: 2p0m) (cyan), pALOX15 (PDB ID: 3rde) cocrystallized with a substrate analogue inhibitor (green), and AA carbanion-intermediate docked model of hALOX12 from this work (magenta). The side chains of R182 from helix α 2 of cALOX8, Q596 from helix α 21 of pALOX15, H596 from helix α 11 of hALOX12, and R403 from helix α 11 of rALOX15, which coordinate with the carboxylate group of the fatty acid, are also shown. Nitrogen, oxygen, and hydrogen atoms are shown in blue, red, and white respectively.

2.5 Conclusion

Human platelet ALOX12 is a critical enzyme in a variety of human biological processes; therefore, understanding its mechanism of action is highly important. In this report, we have performed extensive site-directed mutagenesis and molecular modeling to better understand the binding of fatty acids to the active site of hALOX12. We observed that the conserved R402 in hALOX12 displays minimal interactions with the carboxylate end of AA, as opposed to the large interaction reported for hALOX15.²⁵ H596 in hALOX12 appears to be better positioned to interact with the carboxylic acid, but its effects on hALOX12 catalysis are still not as great as that seen for R402 with hALOX15. We also determined that F414 in hALOX12 interacts with the Δ^{11} double bond of AA, similar to that seen in hALOX15, indicating a common π - π stacking determinant for both hALOX12 and hALOX15.²⁵ Our results also demonstrate that A417 and V418 are determinants for positional specificity in hALOX12, as observed previously for hALOX15, because of

their defining of the cavity depth.²⁸ In addition, we observe that S594 also contributes to the positional specificity of hALOX12 by narrowing the cavity and restricting the degrees of freedom the methyl tail of AA can sample, thus increasing 15-HETE production. Finally, L407 appears to provide a restriction in the active site, which constrains the substrate such that the hydrogen from C10 is abstracted with high efficiency. These findings are summarized in **Figure 4**, which highlight the key substrate determinants for hALOX12.

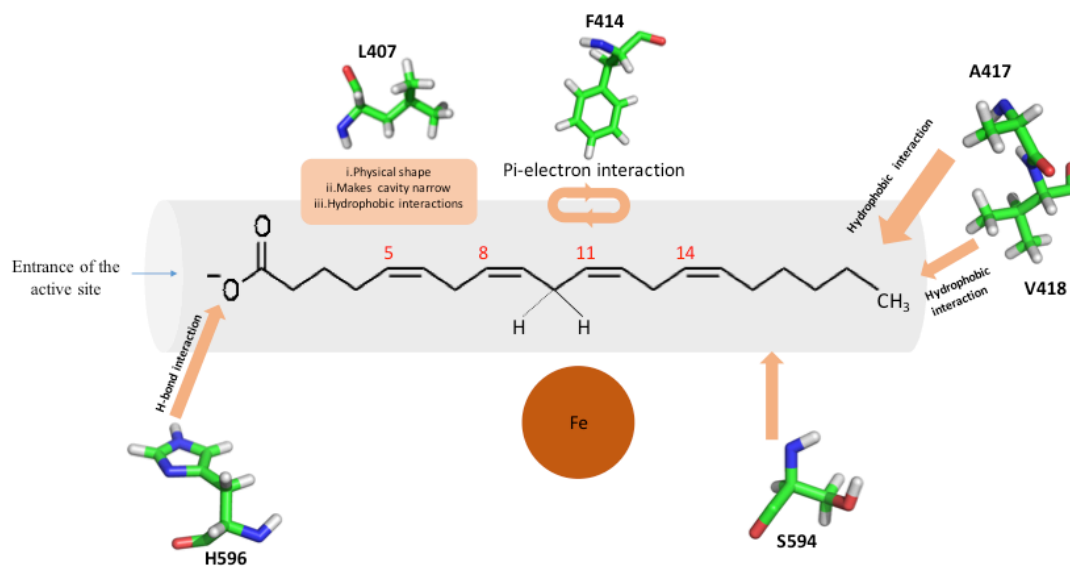


Figure 4. Schematic diagram of the proposed binding determinants of human 12-lipoxygenase. The active site is depicted to be straight instead of boot-shaped for easy understanding. This schematic approximates the position of the amino acids relative to carbon in arachidonic acid.

2.6 Abbreviation

LOX, lipoxygenase; hALOX15 (h15-LOX-1), human reticulocyte 15-lipoxygenase-1;

rALOX15 (r15-LOX-1), rabbit reticulocyte 15-lipoxygenase-1; hALOX12

(h12-LOX), human platelet 12-lipoxygenase; pALOX15 (p12-LOX), porcine

leukocyte 12-lipoxygenase; cALOX8 (8R-LOX), Plexaura homomalla (black sea

whip coral) 8R-lipoxygenase; PUFA, polyunsaturated fatty acids; AA, arachidonic

acid; DHA, docosahexaenoic acid; EDA, 11Z, 14Z-eicosadienoic acid; LA, 9Z,

12Z-linoleic acid; GLA, gamma-6Z, 9Z, 12Z- linolenic acid; HETE,

hydroxy-eicosatetraenoic acid; HpETE, hydroperoxy-eicosatetraenoic acid; 12-HETE,

12-hydroxy- eicosatetraenoic acid; 12-HpETE, 12-hydroperoxy-

5Z,8Z,10E,14Z-eicosatetraenoic acid; 11-HETE, 11-hydroxy- eicosatetraenoic acid;

15-HETE, 15-hydroxy-eicosatetraenoic acid; 15-HpETE,

15-hydroperoxy-5Z,8Z,10Z,13E-eicosatetrae- noic acid; 15-HpEDA,

15(S)-hydroperoxy-11Z,13E-eicosadie- noic acid; 13-HODE,

13(S)-hydroxy-9Z,11E-octadecadienoic acid; 13-HpODE,

13(S)-hydroperoxy-9Z,11E-octadecadienoic acid; 13-HOTrE,

13(S)-hydroxy-6Z,9Z,11E-octadecatrienoic acid; 13-HpOTrE,

13(S)-hydroperoxy-6Z,9Z,11E-octadeca- trienoic acid; 10-HpOTrE,

10(S)-hydroperoxy-6Z,8E,12Z- octadecatrienoic acid

Reference

- (1) Newcomer, M. E., and Brash, A. R. (2015) The structural basis for specificity in lipoxygenase catalysis. *Protein Sci.* 24, 298–309.
- (2) Brash, A. R. (1999) Lipoxygenases: Occurrence, Functions, Catalysis, and Acquisition of Substrate. *J. Biol. Chem.* 274, 23679– 23682.
- (3) Kuhn, H., Saam, J., Eibach, S., Holzhütter, H.-G., Ivanov, I., and Walther, M. (2005) Structural biology of mammalian lipoxygenases: Enzymatic consequences of targeted alterations of the protein structure. *Biochem. Biophys. Res. Commun.* 338, 93–101.
- (4) Lauretti, E., and Pratico, D. (2018) Novel Key Players in the Development of Tau Neuropathology: Focus on the 5-Lipoxygenase. *J. Alzheimer's Dis.* 64, S481–S489.
- (5) Tersey, S. A., Bolanis, E., Holman, T. R., Maloney, D. J., Nadler, J. L., and Mirmira, R. G. (2015) Minireview: 12-Lipoxygenase and Islet beta-Cell Dysfunction in Diabetes. *Mol. Endocrinol.* 29, 791–800.
- (6) Ivanov, I., Kuhn, H., and Heydeck, D. (2015) Structural and functional biology of arachidonic acid 15-lipoxygenase-1 (ALOX15). *Gene* 573, 1–32.
- (7) Kagan, V. E., Mao, G., Qu, F., Angeli, J. P., Doll, S., Croix, C. S., Dar, H. H., Liu, B., Tyurin, V. A., Ritov, V. B., Kapralov, A. A., Amoscato, A. A., Jiang, J., Anthonymuthu, T., Mohammadyani, D., Yang, Q., Proneth, B., Klein-Seetharaman, J., Watkins, S., Bahar, I., Greenberger, J., Mallampalli, R. K., Stockwell, B. R., Tyurina, Y. Y., Conrad, M., and Bayir, H. (2017) Oxidized arachidonic and adrenic PEs navigate cells to ferroptosis. *Nat. Chem. Biol.* 13, 81–90.
- (8) Drefs, M., Thomas, M. N., Guba, M., Angele, M. K., Werner, J., Conrad, M., Steib, C. J., Holdt, L. M., Andrassy, J., Khandoga, A., and Rentsch, M. (2017)

Modulation of Glutathione Hemostasis by Inhibition of 12/15-Lipoxygenase Prevents ROS-Mediated Cell Death after Hepatic Ischemia and Reperfusion. *Oxid. Med. Cell. Longevity* 2017, 8325754.

(9) Friedmann Angeli, J. P., Schneider, M., Proneth, B., Tyurina, Y. Y., Tyurin, V. A., Hammond, V. J., Herbach, N., Aichler, M., Walch, A., Eggenhofer, E., Basavarajappa, D., Radmark, O., Kobayashi, S., Seibt, T., Beck, H., Neff, F., Esposito, I., Wanke, R., Forster, H., Yefremova, O., Heinrichmeyer, M., Bornkamm, G. W., Geissler, E. K., Thomas, S. B., Stockwell, B. R., O'Donnell, V. B., Kagan, V. E., Schick, J. A., and Conrad, M. (2014) Inactivation of the ferroptosis regulator Gpx4 triggers acute renal failure in mice. *Nat. Cell Biol.* 16, 1180– 1191.

(10) Toppo, S., Flohe, L., Ursini, F., Vanin, S., and Maiorino, M. (2009) Catalytic mechanisms and specificities of glutathione peroxidases: variations of a basic scheme. *Biochim. Biophys. Acta, Gen. Subj.* 1790, 1486–1500.

(11) Sutherland, M., Shankaranarayanan, P., Schewe, T., and Nigam, S. (2001) Evidence for the presence of phospholipid hydroperoxide glutathione peroxidase in human platelets: implications for its involvement in the regulatory network of the 12-lipoxygenase pathway of arachidonic acid metabolism. *Biochem. J.* 353, 91–100.

(12) Schnurr, K., Belkner, J., Ursini, F., Schewe, T., and Kuhn, H. (1996) The selenoenzyme phospholipid hydroperoxide glutathione peroxidase controls the activity of the 15-lipoxygenase with complex substrates and preserves the specificity of the oxygenation products. *J. Biol. Chem.* 271, 4653–4658.

(13) Boeglin, W. E., Kim, R. B., and Brash, A. R. (1998) A 12R- lipoxygenase in human skin: mechanistic evidence, molecular cloning, and expression. *Proc. Natl. Acad. Sci. U. S. A.* 95, 6744–6749.

(14) Chen, X. S., Brash, A. R., and Funk, C. D. (1993) Purification and characterization of recombinant histidine-tagged human platelet 12-lipoxygenase expressed in a baculovirus/insect cell system. *Eur. J. Biochem.* 214, 845–852.

- (15) Hussain, H., Shornick, L. P., Shannon, V. R., Wilson, J. D., Funk, C. D., Pentland, A. P., and Holtzman, M. J. (1994) Epidermis contains platelet-type 12-lipoxygenase that is overexpressed in germinal layer keratinocytes in psoriasis. *Am. J. Physiol.* 266, C243–253.
- (16) Connolly, J. M., and Rose, D. P. (1998) Enhanced angiogenesis and growth of 12-lipoxygenase gene-transfected MCF-7 human breast cancer cells in athymic nude mice. *Cancer Lett.* 132, 107–112.
- (17) Natarajan, R., and Nadler, J. (1998) Role of lipoxygenases in breast cancer. *Front. Biosci., Landmark Ed.* 3, E81–88.
- (18) Ding, X. Z., Iversen, P., Cluck, M. W., Knezetic, J. A., and Adrian, T. E. (1999) Lipoxygenase inhibitors abolish proliferation of human pancreatic cancer cells. *Biochem. Biophys. Res. Commun.* 261, 218–223.
- (19) Shappell, S. B., Olson, S. J., Hannah, S. E., Manning, S., Roberts, R. L., Masumori, N., Jisaka, M., Boeglin, W. E., Vader, V., Dave, D. S., Shook, M. F., Thomas, T. Z., Funk, C. D., Brash, A. R., and Matusik, R. J. (2003) Elevated expression of 12/15-lipoxygenase and cyclooxygenase-2 in a transgenic mouse model of prostate carcinoma. *Cancer Res.* 63, 2256–2267.
- (20) Thomas, C. P., Morgan, L. T., Maskrey, B. H., Murphy, R. C., Kühn, H., Hazen, S. L., Goodall, A. H., Hamali, H. A., Collins, P. W., and O'Donnell, V. B. (2010) Phospholipid-esterified eicosanoids are generated in agonist-activated human platelets and enhance tissue factor-dependent thrombin generation. *J. Biol. Chem.* 285, 6891–6903.
- (21) Holinstat, M., Boutaud, O., Apopa, P. L., Vesce, J., Bala, M., Oates, J. A., and Hamm, H. E. (2011) Protease-activated receptor signaling in platelets activates cytosolic phospholipase A2 α differently for cyclooxygenase-1 and 12-lipoxygenase catalysis. *Arterioscler., Thromb., Vasc. Biol.* 31, 435–442.

- (22) Kaur, G., Jalagadugula, G., Mao, G., and Rao, A. K. (2010) RUNX1/core binding factor A2 regulates platelet 12-lipoxygenase gene (ALOX12): studies in human RUNX1 haplodeficiency. *Blood* 115, 3128–3135.
- (23) Ma, K., Nunemaker, C. S., Wu, R., Chakrabarti, S. K., Taylor- Fishwick, D. A., and Nadler, J. L. (2010) 12-Lipoxygenase Products Reduce Insulin Secretion and β -Cell Viability in Human Islets. *J. Clin. Endocrinol. Metab.* 95, 887–893.
- (24) Sloane, D. L., Leung, R., Barnett, J., Craik, C. S., and Sigal, E. (1995) Conversion of human 15-lipoxygenase to an efficient 12- lipoxygenase: the side-chain geometry of amino acids 417 and 418 determine positional specificity. *Protein Eng., Des. Sel.* 8, 275–282
- (25) Gan, Q. F., Browner, M. F., Sloane, D. L., and Sigal, E. (1996) Defining the arachidonic acid binding site of human 15-lipoxygenase. Molecular modeling and mutagenesis. *J. Biol. Chem.* 271, 25412– 25418.
- (26) Borngräber, S., Kuban, R. J., Anton, M., and Kühn, H. (1996) Phenylalanine 353 is a primary determinant for the positional specificity of mammalian 15-lipoxygenases. *J. Mol. Biol.* 264, 1145– 1153.
- (27) Borngräber, S., Kuban, R. J., and Kühn, H. (1999) Sequence determinants for the positional specificity of mammalian and plant lipoxygenases. *Adv. Exp. Med. Biol.* 469, 91–97.
- (28) Vogel, R., Jansen, C., Roffeis, J., Reddanna, P., Forsell, P., Claesson, H.-E., Kuhn, H., and Walther, M. (2010) Applicability of the triad concept for the positional specificity of mammalian lipoxygenases. *J. Biol. Chem.* 285, 5369–5376.
- (29) Di Venere, A., Horn, T., Stehling, S., Mei, G., Masgrau, L., González-Lafont, A., Kühn, H., and Ivanov, I. (2013) Role of Arg403 for thermostability and catalytic activity of rabbit 12/15-lipoxygenase. *Biochim. Biophys. Acta, Mol. Cell Biol. Lipids* 1831, 1079–1088.

- (30) Suzuki, H., Kishimoto, K., Yoshimoto, T., Yamamoto, S., Kanai, F., Ebina, Y., Miyatake, A., and Tanabe, T. (1994) Site-directed mutagenesis studies on the iron-binding domain and the determinant for the substrate oxygenation site of porcine leukocyte arachidonate 12-lipoxygenase. *Biochim. Biophys. Acta, Lipids Lipid Metab.* 1210, 308–316.
- (31) Chen, X. S., and Funk, C. D. (1993) Structure-function properties of human platelet 12-lipoxygenase: chimeric enzyme and in vitro mutagenesis studies. *FASEB J.* 7, 694–701.
- (32) McGovern, S. L., and Shoichet, B. K. (2003) Information decay in molecular docking screens against holo, apo, and modeled conformations of enzymes. *J. Med. Chem.* 46, 2895–2907.
- (33) Amagata, T., Whitman, S., Johnson, T. A., Stessman, C. C., Loo, C. P., Lobkovsky, E., Clardy, J., Crews, P., and Holman, T. R. (2003) Exploring sponge-derived terpenoids for their potency and selectivity against 12-human, 15-human, and 15-soybean lipoxygenases. *J. Nat. Prod.* 66, 230–235.
- (34) Hermann, J. C., Ghanem, E., Li, Y., Raushel, F. M., Irwin, J. J., and Shoichet, B. K. (2006) Predicting substrates by docking high- energy intermediates to enzyme structures. *J. Am. Chem. Soc.* 128, 15882–15891.
- (35) Neau, D. B., Bender, G., Boeglin, W. E., Bartlett, S. G., Brash, A. R., and Newcomer, M. E. (2014) Crystal structure of a lipoxygenase in complex with substrate: the arachidonic acid-binding site of 8R- lipoxygenase. *J. Biol. Chem.* 289, 31905–31913.
- (36) Kutzner, L., Goloshchapova, K., Heydeck, D., Stehling, S., Kuhn, H., and Schebb, N. H. (2017) Mammalian ALOX15 orthologs exhibit pronounced dual positional specificity with docosahexaenoic acid. *Biochim. Biophys. Acta, Mol. Cell Biol. Lipids* 1862, 666–675.

- (37) Nelson, M. J., Cowling, R. A., and Seitz, S. P. (1994) Structural characterization of alkyl and peroxy radicals in solutions of purple lipoxygenase. *Biochemistry* 33, 4966–4973.
- (38) Ivanov, I., Heydeck, D., Hofheinz, K., Roffeis, J., O'Donnell, V. B., Kuhn, H., and Walther, M. (2010) Molecular enzymology of lipoxygenases. *Arch. Biochem. Biophys.* 503, 161–174.
- (39) Sloane, D., Leung, R., Craik, C., and Sigal, E. (1991) A Primary Determinant for Lipoxygenase Positional Specificity. *Nature* 354, 149–152.
- (40) Ikei, K. N., Yeung, J., Apopa, P. L., Ceja, J., Vesci, J., Holman, T. R., and Holinstat, M. (2012) Investigations of human platelet-type 12- lipoxygenase: role of lipoxygenase products in platelet activation. *J. Lipid Res.* 53, 2546–2559.
- (41) Armstrong, M., van Hoorebeke, C., Horn, T., Deschamps, J., Freedman, J. C., Kalyanaraman, C., Jacobson, M. P., and Holman, T. (2016) Human 15-LOX-1 active site mutations alter inhibitor binding and decrease potency. *Bioorg. Med. Chem.* 24, 5380–5387.
- (42) Knapp, M. J., Rickert, K., and Klinman, J. P. (2002) Temperature-dependent isotope effects in soybean lipoxygenase-1: Correlating hydrogen tunneling with protein dynamics. *J. Am. Chem. Soc.* 124, 3865–3874.
- (43) Neau, D. B., Gilbert, N. C., Bartlett, S. G., Boeglin, W., Brash, A. R., and Newcomer, M. E. (2009) The 1.85 Å structure of an 8R- lipoxygenase suggests a general model for lipoxygenase product specificity. *Biochemistry* 48, 7906–7915.
- (44) Xu, S., Mueser, T. C., Marnett, L. J., and Funk, M. O., Jr. (2012) Crystal structure of 12-lipoxygenase catalytic-domain-inhibitor complex identifies a substrate-binding channel for catalysis. *Structure* 20, 1490–1497.

Chapter 3

In Vitro Biosynthetic Pathway Investigations of Neuroprotectin D1 (NPD1) and

Protectin DX (PDX) by Human 12-Lipoxygenase, 15-Lipoxygenase-1 and

15-Lipoxygenase-2

3.1 Abstract

In this paper, human platelet 12-lipoxygenase (h12-LOX (ALOX12)), human reticulocyte 15-lipoxygenase-1 (h15-LOX-1 (ALOX15)), and human epithelial 15-lipoxygenase-2 (h15-LOX-2 (ALOX15B)) were observed to react with docosahexaenoic acid (DHA) and produce 17S-hydroperoxy-4Z,7Z,10Z,13Z,15E,19Z-docosahexaenoic acid (17S-HpDHA). The k_{cat}/K_M values with DHA for h12-LOX, h15-LOX-1 and h15-LOX-2 were 12, 0.35 and 0.43 $\text{sec}^{-1} \cdot \mu\text{M}^{-1}$, respectively, which demonstrate h12-LOX as the most efficient of the three. These values are comparable to their counterpart k_{cat}/K_M values with arachidonic acid (AA), 14, 0.98 and 0.24 $\text{sec}^{-1} \cdot \mu\text{M}^{-1}$, respectively. Comparison of their product profiles with DHA demonstrate that the three LOX isozymes produce 11S-HpDHA, 14S-HpDHA and 17S-HpDHA, to varying degrees, with 17S-HpDHA being the majority product only for the 15-LOX isozymes. The effective k_{cat}/K_M values ($k_{cat}/K_M \cdot \% \text{ product formation}$) for 17S-HpDHA of the three isozymes

indicate that h12-LOX had a 2.8-fold greater *in vitro* value than that of h15-LOX-1 and a 1.3-fold greater value than h15-LOX-2. 17S-HpDHA was an effective substrate for h12-LOX and h15-LOX-1, with four products being observed under reducing conditions; Protectin DX (PDX), 16S,17S-epoxy-4Z,7Z,10Z,12E,14E,19Z-docosahexaenoic acid (16S,17S-epoxyDHA), the key intermediate in neuroprotection D1 biosynthesis (NPD1, also known as protectin D1 (PD1)), 11,17S-diHDHA and 16,17S-diHDHA. However, h15-LOX-2 did not react with 17-HpDHA. With respect to their effective k_{cat}/K_M values, h12-LOX was markedly less effective than h15-LOX-1 in reacting with 17S-HpDHA, with a 55-fold lower effective k_{cat}/K_M in producing 16S,17S-epoxyDHA and a 27-fold lower effective k_{cat}/K_M in generating PDX. This is the first direct demonstration of h15-LOX-1 catalyzing this reaction and reveals an *in vitro* pathway for PDX and NPD1 intermediate biosynthesis. In addition, the epoxide formation from 17S-HpDHA and h15-LOX-1 was negatively affected through allosteric regulation by 17S-HpDHA ($K_d = 5.9 \mu\text{M}$),

12S-hydroxy-5Z,8Z,10E,14Z-eicosatetraenoic acid (12S-HETE) ($K_d = 2.5 \mu\text{M}$), and 17S-hydroxy-13Z,15E,19Z-docosatrienoic acid (17S-HDTA) ($K_d = 1.4 \mu\text{M}$), suggesting a possible regulatory pathway in reducing epoxide formation. Finally, 17S-HpDHA and PDX inhibited platelet aggregation, with EC_{50} values of approximately 1 and 3 μM , respectively. These *in vitro* results may help guide *in vivo* PDX and NPD1 intermediate (i.e. 16S,17S-epoxyDHA) biosynthetic investigations and implicate the benefits of diets rich in DHA.

3.2 Introduction

There are two types of inflammation; acute and chronic. Acute inflammation is the initial response of the body to injury and infection and is initiated by neutrophils, eosinophils, and M1-polarized macrophages, which are amplified by bioactive molecules, such as prostaglandins and leukotrienes¹. However, an uncontrolled immune response promotes chronic inflammation and unresolved tissue damage^{2, 3}.

At the peak of the acute inflammatory response, the immune cells undergo a temporal lipid mediator class switch and start producing specialized pro-resolving mediators (SPMs)^{4, 5}. To date, there are more than 20 different SPMs that have been identified, which can be subdivided into six main classes: AA-derived lipoxins (LXs), EPA-derived E-series resolvins (RvEs), DHA-derived D-series resolvins (RvDs), neuroprotectins (i.e. NPD1, also known as protectin-1 (PD1)) and their conjugates (PCTRs), maresins (Mar1) and their conjugates (MCTRs), and DPA-derived 13-series resolvins (RvTs)³. The failure to transition from inflammation to resolution

has been revealed to cause a variety of chronic inflammatory diseases, such as cardiovascular disease, Alzheimer's disease (AD), amyotrophic lateral sclerosis (ALS) and cancer⁶. Nonsteroidal anti-inflammatory drugs (NSAIDs) have so far been the major therapeutics for acute inflammation by inhibiting the cyclooxygenase (COX) activity; however, these drugs show limited effect on resolving chronic inflammatory diseases. The challenge for treatment of chronic inflammation is simultaneously inhibiting the pro-inflammatory processes while stimulating the pro-resolution processes. This goal is complicated by the fact that production of both pro-inflammatory and pro-resolving molecules is catalyzed from the same enzymes, lipoxygenase (LOX) and cyclooxygenase (COX) isozymes^{5,7}. Therefore, it is critical to characterize the specific roles the LOX and COX isozymes play in the production of SPMs in order to develop the most effective therapeutic treatment for chronic inflammatory diseases.

Neuroprotectin D1 (NPD1) was the first identified neuro-protective mediator of docosahexaenoic acid (DHA) belonging to the SPMs and was fully assigned by

matching the biological sample with stereo-chemically pure and enantio-enriched isomers obtained by total synthesis⁸. The name “neuroprotectin D1” was based on its neuroprotective bioactivity in brain ischemia reperfusion (BIR) and oxidatively stressed retina pigment epithelial (RPE) cells, as well as its ability to protect cells from oxidative stress-induced apoptosis^{9, 10}. It can also up-regulate the stimulation of the anti-apoptotic protein, Bcl-2, and decrease the pro-apoptotic protein, Bax, in ARPE-19 cells during oxidative stress⁹.

Protectin DX (PDX), another SPM and stereoisomer of NPD1, was first obtained enzymatically by Serhan et al. *in vitro* then its structure was re-examined later by Butovich et al. to confirm the geometry of the double bonds of the conjugated triene unit and the stereo-configuration at carbon 10¹¹⁻¹³. The bioactivity of PDX revealed that it can inhibit inflammation associated with cyclooxygenase (COX) activities, reactive oxygen species (ROS) formation and influenza virus replication.¹⁴ The biosynthesis of NPD1 and PDX are both proposed to be catalyzed by LOX isozymes, however, the specific LOX isozymes involved and the detailed biosynthetic pathway

are not well characterized.

Lipoxygenases (LOX) are non-heme iron-containing enzymes with the primary reactivity of abstracting a hydrogen atom from a cis,cis-1,4-pentadiene of a polyunsaturated fatty acid (PUFA), followed by oxygen insertion to generate a hydroperoxide product. In humans, there are six LOX isozymes and the naming of specific LOX isozymes is dependent on the carbon of the substrate that becomes oxidized¹⁵. The oxygenation site depends on which end of the substrate enters the active site first. For example, human reticulocyte 15-lipoxygenase-1 (h15-LOX-1 (ALOX15)) mostly produces the ω -6 product, 15S-hydroperoxy-5Z,8Z,11Z,13E-eicosatetraenoic acid (15S-HpETE), from arachidonic acid (AA) and 17S-hydroperoxy-4Z,7Z,10Z,13Z,15E,19Z-docosahexaenoic acid (17S-HpDHA) from DHA because the fatty acid substrate enters into the active site methyl-end first (**Figure 1**).

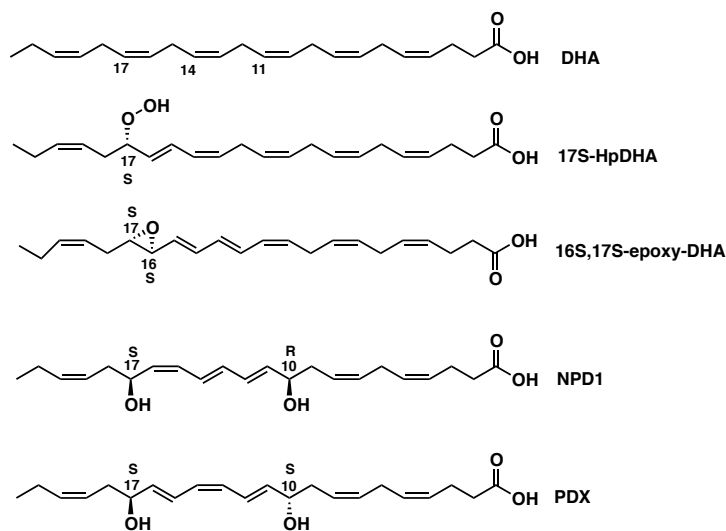


Figure 1. Structures of DHA, 17S-HpDHA, 16S,17S-epoxyDHA, NPD1 and PDX.

In addition to oxygenation reactions, LOX isozymes can also perform dehydration reactions when the hydroperoxide oxylipins is the substrate, to produce an epoxide intermediate. For dehydration, LOX isozymes abstract a hydrogen atom from the adjacent bis-allylic methylene carbon to the hydroperoxide, generating a septa-dienyl radical, similar to the oxygenation reaction. However, instead of oxygen attacking the septa-dienyl radical intermediate, the hydroperoxide moiety dehydrates to form an epoxide. One of the examples of this dehydration mechanism is the reaction of human reticulocyte 15-LOX-1 (h15-LOX-1 (ALOX15)) and human platelet 12-LOX (h12-LOX (ALOX12)) with 5S,15S-diHpETE to generate lipoxin

B4 (LXB₄), through the 14,15-epoxide intermediate¹⁶.

The proposed biosynthetic pathway for NPD1 biosynthesis utilizes both LOX oxygenation and dehydration reactions. First, h15-LOX-1 is proposed to generate 17S-HpDHA and then it abstracts a hydrogen atom from the ω -11 carbon of 17S-HpDHA, which dehydrates to form the critical NPD1 intermediate, 16S,17S-epoxy-4Z,7Z,10Z,12E,14E,19Z-docosahexaenoic acid (16S,17S-epoxyDHA). This epoxide is then enzymatically hydrolyzed to form the final product, NPD1 (**Figure 1**)¹⁷. In addition to h15-LOX-1, both h12-LOX and human epithelial 15-LOX-2 (h15-LOX-2 (ALOX15B)) could also be considered as biocatalysts for NPD1 production due to their known DHA reactivity. While h12-LOX mostly generates the ω -9 product, 14S-HpDHA, it also produces the ω -6 side product, 17S-HpDHA¹⁸. h15-LOX-2 exhibits similar reaction specificity as h15-LOX-1 with the ω -6 oxygenation product, 17S-HpDHA, as the dominant product. Nevertheless, the dehydration step to generate the 16S,17S-epoxyDHA has not been reported for either h12-LOX or h15-LOX-2¹⁹. Regarding PDX, soybean LOX has

been shown to produce it by double oxygenation of DHA, with subsequent reduction to the di-alcohol¹². The ability of h12-LOX, h15-LOX-1 and h15-LOX-2 to generate 17S-HpDHA indicates that they could participate in the biosynthesis of PDX, however the subsequent production of 10S,17S-diHpDHA is less obvious since human LOXs manifest unusual LOX reactivity with oxylipins^{20, 21}.

Given these possible biosynthetic pathways for producing NPD1 and PDX, the current work investigated the reactivities and kinetics of h12-LOX, h15-LOX-1 and h15-LOX-2 with the goal of determining their relative *in vitro* biosynthetic properties. By understanding which LOX enzyme is involved in the *in vitro* biosynthesis of NPD1 and PDX, these results may be extrapolated to their *in vivo* biosynthetic pathways which could help predict the cellular consequences of specific LOX inhibition in the treatment of human disease.

3.3 Materials and Methods

Chemicals

4Z,7Z,10Z,13Z,16Z,19Z-docosahexaenoic acid (DHA) and 13Z,16Z,19Z-docosatrienoic acid (DTA) were purchased from Nu Chek Prep, Inc at greater than 99% purity. Oxylin mass spectrometry standards were purchased from Cayman Chemical. All other solvents and chemicals were of reagent grade or better and purchased from Fisher Scientific, Pittsburgh, PA, USA and were used as purchased without further purification.

Synthesis and Purification of Oxylin

17S-hydroperoxy-4Z,7Z,10Z,13Z,15E,9Z-docosahexaenoic acid (17S-HpDHA) was made from the reaction of DHA (50 μ M) with soybean lipoxygenase-1 (sLOX-1) in 200 mL of 50 mM Borate buffer (pH 9.2). The absorbance was monitored at 234 nm until the reaction was completed and quenched with 1% (v/v) of glacial acetic acid. The reaction was extracted three times with 200 mL of dichloromethane (DCM)

and then concentrated under reduced pressure. The crude product was resuspended with 250 μ L of methanol and purified isocratically via high performance liquid chromatography (HPLC) on a Higgins Haisil Semi-preparative (5 μ m, 250mm x 10mm) C18 column with 60:40 of 99.9% acetonitrile, 0.1% acetic acid and 99.9% water, 0.1% acetic acid, with a flow rate of 2 mL/min.

17S-hydroxy-4Z,7Z,10Z,13Z,15E,9Z-docosahexaenoic acid (17S-HDHA) was synthesized as previously described for 17S-HpDHA, but with the reductant, trimethyl phosphite, added prior to HPLC.

12S-hydroxy-5E,8Z,10Z,14Z-eicosatetraenoic acid (12S-HETE) was synthesized from the reaction of AA (50 μ M) with h12-LOX in 200 mL of 25 mM HEPES buffer (pH 8.0). The purity of the isolated products was assessed via LC-MS/MS to be greater than 90%, with the following parameters: 17S-HpDHA ($UV_{max}=234$ nm, parent m/z 359.2, major MS/MS fragments m/z 341, 245), 17S-HDHA ($UV_{max}=234$ nm, parent m/z 343.2, major MS/MS fragments m/z 281, 245), 12S-HETE ($UV_{max}=234$ nm, parent m/z 319.2, major MS/MS fragments m/z 301, 179).

h12-LOX and h15-LOX-1 Expression and Purification

The overexpression and purification of h15-LOX-1,²² h12-LOX²² and h15-LOX-2²³ were performed as previously described. Briefly, h15-LOX-1, h12-LOX and h15-LOX-2 were expressed as fusion proteins with a 6-His TAG on the N-terminus and purified by FPLC (Biorad) with an affinity nickel-iminodiacetic acid agarose column (4° C). The purity of h15-LOX-1, h12-LOX and h15-LOX-2 were determined by SDS-PAGE analysis to be greater than 90%. The iron content of all the enzymes was assessed on the Thermo Element XR inductively coupled plasma mass spectrometry (ICP-MS) via comparison with iron standard solution. Cobalt-EDTA was used as an internal standard.

Steady State Kinetics of h12-LOX or h15-LOX-1 or h15-LOX-2 with DHA, 17S-HpDHA and 17S-HDHA

h15-LOX-1 reactions were performed in a 1 cm quartz cuvette containing 2 mL of 25 mM HEPES buffer (pH 7.5) with substrate (DHA, 17S-HpDHA or 17S-HDHA) and stirred constantly. h12-LOX and h15-LOX-2 reactions were performed in a

similar manner as the h15-LOX-1 reactions, but the reaction pH was 8.0. The reactions were initiated by adding approximately 40 nM of enzyme to a 2 mL reaction containing 1-20 μM DHA, or 1-50 μM 17S-HpDHA or 1-100 μM 17S-HDHA. For the DHA reactions, the formation of the conjugated diene products was monitored at 234 nm ($\epsilon = 25,000 \text{ M}^{-1}\text{cm}^{-1}$) with the PerkinElmer Lambda 40 UV/Vis spectrophotometer. The 17S-HpDHA and 17S-HDHA reactions were monitored simultaneously on the Hewlett Packard 8453 diode-array spectrophotometer at 270 nm for 10S,17S-diHpDHA, 10R/S,17S-dihydroxy-4Z,7Z, 11E,13E,15E,19Z-docosahexaenoic acid (10R/S,17S-EEE-diHDHA) and 16,17S-diHpDHA formation using the estimated extinction coefficient for a conjugated triene in buffer, $\epsilon_{270} = 40,000 \text{ M}^{-1}\text{cm}^{-1}$ ²⁴ and 254 nm for 11,17S-diHpDHA formation to account for the loss of the substrate, whose 242 nm absorption band overlaps with the product. It should be noted that 11,17S-diHpDHA has two unconjugated diene moieties, which we observe to have a lambda max of 242 nm (**Supporting information, Figure S1**) Since the chromophore for 11,17S-diHpDHA

is similar to that of the previously published methyl ester 9,15-diHpETE,²⁵ we used the published extinction coefficient ($\epsilon_{242} = 49,600 \text{ M}^{-1}\text{cm}^{-1}$)²⁵. It should be noted that the mono-hydroperoxides are produced from the alcohol substrate, but the di-hydroperoxides are produced from the hydroperoxide substrate, with the same epsilon values used for both. Kinetic parameters were calculated by using KaleidaGraph to fit initial rates, at less than 20% turnover.

Product Analysis of LOX isozyme reactions with DHA, 17S-HpDHA and 17S-HDHA

DHA (10 μM), 17S-HpDHA (1 μM) or 17S-HDHA (1 μM) were reacted with 300 nM of h12-LOX, h15-LOX-1 or h15-LOX-2 in 2 mL of 25 mM HEPES buffer (pH 7.5 for h15-LOX-1 and pH 8.0 for h12-LOX and h15-LOX-2) for 3 to 10 minutes as monitored by UV-Vis spectrophotometer. The reactions were quenched with 1% (v/v) glacial acetic acid and extracted three times with 2 mL of dichloromethane (DCM). The reactions were done in parallel with enzyme absent as control for background oxidation. In addition to the native reactions, a reaction was

reduced with trimethyl phosphite for comparison. The products were dried under a stream of the N₂ gas, and then reconstituted in 50 μL of acetonitrile and 50 μL of water with 0.1% formic acid. Chromatographic separation was performed on a Sciex ExcisionLC using a C₁₈ column (Phenomenex Kinetex, 4μm, 150 mm x 2.0 mm). Mobile phase A consisted of water with 0.1% (v/v) formic acid, and mobile phase B was acetonitrile with 0.1% (v/v) formic acid. The column was run isocratically with 60:40 of mobile phase A and mobile phase B, with a flow rate of 0.400 mL/min. Analytes were ionized through electrospray ionization with a -4.0 kV spray voltage and 50, 50, and 20 PSI for ion source gas 1, 2, and curtain gas respectively. The CAD (Collisionally Activated Dissociation) gas was set to 7 and the probe temperature was at 550° C. MS/MS acquisition was performed using SWATH and the parent mass used for the HDHA products was 343.2 and 359.2 for the diHDHA products. With known standards, the products were identified by matching their retention times, UV spectra and MS/MS patterns, while the molecules without standards were deduced

from comparison to theoretical fragments and their double bond geometry determined through their UV spectra.

Allosteric Regulation of Epoxidation of h15-LOX-1 and h12-LOX

The allosteric effects were investigated using varied concentrations of 17S-HpDHA (1-50 μM) and h15-LOX-1 (0.2 μM) with a 10-minute reaction. In addition, 12S-HETE or 17S-hydroxy-13Z,15E,19Z-docosatrienoic acid (17S-HDTA) were added at varying concentrations (1-25 μM), with 1 μM 17S-HpDHA and the products percentages calculated (N=3). Products were reduced and analyzed via LC/MS as described previously in the product analysis section.

Effect of 17S-HpDHA on Human Platelet Aggregation and Lipidomics

The University of Michigan Institutional Review Board approved all research involving human volunteers. A written informed consent was obtained from self-reported healthy donors prior to the blood draws. Whole blood was collected via venipuncture into vacutainers containing sodium citrate (3.2%; Greiner Bio-One, Monroe, NC). Platelets were isolated through serial centrifugation. Platelet-rich

plasma was treated with acid citrate dextrose (2.5% sodium citrate basic, 1.5% citric acid, and 2.0% D-glucose) and apyrase (0.02 U/ml) and then centrifuged for 10 minutes at 2000g to pellet the platelets²⁶. Tyrode's buffer (10 mM N-2-hydroxyethylpiperazine-N9-2-ethanesulfonic acid, 12 mM sodium bicarbonate, 127 mM sodium chloride, 5mM potassium chloride, 0.5 mM monosodium phosphate, 1 mM magnesium chloride, and 5mM glucose) at 3×10^8 platelets/ml as determined by a complete blood cell counter (Hemavet 950FS; Drew Scientific, Miami Lakes, FL). For aggregation assays, 250 μ L of washed human platelets (3×10^8 /mL) were incubated with 1-10 μ M 17S-HpDHA, 10R/S,17S-EEE-diHDHA, PDX, or the control oxylin, 12S-hydroxy-8Z,10E,14Z-eicosatrienoic acid (12S-HETrE), for 10 minutes at 37°C in a glass cuvette. The oxylin treated platelets were stimulated with 0.25 μ g/mL of collagen while stirring at 1100 rpm in a Chrono-log model 700 aggregometer and aggregation was analyzed via a decrease in light transmittance. For lipidomics, 1×10^9 platelets were resuspended in one mL of Tyrode's buffer, incubated with 3 μ M 17S-HpDHA for 10 minutes and stimulated with collagen. Supernatants

and pellets from washed platelets were acidified with HCl, extracted 3 times with 2 mL of DCM and 50 ng of d5-MaR1 as an internal standard. The reactions were treated with trimethyl phosphite as the reductant, blown down under a stream of N₂, and resuspended in 500 µL of H₂O with 0.1% Formic Acid and Acetonitrile at a 1:4 ratio. The proteins were precipitated out by freezing the samples in a -80 freezer for 20 minutes, then spinning down at 13K for 15 minutes. The supernatants were removed and dried under N₂. The samples were reconstituted in acetonitrile and H₂O with 0.1% Formic Acid (50:50 ratio) and analyzed by LC/MS. The m/z transitions used for 10,17-diHDHA isomers 359.2→153.1

Molecular Docking

A homology model of h15-LOX-1 was built using the substrate-mimetic inhibitor-bound porcine 12-LOX structure (pdb-id 3rde). PRIME homology modeling software (Schrodinger Inc) was used to build the model.¹⁸ During homology modeling the metal ion (Fe³⁺), a hydroxide ion that coordinated the metal ion and the co-crystallized inhibitor were retained. Prior to docking, the model was subjected to a

protein-preparation step using Protein Preparation Wizard (Schrodinger Inc). During this step, hydrogen atoms were optimized to make better hydrogen bonding interactions, protonation states of titratable residues were assigned, rotameric states of Asn, Gln, Ser, Thr and Tyr residues were optimized and the model was energy-minimized with restraints, such that heavy atoms did not move beyond 0.3Å. The three-dimensional (3D) structure of 17S-HpDHA was prepared from the SMILES string using LigPrep software (Schrodinger Inc). Both the neutral and charged carboxylic acid forms of the substrate were generated, but neither protonation state of the substrate successfully docked to the active site using the standard rigid receptor docking using Glide (Schrodinger Inc). Therefore, we used InducedFit docking to predict conformational changes necessary to accommodate these ligands. The metal ion, hydroxide ion and metal ion coordinating residues (His360, His365, His540, His544 and Ile662) were kept fixed during the InducedFit docking; all other active site residue side chains, as well as the substrate, were sampled extensively. During InducedFit docking, extra-precision (XP) scoring function was used for Glide

redocking. InducedFit score was used for ranking docking poses.

3.4 Results

Production of 17S-HpDHA, the Neuroprotectin D1 (NPD1) and PDX

Intermediate, through h15-LOX-1, h15-LOX-2 and h12-LOX

The biosynthesis of the potent anti-inflammatory molecules, NPD1 and PDX, is dependent on the production of the intermediate, 17S-hydroperoxy-4Z,7Z,10Z,13Z,15E,19Z-docosahexaenoic acid (17S-HpDHA). To generate 17S-HpDHA from DHA by LOX isozymes, the hydrogen atom on C15 (ω -8) must be abstracted, with a subsequent oxygen insertion at C17 (ω -6). h12-LOX, h15-LOX-1 and h15-LOX-2 were all able to produce 17S-HpDHA from DHA, as determined by LC/MS/MS and therefore their product profiles and steady state kinetics were determined to establish the specificity and catalytic efficiency of these reactions.

Product Profile and Steady-States Kinetics of h15-LOX-1 with DHA

The product profile for the reaction of DHA with h15-LOX-1 showed

17S-HpDHA (49+/-2%), 14S-HpDHA (37+/-2%) and 11S-HpDHA (14+/-2%) (Table 1), consistent with previous work with purified enzyme^{18, 19}. These results are also in agreement with the literature where h15-LOX-1 is capable of making both the ω -6 and ω -9 oxylipins when using AA as the substrate, 15S-HpETE and 12S-HpHETE respectively. However, the increased production of the ω -9 oxylipin with DHA as the substrate (37% 14S-HpDHA vs 10% 12S-HpETE) supports the hypothesis that the increased unsaturation and aliphatic chain length of DHA allows for a deeper active site insertion than that of AA, as has been seen previously^{18, 21}. Regarding the kinetics of h15-LOX-1 and DHA, the k_{cat}/K_M was determined to be $0.35 \pm 0.08 \mu\text{M}^{-1}\text{s}^{-1}$, which was 3-fold slower than that of AA. The k_{cat} was observed to be $2.3 \pm 0.6 \text{ s}^{-1}$, only 2-fold less than the rate seen with AA, indicating DHA is a comparable substrate to AA with h15-LOX-1 (Table 2).

Enzyme + DHA	17S-HpDHA	14S-HpDHA	11S-HpDHA
h15-LOX-1*	49 ± 2%	37 ± 2%	14 ± 2%
h15-LOX-2	84 ± 1%	16 ± 1%	0%
h12-LOX	4 ± 1%	78 ± 1%	18 ± 1%

Table 1. Product profiles of h15-LOX-1, h15-LOX-2 and h12-LOX when reacted with 10 μ M of DHA. *Note that trace amounts of 20S-HpDHA were found to be less than 3% in the reaction of DHA and h15-LOX-1.

Enzyme	Substrate	k_{cat} (s^{-1})	K_M (μ M)	k_{cat}/K_M ($s^{-1}\mu M^{-1}$)	Relative k_{cat}/K_M^*
h15-LOX-1	AA	4.1 ± 0.2	4.2 ± 0.5	0.98 ± 0.1	1.0
h15-LOX-1	DHA	2.3 ± 0.6	6.7 ± 3	0.35 ± 0.08	0.36
h15-LOX-2	AA	2.5 ± 0.3	11 ± 2	0.24 ± 0.02	0.24
h15-LOX-2	DHA	4.2 ± 0.3	9.8 ± 1	0.43 ± 0.03	0.44
h12-LOX	AA	17 ± 0.5	1.2 ± 0.2	14 ± 0.5	14
h12-LOX	DHA	14 ± 0.5	1.2 ± 0.2	12 ± 2	12

Table 2. Steady-state kinetics parameters for h15-LOX-1, h15-LOX-2 and h12-LOX with AA and DHA. The h15-LOX-1, h15-LOX-2 and h12-LOX rates with AA were consistent with previous literature values²⁶⁻²⁸. *The relative k_{cat}/K_M values were set to the reaction of h15-LOX-1 and AA being set to 1.

Product Profile and Steady-States Kinetics of h15-LOX-2 with DHA

The product preference for the reaction of DHA with h15-LOX-2 revealed the production of 17S-HpDHA (84+/-1%) as the major product and 14S-HpDHA (16+/-1%) as the minor product (**Table 1**). This result is consistent with the preference of h15-LOX-2 to abstract a hydrogen atom from the ω -8 carbon with

oxygenation on the ω -6 carbon, however, the large percentage of 14S-HpDHA is unusual. In the case of AA, h15-LOX-2 produces only the ω -6 product, 15S-HpETE, consistent with the hypothesis that the increased length and unsaturation allows DHA to insert deeper into the h15-LOX-2 active site, as seen with h15-LOX-1 (*vide supra*)¹⁹. For kinetics, the $k_{\text{cat}}/K_{\text{M}}$ of this reaction was measured to be $0.43 \pm 0.03 \mu\text{M}^{-1}\text{s}^{-1}$, which is similar to that with AA ($k_{\text{cat}}/K_{\text{M}} = 0.24 \pm 0.02 \mu\text{M}^{-1}\text{s}^{-1}$). However, the k_{cat} for DHA was found to be $4.2 \pm 0.3 \text{ s}^{-1}$, which was comparable to that of AA ($k_{\text{cat}} = 2.5 \pm 0.3 \text{ s}^{-1}$) (**Table 2**).

Product Profile and Steady-States Kinetics of h12-LOX with DHA

The product distribution of h12-LOX with DHA was also examined by LC/MS/MS and revealed 17S-HpDHA (4+/-1%), 14S-HpDHA (78+/-1%) and 11S-HpDHA (18+/-1%) (**Table 1**), consistent with previous work¹⁸, where the majority product is from abstraction from the ω -11 carbon, with oxygenation on the ω -9 carbon. As seen with both h15-LOX-1 and h15-LOX-2, DHA inserts deeper into the active site, producing an increased percentage of the ω -12 product, 11S-HpDHA.

With respect to kinetics, the $k_{\text{cat}}/K_{\text{M}}$ was determined to be $12 \pm 2 \mu\text{M}^{-1}\text{s}^{-1}$ and the k_{cat} was found to be $14 \pm 0.5 \text{ s}^{-1}$, which are both comparable to rates of h12-LOX with AA ($k_{\text{cat}}/K_{\text{M}} = 14 \pm 0.5 \mu\text{M}^{-1}\text{s}^{-1}$, $k_{\text{cat}} = 17 \pm 0.5 \text{ s}^{-1}$)²⁶. From these results, we conclude that DHA is a comparable kinetic substrate for h12-LOX as AA (**Table 2**).

In summary, AA and DHA are comparable kinetic substrates for the three LOX isozymes, h15-LOX-1, h15-LOX-2 and h12-LOX, as seen by their kinetic values being within 5-fold of each other. However, the product profiles differ dramatically between AA and DHA, indicating that the structural differences between the substrates affect their active site binding configuration.

Effective $k_{\text{cat}}/K_{\text{M}}$ of 17S-HpDHA production from DHA and h15-LOX-1, h15-LOX-2 or h12-LOX

When comparing the effective $k_{\text{cat}}/K_{\text{M}}$ (i.e. the $k_{\text{cat}}/K_{\text{M}}$ *% product) of 17S-HpDHA, the NPD1 and PDX precursor, the results revealed that h15-LOX-1, h15-LOX-2 and h12-LOX had comparable catalytic efficiencies. h12-LOX manifested a 2.8-fold greater efficiency than h15-LOX-1 (**Table 3**) and 1.3-fold

better than h15-LOX-2. This result is surprising since 17S-HpDHA is the minor h12-LOX product with DHA and the similar abstraction from the ω -8 carbon, with oxygen insertion at the ω -6 position is not observed with AA as the substrate (i.e. 12S-HpETE).

Synthesis of the NPD1 intermediate, 16S,17S-epoxyDHA and 10S,17S-dihydroxy-4Z,7Z,11E,13Z,15E,19Z-docosahexaenoic acid (PDX) from 17S-HpDHA.

The NPD1 biosynthetic pathway is proposed to be initiated by hydrogen abstraction on C12 of 17S-HpDHA by a lipoxygenase isozyme, whose radical intermediate dehydrates to form 16S,17S-epoxyDHA, which in turn is enzymatically hydrolyzed to NPD1⁸. In contrast, the biosynthetic pathway for the production of PDX is proposed to proceed through the oxygenation of 17S-HpDHA (or 17-HDHA) on C10 by a LOX isozyme, which is subsequently reduced by GPx-4 to produce PDX²⁹. Given the potent biological actions of NPD1 and PDX, the current work investigated the possible *in vitro* biosynthetic pathways for both molecules in order to

propose possible *in vivo* biosynthetic routes for NPD1 and PDX biosynthesis.

Enzyme + DHA	17S-HpDHA Effective k_{cat}/K_M	Relative 17S-HpDHA Effective k_{cat}/K_M *
h15-LOX-1	0.17	1
h15-LOX-2	0.36	2.1
h12-LOX	0.48	2.8

Table 3. The effective k_{cat}/K_M (k_{cat}/K_M * % product) for the production of 17S-HpDHA from DHA for h15-LOX-1, h15-LOX-2 and h12-LOX. *The relative 17S-HpDHA effective k_{cat}/K_M values were set to the reaction of h15-LOX-1 and DHA being set to 1.

Product Profile and Steady-States Kinetics of h15-LOX-1 and h15-LOX-2 with 17S-HpDHA and 17S-HDHA

The reaction of h15-LOX-1 with 17S-HpDHA produced a majority of the non-enzymatic hydrolysis products of 16S,17S-epoxyDHA, 10R/S,17S-EEE-diHDHA (54+/-3%) (Table 4).¹⁷ This non-enzymatic hydrolysis product with EEE conjugation was determined by its reduced nature (di-OH) in non-reducing environment (Supporting Information, Figure S2) and its UV_{max} at ~270 nm, whose shoulder at ~280 nm is slightly higher than the shoulder at ~260 nm, consistent with literature values³⁰ (Supporting Information, Figure S1). Under

reducing conditions, three oxygenation products were also observed, PDX (28+/-3%), 11,17S-dihydroxy-4Z,7Z, 9E,13Z,15E,19Z-docosahexaenoic acid (11,17S-diHDHA, 2+/-3%) and 16,17S-dihydroxy-4Z,7Z,10Z,12Z,14E,19Z-docosahexaenoic acid (16,17S-diHDHA, 16+/-3%) (**Supporting Information, Figure S2**). For PDX, it was characterized by comparing its retention time and MS fragmentation to a PDX standard and found to be identical (**Supporting Information, Figure S3**). In addition, the UV spectrum of PDX showed a broad dissymmetric triplet, with a maximum absorption at 269 nm and shoulders at 259 and 280 nm, with the shoulder at 280 nm being slightly less intense than the shoulder at 259 nm, indicating an EZE conjugation and matching the UV pattern of PDX reported previously³⁰ (**Supporting Information, Figure S1**). The characterization of 11,17S-diHDHA and 16,17S-diHDHA were determined by their MS fragmentations and UV absorption spectra (**Supporting Information, Figure S1 & S2**). 11,17S-diHDHA was characterized by its MS fragmentation patterns as m/z 341, 297, 261, 194, 165 and a UV_{max} of 242 nm, indicating two conjugated diene moieties separated by a methylene,

and 16,17S-diHDHA was characterized by its MS fragmentation patterns as m/z 279, 261, 243, 217, 199 and a UV_{max} of 270 nm, indicating one conjugated triene. It should be noted that since there are no commercially available standards for 11,17S-diHDHA and 16,17S-diHDHA, we cannot confirm the stereochemistry of these products. but since they are oxygenation products, it is appropriate to assume their configurations are 11S,17S-diHDHA and 16R,17S-diHDHA, as has been seen previously for similar di-oxygenated LOX products^{18, 21}.

Enzyme + 17S-HpDHA	11,17S- diHDHA	16S,17S- epoxyDHA*	PDX	16,17S- diHDHA
h12-LOX	52 ± 1%	21 ± 1%	22 ± 1%	5 ± 1%
h15-LOX-1	2 ± 3%	54 ± 3%	28 ± 3%	16 ± 3%
h15-LOX-2	n/r	n/r	n/r	n/r

Table 4. Product profile of h12-LOX, h15-LOX-1 and h15-LOX-2 with 2 μ M 17S-HpDHA. *10R/S, 17S-EEE-diHDHA is the detected product from the non-enzymatic hydrolysis of 16S,17S-epoxyDHA *No reaction (n/r) was detectable after the incubation of h15-LOX-2 with 17S-HpDHA.

For h15-LOX-2, there was no observable reaction with either 17S-HpDHA (**Table 4**) or 17S-HDHA (**Table 5**). These results reinforce the selective reactivity of h15-LOX-2 to abstract predominately from the ω -8 carbon to produce the ω -6

oxygenation product, which is unavailable with these 17-oxylin substrates.

The mechanism of these products can be explained as follows. For the generation of the major product, 16S,17S-epoxyDHA, 17S-HpDHA enters the active site methyl-end first and h15-LOX-1 abstracts a hydrogen atom from C12 (ω -11), leading to dehydration and epoxide formation. For 16,17S-diHpDHA, the mechanism is the same as for 16S,17S-epoxyDHA, however, in this case oxygen attacks the radical on C16. Normally, h15-LOX-1 would oxygenate on C17, as it does with DHA, but since C17 is already oxygenated, C16 is the closest carbon for attack. For the other oxygenation product, 11,17S-diHpDHA, it is most likely formed with a methyl-end first entry by 17S-HpDHA, followed by a hydrogen abstraction from C9 (ω -14) and subsequent oxygenation on C11, as seen with DHA in **Table 1**. PDX, however, cannot be explained by this mechanism since the radical generated by a C9 activation cannot resonate onto C10 with a methyl-end first substrate binding. To produce PDX, our hypothesis is that 17S-HpDHA enters into the active site with the carboxylate-end first, positioning C12 for hydrogen atom abstraction and oxygenation

on C10. This is a reasonable assumption since C12 is the “ ω -13” position from the carboxylate-end, if the oxygen atom is included. This is consistent with previous work which demonstrated that the methyl-end first binding favors a +2 radical rearrangement, while the carboxyl-end first favors a -2 radical rearrangement^{31, 32}.

With the proposed carboxylate-end first entry binding mode for the production of PDX, it's reasonable to suppose that a negatively charged carboxylate on the substrate would retard entry into the hydrophobic cavity, as observed previously with 14S-HpDHA¹⁸. To test this hypothesis, we examined PDX production with h15-LOX-1 and 17S-HpDHA at various pH conditions and observed a decrease in PDX production under basic conditions (**Figure S4**), which supports the hypothesis that deprotonation of the carboxylic acid at high pH inhibits carboxyl-end first binding in the active site. It should be noted that fatty acids are known to have high pKa values, with both LA and DHA having approximate pKa values from 7 to 8³³⁻³⁵, however, the oxylipins will presumably have lower pKa values due to the disruption of the detergent effect.

The reduced oxylipin, 17S-HDHA, was next reacted with h15-LOX-1, but only the oxygenation product, 16,17S-diHDHA, was observed (**Table 5**), which is predicted to be in the 16R,17S configuration, based on previous work with 15S-HETE products.^{36, 37} This is consistent with the fact that the hydroperoxide of 17S-HpDHA is essential to produce the epoxide intermediate for NPD1 biosynthesis, 16S,17S-epoxyDHA. Amazingly, PDX was not detected in the reaction of h15-LOX-1 with 17S-HDHA, suggesting that the decreased size and hydrophobicity of the C17 alcohol inhibits either the carboxylate-end first binding mode or the oxygenation of C10.

Enzyme + 17S-HDHA	11,17S-diHDHA	PDX	16,17S-diHDHA
h12-LOX	73 ± 2%	4 ± 2%	23 ± 2%
h15-LOX-1	0%	0%	100%
h15-LOX-2	n/r	n/r	n/r

Table 5. h12-LOX, h15-LOX-1 and h15-LOX-2 product profile with 2 μM 17S-HDHA. *No reaction (n/r) was detectable after the incubation of h15-LOX-2 with 17S-HDHA

A. Enzyme	Substrate	k_{cat} (s^{-1})	K_M (μM)	k_{cat}/K_M ($s^{-1}\mu M^{-1}$)	Relative k_{cat}/K_M^*
h15-LOX-1	DHA	2.3 ± 0.6	6.7 ± 3	0.35 ± 0.08	1
h15-LOX-1	17S-HpDHA	1.8 ± 0.1	2.4 ± 0.6	0.75 ± 0.2	2.1
h15-LOX-1	17S-HDHA	0.27 ± 0.02	37 ± 9	0.0070 ± 0.001	0.02

B. Enzyme	Substrate	k_{cat} (s^{-1})	K_M (μM)	k_{cat}/K_M ($s^{-1}\mu M^{-1}$)	Relative k_{cat}/K_M^*
h12-LOX	DHA	14 ± 0.5	1.2 ± 0.2	12 ± 2	1
h12-LOX	17S-HpDHA	0.19 ± 0.01	12 ± 1.9	0.017 ± 0.002	0.0015
h12-LOX	17S-HDHA	0.25 ± 0.02	29 ± 6.3	0.0080 ± 0.001	0.0007

Table 6. Steady-state kinetics of (A) h15-LOX-1 and (B) h12-LOX with DHA, 17S-HpDHA and 17S-HDHA. The DHA reactions were monitored at 234 nm for the production of conjugated diene monohydroxylated products. The 17S-HpDHA and 17S-HDHA reactions were monitored at 270 nm for the production of conjugated triene dihydroxylated products. *Relative k_{cat}/K_M values with DHA was set to 1.

Regarding the kinetics of h15-LOX-1 with 17S-HpDHA, the k_{cat}/K_M for the reaction was found to be $0.75 \pm 0.2 s^{-1}\mu M^{-1}$ and the k_{cat} to be $1.8 \pm 0.1 s^{-1}$, which were found to be comparable to that of DHA (**Table 6A**). These results are noteworthy because the hydrogen on 17S-HpDHA that is abstracted is from C12 (ω -11). This is the minority site for hydrogen abstraction for DHA, producing 14S-HpDHA, suggesting a distinct active site binding pose for 17S-HpDHA relative to DHA in the h15-LOX-1

active site. Furthermore, the kinetic parameters of 17S-HDHA were dramatically reduced compared to 17S-HpDHA, which could be due to either the need for activation with an oxylipin, as seen with 15-HETE³⁸, or that the epoxidation reaction is the primary reaction mechanism.

In summary, while the kinetic values between DHA and 17S-HpDHA are comparable for h15-LOX-1, they are not similar for h15-LOX-2 and h12-LOX. h15-LOX-2 does not react with 17S-HpDHA and the kinetic values of h12-LOX are dramatically reduced for 17S-HpDHA, 74-fold lower for k_{cat} and 705-fold lower for $k_{\text{cat}}/K_{\text{M}}$ compared to using DHA as the substrate. These data indicate that h15-LOX-1 can accommodate the oxylipin for catalysis better than both h15-LOX-2 and h12-LOX. Interestingly, soybean 15-LOX does not accommodate oxylipins well, with a 470-fold lower for $k_{\text{cat}}/K_{\text{M}}$ 15-HpETE relative to AA³¹.

Product Profile and Steady-States Kinetics of h12-LOX with 17S-HpDHA and 17S-HDHA

h12-LOX was reacted with 17S-HpDHA to determine its ability to produce the

NPD1 intermediate, 16S,17S-epoxyDHA, and PDX. The major product under reducing conditions was the oxygenation product 11,17S-diHDHA (52+/-1%) and two other minor oxygenation products, PDX (22+/-1%) and 16,17S-diHDHA (5+/-1%). 10R/S,17S-EEE-diHDHA (21+/-1%) was also detected as the non-enzymatic hydrolysis products of 16S,17S-epoxyDHA (**Table 4, Supporting Information, Figure S2**), as seen previously.¹⁷ To confirm these reaction products, h12-LOX was reacted with 17S-HDHA and as seen for h15-LOX-1, only oxygenation products were observed, 11,17S-diHDHA (73+/-2%), 16,17S-diHDHA (23+/-2%) and PDX (4+/-2%) (**Table 5**). These observations are consistent with the reaction of h15-LOX-1 with 17S-HDHA, confirming that the lack of the hydroperoxide moiety prohibits epoxidation and thus only oxygenation products are detected.

The kinetics of h12-LOX with 17S-HpDHA was dramatically slower than that of h15-LOX-1 with 17S-HpDHA, with the k_{cat}/K_M being $0.017 \pm 0.002 \text{ s}^{-1}\mu\text{M}^{-1}$ and the k_{cat} being $0.19 \pm 0.01 \text{ s}^{-1}$ (**Table 6B**), which are 45-fold and 10-fold slower than that

of h15-LOX-1 reaction, respectively. These data indicate that 17S-HpDHA is a poor substrate for h12-LOX, relative to h15-LOX-1. This difference is significant since the hydrogen atom abstraction step for both LOX isozymes is from C12 (ω -11) on 17S-HpDHA, which is the preferable hydrogen abstraction position seen for h12-LOX when DHA is the substrate (**Table 1**). The kinetics parameters of h12-LOX with the reduced substrate, 17S-HDHA, were found to be half as efficient as with 17-HpDHA, consistent with a loss of the epoxide generating pathway (**Table 6B**).

Effective k_{cat}/K_M of 16S,17S-epoxyDHA and PDX from the catalysis of h15-LOX-1 and h12-LOX with 17S-HpDHA and 17S-HDHA

When comparing the effective k_{cat}/K_M (i.e. $k_{\text{cat}}/K_M * \% \text{ Product}$) of 16S,17S-epoxyDHA by both h15-LOX-1 and h12-LOX with 17S-HpDHA as the substrate, it was observed that h15-LOX-1 is 55 times more efficient than h12-LOX in producing 16S,17S-epoxyDHA, the precursor of NPD1(**Table 7**). We also compared the biosynthetic flux for PDX by h15-LOX-1 and h12-LOX with 17S-HpDHA as the substrate and determined that h15-LOX-1 is over 27 times more

efficient than h12-LOX and 159 times more efficient than h12-LOX with 17S-HDHA (Table 8). From these results, it is apparent that h15-LOX-1 is more efficient in making the NPD1 intermediate, 16S,17S-epoxyDHA, and PDX than h12-LOX *in vitro*, suggesting that h15-LOX-1 could contribute significantly to NPD1 and PDX formation *in vivo*.

Allosteric Regulation of 17S-HpDHA and h15-LOX-1 epoxidation

The reaction of h15-LOX-1 with 17S-HpDHA (10 μ M) favors the epoxidation pathway, however, it was observed that this percentage increased with decreasing 17S-HpDHA concentration (1 μ M), resulting in the formation of non-enzymatic epoxide hydrolysis product, 10R/S,17S-EEE-diHDHA, as the major product (93 \pm 1%). However, at high 17S-HpDHA concentration (50 μ M), the oxygenation pathway was dominant producing 67 \pm 1% of oxygenation products (Figure 2). This substantial switch from epoxidation to oxygenation, with an approximately 70% increase in oxygenation products, suggests a possible allosteric regulation, as previously observed with 14S-HpDHA¹⁸. Furthermore, when the data was fit to a

hyperbolic curve, it resulted in a K_D value of $5.9 \pm 1.6 \mu\text{M}$, comparable in magnitude to previous allosteric regulators which also decreased epoxide production¹⁸.

Enzyme + 17S-HpDHA	16S,17S-epoxyDHA Effective k_{cat}/K_M	Relative 16S,17S-epoxyDHA Effective k_{cat}/K_M^*
h12-LOX	0.0075	1
h15-LOX-1	0.41	55

Table 7. Effective k_{cat}/K_M (k_{cat}/K_M * % Product at 270 nm) of 16S,17S-epoxyDHA of h-12-LOX and h-15-LOX-1 react with 2 μM 17S-HpDHA. *Relative 16S,17S-epoxyDHA effective k_{cat}/K_M for h-12-LOX+17S-HpDHA reaction was set to 1.

Enzyme	Substrate	PDX Effective k_{cat}/K_M	Relative PDX Effective k_{cat}/K_M^*
h12-LOX	17S-HpDHA	0.0078	1
h12-LOX	17S-HDHA	0.0013	0.17
h15-LOX-1	17S-HpDHA	0.21	27
h15-LOX-1	17S-HDHA	0	0

Table 8. Effective k_{cat}/K_M (k_{cat}/K_M * % Product at 270 nm) of PDX of h12-LOX and h15-LOX-1 react with 17S-HpDHA and 17S-HDHA. *Relative PDX effective k_{cat}/K_M for h-12-LOX+17S-HpDHA reaction was set to 1.

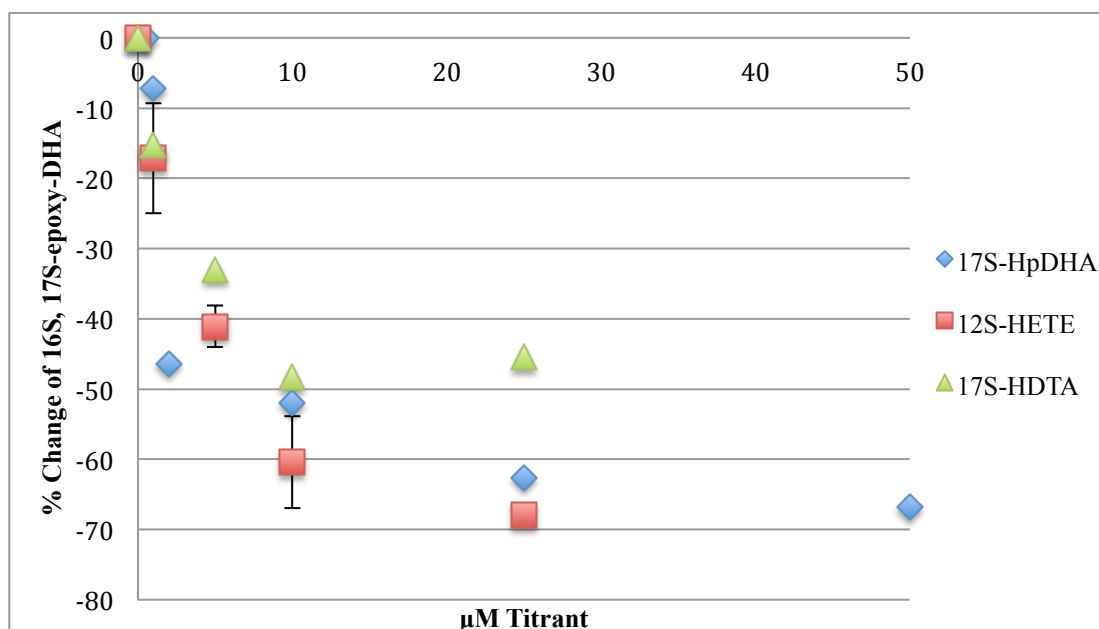


Figure 2. Percent Change in 16S,17S-epoxyDHA through h15-LOX-1 allosteric regulation of 17S-HpDHA epoxidation. h15-LOX-1 reacted with increasing [17S-HpDHA] (blue diamonds), 17S-HpDHA (1 μ M) with increasing [12S-HETE] (red squares) and 17S-HpDHA (1 μ M) with increasing [17S-HDTA] (green triangles) concentration. Note, 1 μ M of 17S-HpDHA is required for the second two reactions since 12S-HETE and 17S-HDTA are not substrates.

To further investigate this hypothesis, a previously reported allosteric modulator, 12S-HETE and a similar oxylipin to 17S-HDHA, 17S-HDTA, were titrated into the reaction mixture of h15-LOX-1 and 17S-HpDHA (1 μ M) and the epoxidation/oxygenation ratio of 17S-HpDHA recorded. It should be noted that 12S-HETE and 17S-HDTA were selected as allosteric regulators of h15-LOX-1 since they have minimal reactivity with h15-LOX-1. Titration of 12S-HETE, from 0 to 25

μM , lowered epoxide production from 93 \pm 1% to 30 \pm 1%, which resulted in a K_D value of $2.5 \pm 0.8 \mu\text{M}$. A titration of 17S-HDTA also decreased the epoxidation product, from 93 \pm 1% to 51 \pm 1%, with a K_D value of $1.4 \pm 0.5 \mu\text{M}$ (**Figure 2**). Taken together, we conclude that these oxylipins bind to the previously identified allosteric site of h15-LOX-1^{18, 27}, regulating the epoxidation/oxygenation ratio of 17S-HpDHA. It should be noted that these experiments could not be performed with h12-LOX due to its limited reactivity.

17S-HpDHA Docking to h12-LOX and h15-LOX-1

As we mentioned earlier, h15-LOX-1 is markedly more efficient than h12-LOX in reacting with 17S-HpDHA in the *in vitro* experiments. To get a better understanding of this result, computational docking was performed to predict the binding mode of 17S-HpDHA against the active site of h15-LOX-1 and h12-LOX. First, 17S-HpDHA was docked into h15-LOX-1 with lowest energy docking pose being the methyl-end first entry pose (**Figure 3A**). The carboxylate group of 17S-HpDHA makes a bidentate hydrogen bond with the residue Arg402 and the

aliphatic tail of 17S-HpDHA was positioned deep in the hydrophobic pocket created by residues Phe352, Phe414, Ile417, Met418 and Cys559. The hydroperoxide group on C17 makes hydrogen bonds with residues Glu356 and Gln547. These interactions help position the reactive C12 close (4.5 Å) to the oxygen atom of the hydroxide ion.

Next we docked the unprotonated 17S-HpDHA into the active site of h12-LOX with the lowest energy docking pose being the methyl-end first entry pose (**Figure 3C**). The carboxylate group of 17S-HpDHA makes hydrogen bonds with residues Arg402 and Gln406, and the hydroperoxide hydrogen atom forms a hydrogen bond with Glu356. From this lowest energy docking pose we observed that the reactive C12 was located farther from the oxygen atom of hydroxide ion than that seen for h15-LOX-1 (5.5 Å). The larger distance between the reacting centers for h12-LOX than for h15-LOX-1 is consistent with the lowered reactivity of h12-LOX compared to h15-LOX-1.

Molecular docking of 17S-HpDHA to h15-LOX-1 and h12-LOX also support the hypothesis that the production of PDX is through protonated carboxylate-end first

entry, as observed with the decreased production of PDX at high pH. 17S-HpDHA was docked into h15-LOX-1 with the protonated carboxylic acid-first entry (**Figure 3B**). The proton of the carboxylic acid of 17S-HpDHA does not make hydrogen bond with any residue. However, the hydrogen atom of the hydroperoxide moiety makes a hydrogen bond with the c-terminus of residue Ile662. In this binding pose, the reactive C12 is 4.1 Å from the oxygen of the hydroxide ion, which is comparable to the distance seen for the methyl-end first entry docking pose and suggests that this “flipped” docking pose is catalytically viable.

Protonated 17S-HpDHA was also docked into h12-LOX with carboxylic acid-first entry (**Figure 3D**). The hydrogen atom of the carboxylic acid does not make a hydrogen bond with any active site residue, but the hydrogen of the hydroperoxide group forms a hydrogen bond with the oxygen atom of the iron-bound hydroxide ion. The reactive C12 is far away from the oxygen atom of hydroxide ion (7.5 Å), which supports the observation that h15-LOX-1 is over 27 times more efficient than h12-LOX in producing PDX from 17S-HpDHA.

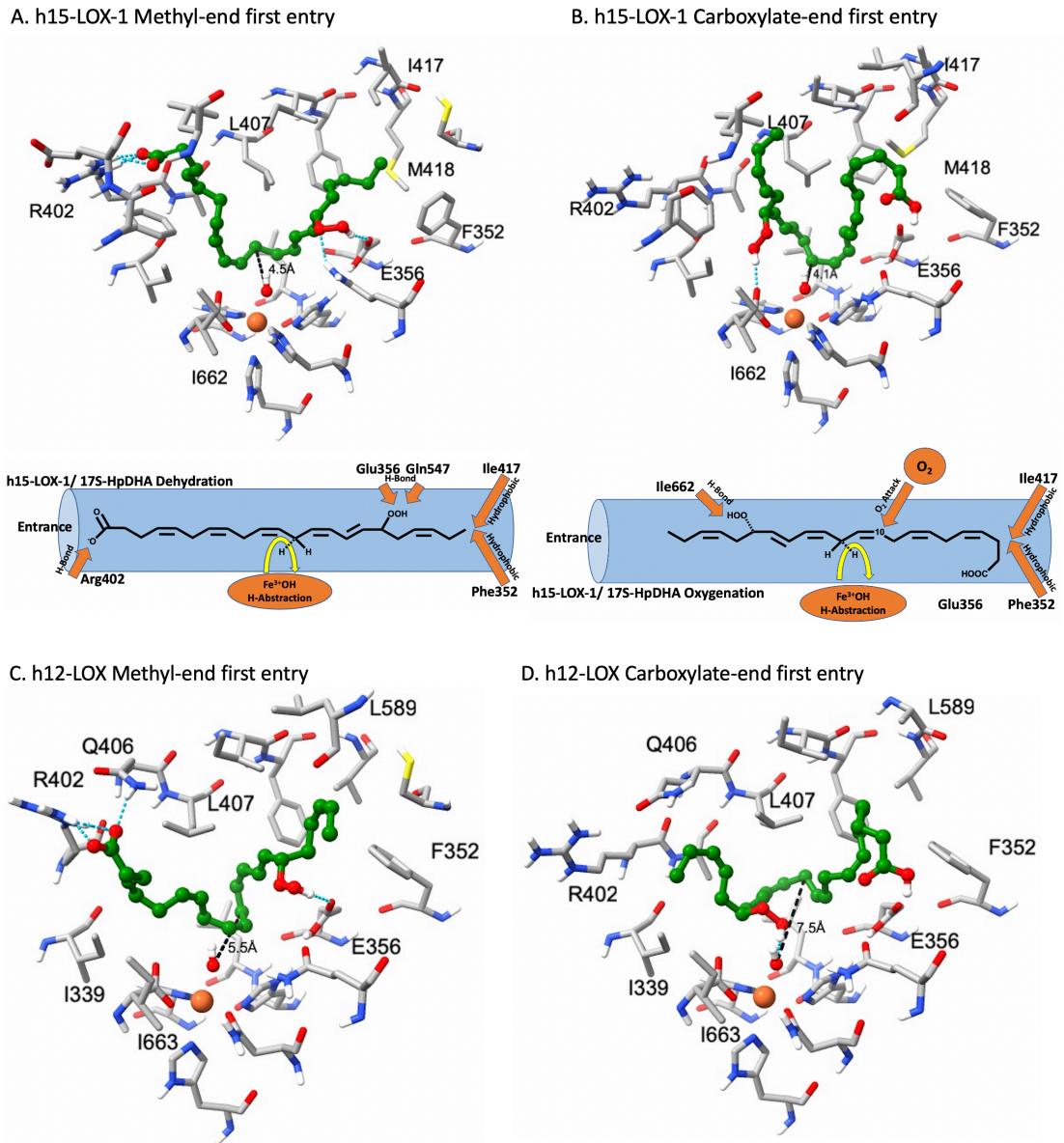


Figure 3. Docking poses of charged and neutral 17S-HpDHA against h12-LOX and h15-LOX-1. A) Charged 17S-HpDHA docked to h15-LOX-1. B) Neutral 17S-HpDHA docked to h15-LOX-1. C) Charged 17S-HpDHA docked to h12-LOX. D) Neutral 17S-HpDHA docked to h12-LOX. Carbon atoms of the protein and substrate are shown in gray and green colors respectively. Nitrogen, oxygen, hydrogen, sulfur and Fe^{3+} are shown respectively in blue, red, white, yellow and tan color. Residues providing polar and hydrophobic interactions to the substrate are

labeled. Distance between oxygen atom of the hydroxide ion and C12 of the substrate are shown. Hydrogen bonds between the substrate and the protein are shown in cyan color.

Metabolites of 17S-HpDHA Obtained After *Ex vivo* Incubations with Human Platelets

Human platelets have been shown to contain a large amount of h12-LOX, which can produce a great variety of oxylipins when fatty acids in the platelet membrane are cleaved from the phospholipid by phospholipase A2²⁶. Considering that h12-LOX is capable of producing the NPD1 intermediate *in vitro* (Table 4), 17S-HpDHA was administered to human platelets to determine if the *ex vivo* metabolites were of comparable ratios. Human platelets treated with 17S-HpDHA (3 μ M or 1080 ng/ 1×10^9 platelets) only produced 0.5% di-oxylipins, with the primary metabolite being the hydrolysis product of 16S,17S-epoxyDHA (3.7 ng/ 1×10^9 platelets, $75 \pm 4\%$ of the total di-oxylipins produced), and the minor metabolite being PDX (1.2 ng/ 1×10^9 platelets, $25 \pm 4\%$ of the total di-oxylipins produced). The observed percentage of PDX production in platelets is similar to that observed *in vitro* ($22 \pm 1\%$), but surprisingly, there was no production of 11,17S-diHDHA in platelets, which

was shown to be the major metabolite *in vitro* ($52 \pm 1\%$). The lack of production of the 11-oxygenation product from 17S-HpDHA (i.e. 11,17S-diHDHA) in platelets could be explained from previous work where incubation of human platelets with DHA made vanishingly small amounts of the 11-product (14S-HDHA:11S-HDHA = 94:6) compared to the *in vitro* results (14S-HDHA:11S-HDHA = 81:19)¹⁸. The major metabolite produced in platelets was the hydrolysis product of 16S,17S-epoxyDHA ($75 \pm 4\%$). It should be noted that we assume that much of the 17S-HpDHA added to the platelets is reduced to the alcohol, but in detecting the hydrolysis product of 16S,17S-epoxyDHA, it confirms the hydroperoxide enters the platelet since 16S,17S-epoxyDHA can only be produced starting with the hydroperoxide oxylin.

With respect to the overall turnover in platelets, the amount of oxylin products produced with 17S-HpDHA as the substrate is considerably low. With the addition of 17S-HpDHA (1080 ng total), 3.7 ng of 16S,17S-epoxyDHA and 1.2 ng of PDX were produced per 1×10^9 platelets, which is that less than 1% of the total 17S-HpDHA that was presented to the platelets. This observation was seen previously with the

incubation of 14S-HpDHA with human platelets¹⁸ and is consistent with its poor *in vitro* activity, indicating that 17S-HpDHA is a poor substrate for h12-LOX *ex vivo*.

Effect of 17S-HpDHA, PDX and 10R/S,17S-EEE-diHDHA on Human Platelet

Aggregation

In order to determine whether these oxylipins can inhibit human platelet activation, isolated human platelets from five different donors were titrated with 17S-HpDHA, PDX and 10R/S,17S-EEE-diHDHA (1 to 10 μM) for ten minutes and then stimulated with collagen (0.25 $\mu\text{g}/\text{mL}$). DMSO was used as the vehicle control (represented as 0 μM) and 12S-HETrE was chosen as positive control for comparison²⁶. Compared to vehicle control, 17S-HpDHA inhibited platelet aggregation in response to collagen stimulation with an $\text{EC}_{50} < 1 \mu\text{M}$ and had over a 90% reduction in platelet aggregation with a concentration $\geq 3 \mu\text{M}$ (**Figure 4**). This response is significantly more potent than that observed for 12S-HETrE²⁶ but comparable to that of 11S-HDPA_{n-6} and 14S-HDPA_{n-6}³⁹ ($\text{EC}_{50} < 1 \mu\text{M}$), indicating that 17S-HpDHA is a potent anti-aggregation molecule. The antiplatelet effects of the dihydroxylated

oxylipins, PDX and 10R/S,17S-EEE-diHDHA, were also investigated. PDX showed antiplatelet activity with an EC₅₀ at low-micromolar concentration (between 1 to 3 μM) and an over 90% reduction with a concentration ≥ 5μM, comparable to previous work¹². However, 10R/S,17S-EEE-diHDHA was markedly less potent, with an EC₅₀ of greater than 5 μM, with a 90% reduction at ≥ 15 μM. This result was consistent with the observation that poxytrins, dihydroxylated fatty acids with an EZE-conjugated triene motif, were potent human platelet aggregation inhibitors (approximately 60% inhibition at 1 μM), however, dihydroxylated fatty acids with an EEE-conjugated triene motif were less potent (approximately 5% inhibition at 1 μM)⁴⁰.

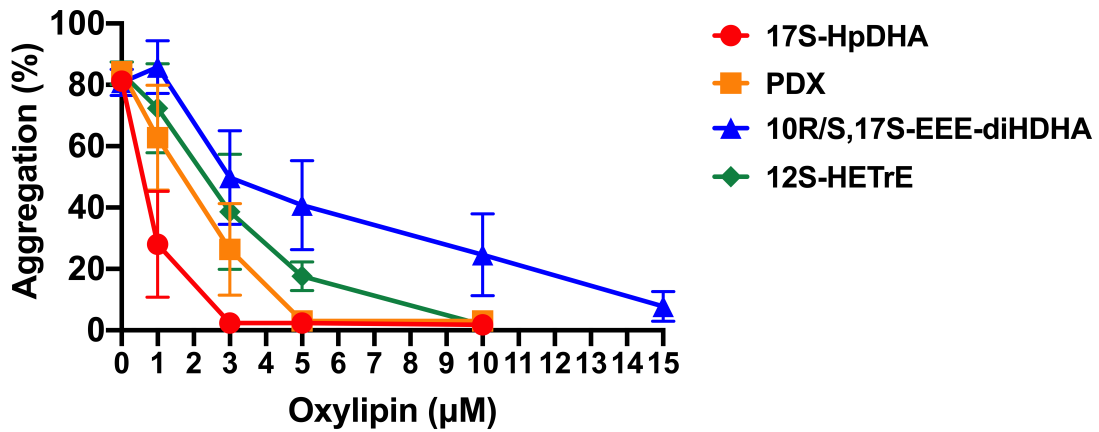


Figure 4. Inhibition of collagen-stimulated platelet aggregation by 17S-HpDHA, PDX, 10R/S,17S-EEE-diHDHA and 12S-HETrE. 17S-HpDHA, PDX, and 10R/S,17S-EEE-diHDHA (ranging from 1 to 15 μM) were incubated with isolate human platelets and then stimulated with collagen (0.25 μg/mL). Data represent mean ± S.E.M of the maximum aggregation of 5 independent experiments.

3.5 Discussion

Neuroprotectin D1 (NPD1) is classified as a specialized pro-resolving mediator (SPM), based on its potent anti-inflammatory activity and pro-resolving action⁴¹. It has been shown to inhibit polymorphonuclear leukocyte infiltration and macrophage efferocytosis.^{8, 42} PDX is less potent than NPD1 in resolving inflammation, but it does inhibit collagen-induced platelet aggregation at submicromolar concentrations.⁴⁰ For the biosynthesis of these two molecules, it was observed that h15-LOX-1 was involved in the biosynthesis of NPD1 in human macrophage through the 16S,17S-epoxyDHA intermediate¹⁷, however, no human LOX isozymes have yet been identified in the biosynthesis of PDX. Only soybean 15-LOX has been identified as a lipoxygenase that could carry out its production¹². In order to obtain further knowledge on the biosynthesis of NPD1 and PDX, *in vitro* investigations were performed to determine potential routes of their *in vivo* biosynthesis.

In the current work, we first investigated which human lipoxygenases were

capable of generating the precursor of NPD1 and PDX, 17S-HpDHA. We determined that h12-LOX was slightly more efficient in producing 17S-HpDHA than h15-LOX-1 and h15-LOX-2 from DHA. The effective $k_{\text{cat}}/K_{\text{M}}$ of h12-LOX was 2.8-fold greater than h15-LOX-1 and 1.3-fold greater than h15-LOX-2 (**Table 3**). This result is surprising since the canonical mechanism of both h15-LOX-1 and h15-LOX-2 is to produce mainly 17S-HpDHA from DHA, while h12-LOX produces primarily 14S-HpDHA as the major product. However, if we take rates into account in the case of DHA as the substrate, $k_{\text{cat}}/K_{\text{M}}$ for h12-LOX is greater than h15-LOX-1 (34-fold) and h15-LOX-2 (28-fold), resulting in increasing its effective $k_{\text{cat}}/K_{\text{M}}$ relative to both h15-LOX isozymes, even though 17S-HpDHA is a minor product for h12-LOX. The other observation that is noteworthy is that the increased percentage of the ω -9 product with DHA relative to AA (i.e. ω -11 hydrogen abstraction), indicates that the increased length and unsaturation allows DHA to insert deeper into both the h15-LOX-1 and h15-LOX-2 active sites, as previously observed¹⁸. This expanded reactivity of h15-LOX-1 and h15-LOX-2 with DHA made us suspect that they might

be capable of contributing to next step of NPD1 and PDX biosynthesis, which requires a ω -11 hydrogen abstraction.

Utilizing 17S-HpDHA as the substrate, it was determined that both h15-LOX-1 and h12-LOX were capable of producing 16S,17S-epoxyDHA, indicating that both these lipoxygenases abstract a hydrogen atom from the C12 (ω -11) of 17S-HpDHA. However, h15-LOX-1 is 44-fold more kinetically efficient (i.e. k_{cat}/K_M) with 17S-HpDHA than h12-LOX. This result is significant since the ω -11 carbon is the preferable hydrogen abstraction position for h12-LOX and yet the reaction rate is slower than expected with the oxylipin. This lowered rate of catalysis for h12-LOX with oxylipins was previously observed for 14S-HpDHA, indicating the active site for h12-LOX is more restrictive with respect to substrate structure¹⁸. We also investigated if h15-LOX-2 could be responsible for the biosynthesis of 16S,17S-epoxyDHA, since it was observed to abstract from the ω -11 carbon and produce the ω -9 product, 14S-HpDHA, from DHA. Surprisingly, no reaction was observed for h15-LOX-2 with 17S-HpDHA or the reduced substrate, 17S-HDHA.

This lack of reactivity is also consistent with previous work where h15-LOX-2 did not react with 14S-HpDHA¹⁸, indicating the active site of h15-LOX-2 is also selective against oxylipins, similar to h12-LOX.

When the reduced form of 17S-HpDHA, 17S-HDHA, was reacted with h15-LOX-1 and h12-LOX and it was confirmed that the lack of the hydroperoxide moiety prohibited the dehydration reaction to make the epoxide and thus only the oxygenation products, 16,17S-diHDHA for h15-LOX-1 and 11,17S-diHDHA, 16,17S-diHDHA and PDX for h12-LOX, were detected under reducing condition. These results build on previous work,^{16, 18} where the chemical nature of the oxylipin is critical to the biosynthesis of lipoxins, maresins and NPD1, to name a few, which all require an epoxide intermediate. However, if the hydroperoxide precursor is reduced by glutathione peroxidases 4 (GPx4) in the cell, then the biosynthesis of these critical SPMs will be greatly diminished, indicating the importance of GPx4 and glutathione concentrations in the inflammatory response. Unexpectedly, the oxygenation product, PDX, is also affected by the nature of the oxylipin substrate.

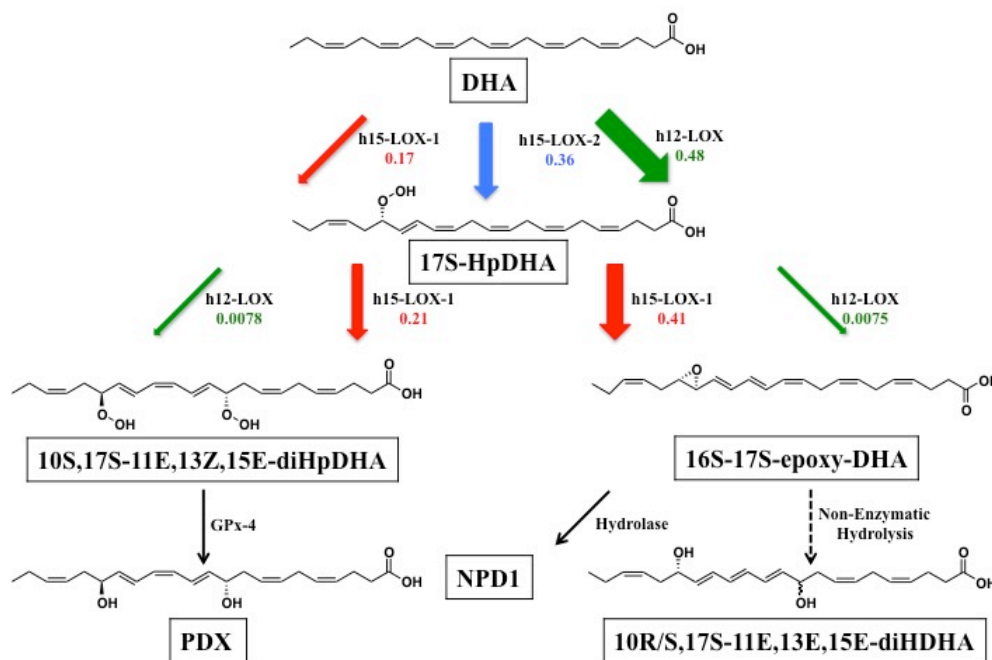
PDX was not detected in the reaction of 17S-HDHA with h15-LOX-1 and was barely detected in the reaction with h12-LOX (4%), suggesting that the synthetic route for PDX could be initiated by 17S-HpDHA as the substrate, not the reduced form, as was suggested in the literature³⁰.

Although both h15-LOX-1 and h12-LOX react with 17S-HpDHA to produce 16S,17S-epoxyDHA and PDX, the efficiency is not comparable. It was observed that the effective k_{cat}/K_M of h15-LOX-1 ($k_{cat}/K_M * \% \text{ Product}$) is 55 times more efficient than that of h12-LOX in producing 16S,17S-epoxyDHA and over 27 times more efficient in generating PDX (**Table 7**), implying that h15-LOX-1 may contribute more than h12-LOX to NPD1 and PDX formation *in vivo*. This is supported by the fact that a significant reduction in NPD1 and PDX production was observed with h15-LOX-1 deficient mice, compared to WT⁴³. Furthermore, the role of h15-LOX-1 in NPD1 and PDX biosynthesis was further corroborated by the challenge of the h15-LOX-1 inhibitor, PD146176, to M2 macrophages, resulting in the decrease of NPD1 and PDX production by 32% and 29%, respectively⁴³. Despite the low

efficiency of 16S,17S-epoxyDHA and PDX production in the reaction of 17S-HpDHA with h12-LOX *in vitro*, a different outcome is possible *in vivo*. Therefore, the production of NPD1 and PDX were monitored with the incubation of 17S-HpDHA with human platelets that contain high quantities of h12-LOX. Our results suggest that the primary metabolite of 17S-HpDHA with human platelets is the epoxidation product, 16S,17S-epoxyDHA ($75 \pm 4\%$), with a minor production of PDX ($25 \pm 4\%$). However, the overall turnover number of 17S-HpDHA by platelets *ex vivo* is low (0.5% converted to the di-oxylin), indicating that this pathway may not be important *in vivo*.

A proposed biosynthetic scheme of NPD1 and PDX from h12-LOX and h15-LOX-1 is presented in **Scheme 1**, with the size of the arrows representing the magnitude of their effective k_{cat}/K_M . It should be noted that the *in vitro* biosynthetic flux values may vary from the *in vivo* results since in the cell there are many variables which could affect these rates, such as protein expression or protein-protein

interactions, as seen with 5-LOX activating protein (FLAP), which can facilitate AA conversion with h5-LOX⁴⁴.



Scheme 1. A proposed biosynthetic scheme of NPD1 and PDX with lipoxygenase isozyme. The size of the arrows is proportional to their effective k_{cat}/K_M (i.e. k_{cat}/K_M * % Product).

As mentioned in the introductory section, NPD1 displays anti-inflammatory and pro-resolving properties during inflammation, while PDX shows more anti-platelet aggregation activity instead of inflammatory resolution. Therefore, a change in the NPD1: PDX ratio in the cell could affect the inflammatory response. Previously, we determined that the epoxide/oxygenated product ratio of 14S-HpDHA with

h15-LOX-1 was affected by allosteric effectors, such as 14S-HpDHA. In the current work, similar results were revealed with increasing concentrations of 17S-HpDHA, where the production of the NPD1 intermediate, 16S,17S-epoxyDHA, decreased and PDX increased, thus suggesting a product-feedback loop for NPD1 and PDX formation. These data suggest that allosteric effectors could change the NPD1/PDX ratio *in vivo* and we are currently investigating if LOX products can regulate this ratio and establish a product-feedback loop in the cell.

The mono- and di-hydroxylated DHA-derived oxylipins were then examined to determine their ability to inhibit collagen induced platelet aggregation. Our findings indicated that 17S-HpDHA was active toward platelet aggregation inhibition, with an EC₅₀ of less than 1 μM. This response is comparable to the effect observed for 14S-HpDHA,¹⁸ 11S-HDPA_{n-6}, and 14S-HDPA_{n-6} oxylipins³⁹, but significantly more potent than 12S-HETrE²⁶. For the di-hydroxylated oxylipins, we observed that PDX showed antiplatelet activity with an EC₅₀ of low-micromolar values (between 1 to 3 μM). However, 10R/S,17S-EEE-diHDHA, the non-enzymatic hydrolysis product of

16S,17S-epoxyDHA, was markedly less potent, with an EC₅₀ of greater than 5 μM. This observation is consistent with previous work, which demonstrated that poxytrins with an EEE-conjugated triene motif were less potent (approximately 5% inhibition at 1 μM)⁴⁰ than poxytrins with an EZE-conjugated triene motif (approximately 60% inhibition at 1 μM), indicating the importance of the double bond conjugation for platelet potency. This hypothesis was further supported with other dihydroxy conjugated trienes with different geometry (ZEE instead of EZE as found in LTB₄) manifested weak inhibition of platelet aggregation, suggesting that the conjugated EZE triene is an important molecular motif against the platelet aggregation.

3.6 Conclusion

In summary, we have shown that while h12-LOX and h15-LOX-1 are both viable enzymes for the production of the NPD1 epoxide intermediate and PDX, h15-LOX-1 is a more efficient pathway to their *in vitro* biosynthesis by over 55-fold and 27-fold, respectively. Moreover, we have demonstrated the allosteric regulation of NPD1 and PDX biosynthesis for h15-LOX-1 by oxylipins can negatively regulate NPD1 epoxide intermediate production. Given that 17S-HpDHA and 12S-HETE have micromolar potency for affecting NPD1:PDX ratio *in vitro*, it is biologically feasible that NPD1 and PDX are regulated by oxylipin concentrations in the cell, which is in agreement with previous work¹⁸. Lastly, 17S-HpDHA was shown to be a highly potent anti-platelet metabolite of DHA, which could imply additional dietary benefits for fish oil consumption. These new insights into the biochemistry of NPD1 and PDX biosynthesis will help direct inhibitor development, as well as possibly guide *in vivo* biosynthetic investigations.

3.7 Abbreviations

DHA, docosahexaenoic acid; DTA, docosatrienoic acid; AA, arachidonic acid;

17S-HpDHA, 17S-hydroperoxy-4Z,7Z,10Z,13Z,15E,19Z-docosahexaenoic acid;

17S-HDHA, 17S-hydroxy-4Z,7Z,10Z,13Z,15E,9Z-docosahexaenoic acid;

16S,17S-epoxyDHA, 16S,17S-epoxy-4Z,7Z,10Z,12E,14E,19Z-docosahexaenoic acid;

10R/S,17S-EEE-diHDHA, 10R/S,17S-dihydroxy-4Z,7Z,
11E,13E,15E,19Z-docosahexaenoic acid; 11,17S-diHDHA, 11,17S-dihydroxy-4Z,7Z,
9E,13Z,15E,19Z-docosahexaenoic acid; 16,17S-diHDHA,
16,17S-dihydroxy-4Z,7Z,10Z,12Z,14E,19Z-docosahexaenoic acid; 15S-HpETE,
15S-hydroperoxy-5Z,8Z,11Z,13E-eicosatetraenoic acid;

12S-HETrE,12S-hydroxy-8Z,10E,14Z-eicosatrienoic acid;

12S-HETE, 12S-hydroxy-5Z,8Z,10E,14Z-eicosatetraenoic acid;

17S-HDTA, 17S-hydroxy-13Z,15E,19Z-docosatrienoic acid;

PDX, protectin DX; NPD1, neuroprotectin D1 (also known as protectin D1 (PD1));

PCTRs, protectin conjugates in tissue regeneration; MCTRs, maresin conjugates in tissue regeneration; LXs, AA-derived lipoxins; RvEs, EPA-derived E-series resolvins; RvDs, DHA-derived D-series resolvins; RvTs, DPA-derived 13-series resolvins; LXB₄, lipoxin B₄; SPM, specialized pro-resolving mediator; PUFA, polyunsaturated fatty acid; ROS, reactive oxygen species; AD, Alzheimer's disease; ALS, amyotrophic lateral sclerosis; NSAIDs, nonsteroidal anti-inflammatory drugs; BIR, brain ischemia reperfusion; RPE, retina pigment epithelial; ICP-MS, inductively coupled plasma mass spectrometry; CAD, Collisionally Activated Dissociation; COX, cyclooxygenase; LOX, lipoxygenase; h15-LOX-1, ALOX15, human reticulocyte 15-lipoxygenase-1; h12-LOX, ALOX12, human platelet 12-lipoxygenase; h15-LOX-2, ALOX15B, human epithelial 15-lipoxygenase-2; sLOX-1, soybean lipoxygenase-1.

Reference

- [1] Chen, L., Deng, H., Cui, H., Fang, J., Zuo, Z., Deng, J., Li, Y., Wang, X., and Zhao, L. (2018) Inflammatory responses and inflammation-associated diseases in organs, *Oncotarget* 9, 7204-7218.
- [2] Tabas, I., and Glass, C. K. (2013) Anti-inflammatory therapy in chronic disease: challenges and opportunities, *Science* 339, 166-172.
- [3] Chiurchiù, V., Leuti, A., and Maccarrone, M. (2018) Bioactive Lipids and Chronic Inflammation: Managing the Fire Within, *Front Immunol* 9, 38.
- [4] Wongrakpanich, S., Wongrakpanich, A., Melhado, K., and Rangaswami, J. (2018) A Comprehensive Review of Non-Steroidal Anti-Inflammatory Drug Use in The Elderly, *Aging Dis* 9, 143-150.
- [5] Serhan, C. N., Chiang, N., and Van Dyke, T. E. (2008) Resolving inflammation: dual anti-inflammatory and pro-resolution lipid mediators, *Nat Rev Immunol* 8, 349-361.
- [6] Sugimoto, M. A., Sousa, L. P., Pinho, V., Perretti, M., and Teixeira, M. M. (2016) Resolution of Inflammation: What Controls Its Onset?, *Front Immunol* 7, 160.
- [7] Wisastra, R., and Dekker, F. J. (2014) Inflammation, Cancer and Oxidative Lipoyxygenase Activity are Intimately Linked, *Cancers (Basel)* 6, 1500-1521.
- [8] Serhan, C. N., Gotlinger, K., Hong, S., Lu, Y., Siegelman, J., Baer, T., Yang, R., Colgan, S. P., and Petasis, N. A. (2006) Anti-inflammatory actions of neuroprotectin D1/protectin D1 and its natural stereoisomers: assignments of dihydroxy-containing docosatrienes, *J Immunol* 176, 1848-1859.
- [9] Bazan, N. G. (2005) Neuroprotectin D1 (NPD1): a DHA-derived mediator that protects brain and retina against cell injury-induced oxidative stress, *Brain*

Pathol 15, 159-166.

- [10] Bazan, N. G. (2009) Neuroprotectin D1-mediated anti-inflammatory and survival signaling in stroke, retinal degenerations, and Alzheimer's disease, *J Lipid Res 50 Suppl*, S400-405.
- [11] Butovich, I. A. (2005) On the structure and synthesis of neuroprotectin D1, a novel anti-inflammatory compound of the docosahexaenoic acid family, *J Lipid Res 46*, 2311-2314.
- [12] Chen, P., Fenet, B., Michaud, S., Tomczyk, N., Vericel, E., Lagarde, M., and Guichardant, M. (2009) Full characterization of PDX, a neuroprotectin/protectin D1 isomer, which inhibits blood platelet aggregation, *FEBS Lett 583*, 3478-3484.
- [13] Hong, S., Gronert, K., Devchand, P. R., Moussignac, R. L., and Serhan, C. N. (2003) Novel docosatrienes and 17S-resolvins generated from docosahexaenoic acid in murine brain, human blood, and glial cells. Autacoids in anti-inflammation, *J Biol Chem 278*, 14677-14687.
- [14] Lagarde, M., Guichardant, M., and Bernoud-Hubac, N. (2020) Anti-inflammatory and anti-virus potential of poxytrins, especially protectin DX, *Biochimie 179*, 281-284.
- [15] Brash, A. R. (1999) Lipoxygenases: occurrence, functions, catalysis, and acquisition of substrate, *J Biol Chem 274*, 23679-23682.
- [16] Green, A. R., Freedman, C., Tena, J., Tourdot, B. E., Liu, B., Holinstat, M., and Holman, T. R. (2018) 5 S,15 S-Dihydroperoxyeicosatetraenoic Acid (5,15-diHpETE) as a Lipoxin Intermediate: Reactivity and Kinetics with Human Leukocyte 5-Lipoxygenase, Platelet 12-Lipoxygenase, and Reticulocyte 15-Lipoxygenase-1, *Biochemistry 57*, 6726-6734.

- [17] Aursnes, M., Tungen, J. E., Colas, R. A., Vlasakov, I., Dalli, J., Serhan, C. N., and Hansen, T. V. (2015) Synthesis of the 16S,17S-Epoxyprotectin Intermediate in the Biosynthesis of Protectins by Human Macrophages, *J Nat Prod* 78, 2924-2931.
- [18] Freedman, C., Tran, A., Tourdot, B. E., Kalyanaraman, C., Perry, S., Holinstat, M., Jacobson, M. P., and Holman, T. R. (2020) Biosynthesis of the Maresin Intermediate, 13S,14S-Epoxy-DHA, by Human 15-Lipoxygenase and 12-Lipoxygenase and Its Regulation through Negative Allosteric Modulators, *Biochemistry* 59, 1832-1844.
- [19] Kutzner, L., Goloshchapova, K., Heydeck, D., Stehling, S., Kuhn, H., and Schebb, N. H. (2017) Mammalian ALOX15 orthologs exhibit pronounced dual positional specificity with docosahexaenoic acid, *Biochim Biophys Acta Mol Cell Biol Lipids* 1862, 666-675.
- [20] Perry, S. C., Horn, T., Tourdot, B. E., Yamaguchi, A., Kalyanaraman, C., Conrad, W. S., Akinkugbe, O., Holinstat, M., Jacobson, M. P., and Holman, T. R. (2020) Role of Human 15-Lipoxygenase-2 in the Biosynthesis of the Lipoxin Intermediate, 5S,15S-diHpETE, Implicated with the Altered Positional Specificity of Human 15-Lipoxygenase-1, *Biochemistry* 59, 4118-4130.
- [21] Perry, S. C., Kalyanaraman, C., Tourdot, B. E., Conrad, W. S., Akinkugbe, O., Freedman, J. C., Holinstat, M., Jacobson, M. P., and Holman, T. R. (2020) 15-Lipoxygenase-1 biosynthesis of 7S,14S-diHDHA implicates 15-lipoxygenase-2 in biosynthesis of resolvin D5, *J Lipid Res* 61, 1087-1103.
- [22] Amagata, T., Whitman, S., Johnson, T. A., Stessman, C. C., Loo, C. P., Lobkovsky, E., Clardy, J., Crews, P., and Holman, T. R. (2003) Exploring sponge-derived terpenoids for their potency and selectivity against 12-human, 15-human, and 15-soybean lipoxygenases, *J Nat Prod* 66, 230-235.

- [23] Vasquez-Martinez, Y., Ohri, R. V., Kenyon, V., Holman, T. R., and Sepulveda-Boza, S. (2007) Structure-activity relationship studies of flavonoids as potent inhibitors of human platelet 12-hLO, reticulocyte 15-hLO-1, and prostate epithelial 15-hLO-2, *Bioorganic & Medicinal Chemistry* 15, 7408-7425.
- [24] Butovich, I. A. (2006) A one-step method of 10,17-dihydro(pero)xydocosa-hexa-4Z,7Z,11E,13Z,15E,19Z-enoic acid synthesis by soybean lipoxygenase, *J Lipid Res* 47, 854-863.
- [25] Jiang, Z. D., and Gerwick, W. H. (1997) Novel oxylipins from the temperate red alga *Polysiphonia latissima*: evidence for an arachidonate 9(S)-lipoxygenase, *Lipids* 32, 231-235.
- [26] Ikei, K. N., Yeung, J., Apopa, P. L., Ceja, J., Vesci, J., Holman, T. R., and Holinstat, M. (2012) Investigations of human platelet-type 12-lipoxygenase: role of lipoxygenase products in platelet activation, *J Lipid Res* 53, 2546-2559.
- [27] Wecksler, A. T., Kenyon, V., Deschamps, J. D., and Holman, T. R. (2008) Substrate specificity changes for human reticulocyte and epithelial 15-lipoxygenases reveal allosteric product regulation, *Biochemistry* 47, 7364-7375.
- [28] Green, A. R., Barbour, S., Horn, T., Carlos, J., Raskatov, J. A., and Holman, T. R. (2016) Strict Regiospecificity of Human Epithelial 15-Lipoxygenase-2 Delineates Its Transcellular Synthesis Potential, *Biochemistry* 55, 2832-2840.
- [29] Guichardant, M., Vericel, E., and Lagarde, M. (2019) Biological relevance of double lipoxygenase products of polyunsaturated fatty acids, especially within blood vessels and brain, *Biochimie* 159, 55-58.
- [30] Balas, L., Guichardant, M., Durand, T., and Lagarde, M. (2014) Confusion

between protectin D1 (PD1) and its isomer protectin DX (PDX). An overview on the dihydroxy-docosatrienes described to date, *Biochimie* 99, 1-7.

- [31] Van Os, C. P., Rijke-Schilder, G. P., Van Halbeek, H., Verhagen, J., and Vliegthart, J. F. (1981) Double dioxygenation of arachidonic acid by soybean lipoxygenase-1. Kinetics and regio-stereo specificities of the reaction steps, *Biochim Biophys Acta* 663, 177-193.
- [32] Hornung, E., Walther, M., Kuhn, H., and Feussner, I. (1999) Conversion of cucumber linoleate 13-lipoxygenase to a 9-lipoxygenating species by site-directed mutagenesis, *Proc Natl Acad Sci U S A* 96, 4192-4197.
- [33] Bild, G. S., Ramadoss, C. S., and Axelrod, B. (1977) Effect of substrate polarity on the activity of soybean lipoxygenase isoenzymes., *Lipids* 12, 732-735.
- [34] Glickman, M. H., and Klinman, J. P. (1995) Nature of Rate-Limiting Steps in the Soybean Lipoxygenase-1 Reaction, *Biochemistry* 34, 14077-14092.
- [35] Dobson, E. P., Barrow, C. J., Kralovec, J. A., and Adcock, J. L. (2013) Controlled formation of mono- and dihydroxy-resolvins from EPA and DHA using soybean 15-lipoxygenase, *Journal of Lipid Research* 54, 1439-1447.
- [36] Maas, R. L., and Brash, A. R. (1983) Evidence for a lipoxygenase mechanism in the biosynthesis of epoxide and dihydroxy leukotrienes from 15(S)-hydroperoxyicosatetraenoic acid by human platelets and porcine leukocytes, *Proc Natl Acad Sci U S A* 80, 2884-2888.
- [37] Radmark, O., Serhan, C., Hamberg, M., Lundberg, U., Ennis, M. D., Bundy, G. L., Oglesby, T. D., Aristoff, P. A., Harrison, A. W., Slomp, G., and et al. (1984) Stereochemistry, total synthesis, and biological activity of 14,15-dihydroxy-5,8,10,12-eicosatetraenoic acid, *J Biol Chem* 259, 13011-13016.

- [38] Kuhn, H., Wiesner, R., Stender, H., Schewe, T., Lankin, V. Z., Nekrasov, A., and Rapoport, S. M. (1986) Requirement of monohydroperoxy fatty acids for the oxygenation of 15LS-HETE by reticulocyte lipoxygenase, *FEBS Lett* 203, 247-252.
- [39] Yeung, J., Adili, R., Yamaguchi, A., Freedman, C. J., Chen, A., Shami, R., Das, A., Holman, T. R., and Holinstat, M. (2020) Omega-6 DPA and its 12-lipoxygenase-oxidized lipids regulate platelet reactivity in a nongenomic PPAR α -dependent manner, *Blood Adv* 4, 4522-4537.
- [40] Chen, P., Vericel, E., Lagarde, M., and Guichardant, M. (2011) Poxyrins, a class of oxygenated products from polyunsaturated fatty acids, potently inhibit blood platelet aggregation, *Faseb j* 25, 382-388.
- [41] Hansen, T. V., Vik, A., and Serhan, C. N. (2018) The Protectin Family of Specialized Pro-resolving Mediators: Potent Immunoresolvents Enabling Innovative Approaches to Target Obesity and Diabetes, *Front Pharmacol* 9, 1582.
- [42] Schwab, J. M., Chiang, N., Arita, M., and Serhan, C. N. (2007) Resolvin E1 and protectin D1 activate inflammation-resolution programmes, *Nature* 447, 869-874.
- [43] Pistorius, K., Souza, P. R., De Matteis, R., Austin-Williams, S., Primdahl, K. G., Vik, A., Mazzacuva, F., Colas, R. A., Marques, R. M., Hansen, T. V., and Dalli, J. (2018) PDn-3 DPA Pathway Regulates Human Monocyte Differentiation and Macrophage Function, *Cell Chem Biol* 25, 749-760 e749.
- [44] Gerstmeier, J., Newcomer, M. E., Dennhardt, S., Romp, E., Fischer, J., Werz, O., and Garscha, U. (2016) 5-Lipoxygenase-activating protein rescues activity of 5-lipoxygenase mutations that delay nuclear membrane association and disrupt product formation, *Faseb j* 30, 1892-1900.

- [45] Dona, M., Fredman, G., Schwab, J. M., Chiang, N., Arita, M., Goodarzi, A., Cheng, G., von Andrian, U. H., and Serhan, C. N. (2008) Resolvin E1, an EPA-derived mediator in whole blood, selectively counterregulates leukocytes and platelets, *Blood* *112*, 848-855.

Chapter 4

Mutagenesis, Hydrogen-Deuterium Exchange, and Molecular Dynamic

Investigations Establish the Dimeric Interface of Human Platelet-type

12-Lipoxygenase

4.1 Abstract

It was previously shown that human platelet 12S-lipoxygenase (h12-LOX) exists as a dimer. In this study, we create a model of the dimer through a combination of computational methods, experimental mutagenesis and hydrogen/deuterium exchange (HDX) investigations. Initially, Leu183 and Leu187 were replaced by negatively charged glutamate residues and neighboring aromatic residues were replaced with alanine residues (F174A/W176A/L183E/L187E/Y191A). This quintuple mutant disrupted both the hydrophobic and π - π interactions, generating a h12-LOX monomer. To refine the determinants for dimer formation further, the L183E/L187E mutant was generated and the equilibrium shifted mostly toward monomer. We then submitted the predicted monomeric structure to protein-protein docking in order to create a model of the dimeric complex. A total of 9 out of the top 10 most energetically favorable docking conformations predict a TOP-to-TOP dimeric arrangement of h12-LOX, with the α -helices containing a Leu-rich region

(L172, L183, L187 and L194), corroborating our experimental results showing the importance of these hydrophobic interactions for dimerization. This model was supported by HDX exchange investigations that demonstrated the stabilization of four, non-overlapping peptides within the $\alpha 2$ helix of the TOP subdomain for wt-h12-LOX, consistent with the dimer interface. Most importantly, our data reveal that the biochemical properties of dimer and monomer of h12-LOX behave differently, suggesting that the structural changes due to dimerization have allosteric effects on active site catalysis and inhibitor binding.

4.2 Introduction

Human platelet 12S- Lipoxygenase (h12-LOX or ALOX12) adds molecular oxygen at C-12 of arachidonic acid (AA) with 'S' chirality to generate 12(S)-hydroperoxyeicosatetraenoic acid (12(S)-HpETE).¹⁻³ This hydroperoxide is further reduced by peroxidases to yield 12(S)-hydroxyeicosatetraenoic acid (12(S)-HETE).⁴⁻⁷ These h12-LOX products, as well as others from different fatty acids, influence platelet aggregation and play a role in many inflammatory diseases,⁸ such as psoriasis,⁹ diabetes,¹⁰⁻¹² cancer,¹³⁻¹⁸ indicating h12-LOX as a possible therapeutic target.^{8, 19, 20} Currently, the main effort in the search for inhibitors targeting lipoxygenases has been directed to the active site, blocking the direct enzymatic activity of fatty acid peroxidation. However, allosteric inhibition with respect to the dimerization state of h12-LOX may also be relevant, as seen for cyclooxygenase (COX).^{21, 22}

The first high-resolution crystal structure of mammalian lipoxygenase, rabbit

15S-LOX-1 (r15-LOX-1 or r12/15-LOX or rALOX15) was reported as dimer,²³ although its interface was not correctly described until 10 years later.²⁴ It took another 5 years until it was postulated that r15-LOX-1, predominantly monomeric in solution, becomes a dimer in the presence of 13S-hydroxyoctadeca-9Z,11E-dienoic acid (13-HODE), the reduced form of its endogenous hydroperoxide product, 13-HpODE.²⁵ In the meantime, the rabbit enzyme monomer has been used as a homology model for other lipoxygenases, with the TOP being defined as a subdomain region from residue 163 to 222, covering the active site in the helical bundle of the catalytic domain. Although the crystal structures suggest oligomers for some lipoxygenases, the nature of their association has not been discussed,²⁶⁻²⁹ except for h12-LOX³⁰ and coral 11R-LOX (c11-LOX),³¹ which were reported stable and active as dimers. There is no crystal structure of an active, full-length h12-LOX, but the wild-type (wt) h12-LOX has been shown experimentally to agglomerate into large clusters³⁰ and there are indications that other human lipoxygenases might not be monomeric either.³² Previously, Shang and co-workers used a combination of

thermodynamic calculations, concerning the stability of molecular assemblies, thermal motion analysis [TLSMD (translation, vibration, and screw rotation motion detection based on crystallographic temperature factor)], and results of small angle X-ray analysis (SAXS) to propose a dimeric structure of h12-LOX connected in a TOP-to-TOP fashion (**Figure 1**), defined by interactions between their $\alpha 2$ helices.³³ The assembly of dimers via the $\alpha 2$ helices, running in opposite directions (anti-symmetric), has been tested in r15-LOX-1 by site-directed mutagenesis and SAXS, supporting a model that such dimers, as found in its crystal structure,²⁴ are stabilized by a leucine zipper motif formed by L179A:L192B and L183A:L188B.²⁵ However, dimerization in coral 11R-LOX was studied by SAXS, and tested by chemical cross-linking and site-directed mutagenesis to reveal that its dimerization interaction is through its PDZ-like domain.³¹ Although a similar PDZ-like domain interaction for h12-LOX was among others predicted by thermodynamic stability calculations, a model of dimerization through this domain was inconsistent with SAXS analysis^{30, 33} and thus was rejected as a possible dimer structure model. In the

current work, results from site-directed mutagenesis, *in silico* modeling, and hydrogen deuterium exchange-mass spectrometry (HDX-MS) are presented which suggest a TOP-to-TOP h12-LOX dimerization model that is mediated by an interaction similar to a leucine-zipper.

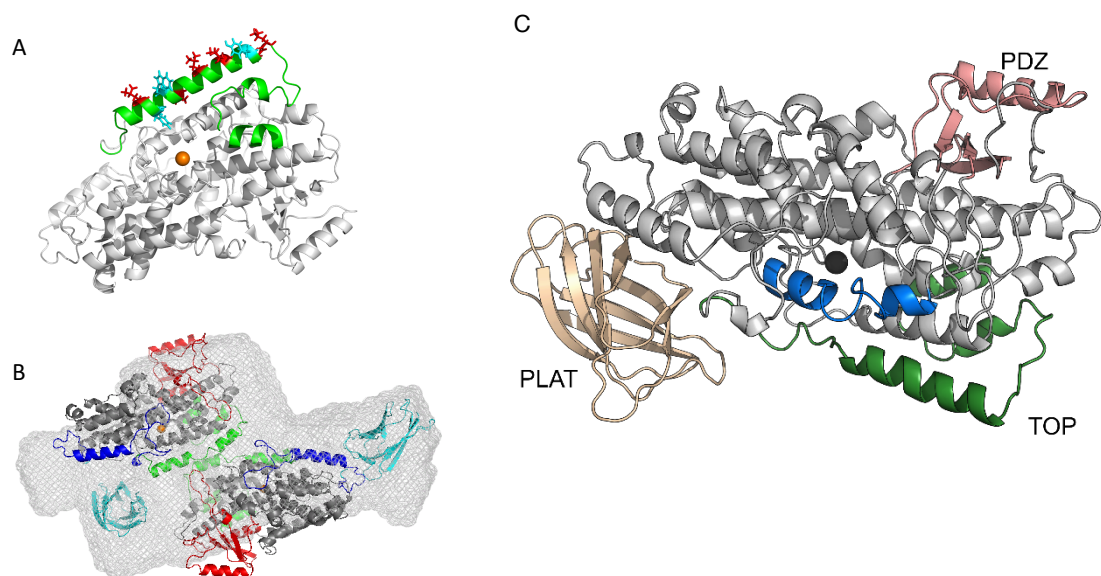


Figure 1. A: Homology model of wt-h12-LOX catalytic domain with TOP region (163-222) depicted in green. Leucines in this region are depicted in red, aromatic amino acids in cyan. B: TOP-to-TOP model (from our earlier publication)³⁰. C: A full-length model of h12-LOX with the various subdomains labeled.

4.3 Materials and Methods

Chemicals.

Fatty acids used in this study were purchased from Nu-Chek Prep, Inc. (MN, USA). Deuterium oxide (99.9%) was purchased from Cambridge Isotope Laboratories (Tewksbury, MA, USA). All other solvents and chemicals were of reagent grade or better and were used as purchased without further purification.

Homology model of h12-LOX.

A crystal structure of h12-LOX is available in the Protein Data Bank (pdb id: 3D3L, resolution 2.6Å), however, this structure is not suitable for the present modeling due to several missing residues. For instance, helix α 11 that forms the entrance to the active site is missing. Also, the entire PLAT domain and helix α 2, which is positioned parallel to helix α 11 in the r15-LOX-1 and porcine 12-LOX structures, is re-oriented horizontally above the active site entrance in the h12-LOX structure (structural superposition is shown in Supplementary Information Figure S1).

Finally, the C-terminal residue, I663, which coordinates the active site ferric ion, is replaced by a heavy construct vector that was not removed. For these reasons, a homology model of h12-LOX (Uniprot accession P18054) was constructed based on the porcine 12-LOX structure (pdb id: 3rde, resolution 1.9 Å) using the software PRIME (v4.7, Schrödinger Inc). During homology modeling, we retained the metal ion (Fe^{3+}), a hydroxide ion that coordinated the metal ion, and the co-crystallized ligand, 3-(4-[(tridec-2-yn-1-yloxy) methyl]phenyl) propanoic acid, from the porcine 12(S)-LOX structure. The h12-LOX model was subsequently energy minimized using Protein Preparation Wizard (Schrödinger Inc). During the protein preparation step, hydrogen atoms were optimized to make better hydrogen bonding interactions and all heavy atoms were relaxed such that they did not move beyond 0.3 Å from their starting position. After the protein preparation step, we separated the protein and the co-crystallized ligand into two separate entries in the Maestro project table. The protein entry included metal (Fe^{3+}) and hydroxide ions.

Site-directed Mutagenesis.

In order to test the TOP-to-TOP model of dimerization in h12-LOX, site-directed mutagenesis was employed to introduce mutations in this region that would abolish the hypothesized hydrophobic and $\pi - \pi$ interactions. The following two mutations were introduced; F174A/W176A/L183E/L187E/Y191A and L183E/L187E. We follow the same residue numbering convention as used in UniProt for the h12-LOX sequence (Accession number P18054). Online QuikChange Primer Design tool (<http://www.genomics.agilent.com/primerDesignProgram.jsp>) from Agilent Technologies (CA, USA) was used to design the primers for all the mutants of h12-LOX. The mutations were introduced using a QuikChange[®] II XL site-directed mutagenesis kit from Agilent Technologies by following the instructions in the provided protocol. The mutations were confirmed by sequencing the LOX insert in the pFastBac1 shuttle vector (Eurofins Genomics, KY, USA).

Protein Expression and Purification.

The expression and purification of h12-LOX and mutant enzymes used in this study were done as previously described.^{34, 35} The wild-type (wt-h12-LOX) enzyme

and its mutants were expressed as fusion proteins with a 6-His tag on the N-terminus and were purified by affinity nickel-iminodiacetic acid agarose using a FPLC (Bio-Rad). The entire purification process was performed at 4°C. The purity of all the proteins was greater than 90%, as determined by SDS-PAGE analysis.

Size Exclusion Chromatography.

Size exclusion chromatography (SEC) was performed on the affinity-purified proteins using an AKTA Pure system. After centrifugation for 13000 rpm for 5 mins (to sediment any debris), the purified protein was loaded onto either a Superdex™ 200, 10/300 GL column (GE Healthcare) for **Figure 2** or a Superdex™ 75, 10/300 GL column (GE Healthcare) for **Figure 3** equilibrated with 25mM HEPES (pH 7.5) at a flow rate of 0.3 mL/min. The elution volume (Ve) for **Figure 2** was compared with the gel filtration standard (Bio-Rad, catalog # 151-1901) containing horse thyroglobulin (MW 670 kDa), bovine γ -globulin (158 kDa), chicken ovalbumin (44 kDa), horse myoglobin (17 kDa) and vitamin B12 (1.35 kDa) and the elution volume (Ve) for **Figure 3** was compared with 69385 Protein Standard Mix 15-600 kDa

(Sigma-Aldrich) containing horse thyroglobulin (MW 670 kDa), bovine γ -globulin (158 kDa), chicken ovalbumin (44 kDa), bovine pancreatic ribonuclease (13.7 kDa) and pABA (0.14 kDa). A standard curve of MWs relative to elution volume was utilized to establish monomer and dimer h12-LOX (**Supporting information, Figure S3**).

Determination of Iron Content using ICP-MS.

The iron content of wt-h12-LOX and all the mutant enzymes was determined on a Thermo Element XR inductively coupled plasma mass spectrometer (ICP-MS). Cobalt EDTA was used as an internal standard. Iron concentrations were determined by comparison with standardized iron solutions (range 20-30% occupancy) and all kinetic data were normalized to the iron content. Protein concentrations were determined by a Bradford assay, with bovine serum albumin as protein standard.

Steady-state Kinetics.

Wt and mutant h12-LOX enzymatic rates were determined in triplicate by following the formation of the conjugated diene product, 12(S)-HpETE ($\epsilon = 25,000$

$M^{-1}cm^{-1}$) at 234 nm with a Perkin-Elmer Lambda 40 UV/Vis spectrophotometer. The reactions were started by adding approximately 40 nM enzyme to a 2 mL reaction mixture containing 1-20 μM AA, in 25 mM HEPES buffer (pH 8.00), in the presence of 0.01% Triton X-100, at room temperature (23°C), with constant stirring. The Triton X-100 is added to reduce substrate inhibition. Kinetic data were obtained by recording initial enzymatic rates at each substrate concentration and then fitting them to the Michaelis-Menten equation using the KaleidaGraph (Synergy) program to determine k_{cat} and k_{cat}/K_M values.

UV-Vis-based IC_{50} assay

IC_{50} values of ML355, an h12-LOX specific inhibitor,³⁶ against h12-LOX and its mutants were determined in the same manner as the steady state kinetic values. The reactions were carried out in 25 mM HEPES buffer (pH 8.00), 0.01% Triton X-100, and 10 μM AA. IC_{50} values were obtained by determining the enzymatic rate at six inhibitor concentrations and plotting them against inhibitor concentration, followed by a hyperbolic saturation curve fit. The data used for the saturation curve fits were

performed in duplicate or triplicate, depending on the quality of the data. Triton X-100 is used to ensure proper solubilization of the inhibitor.

Liquid Chromatography-Tandem Mass Spectrometry Analysis of Enzymatic Products.

To determine the products formed, wt-h12-LOX and the mutant enzymes were reacted, in triplicate, with 10 μ M of AA in 25 mM HEPES buffer (pH 7.5) for 10 minutes. The reactions were quenched with 1% glacial acetic acid, and extracted three times with dichloromethane (DCM). The products were then reduced with trimethylphosphite, and evaporated under a stream of nitrogen gas. The reaction products were reconstituted in methanol and analyzed via liquid chromatography-tandem mass spectrometry (LC-MS/MS). Chromatographic separation was performed using a C18 Synergi (4 μ M) Hydro-RP 80 Angstrom LC column (150 x 2 mm). The injection volume was 20 μ L. The chromatography system had a Thermo PDA Plus UV detector, coupled to a Thermo-Electron LTQ mass spectrometer. All analyses were performed in negative ionization mode at the normal

resolution setting. The mobile phase A consisted of water with 0.1% (volume/volume) formic acid and the mobile phase B consisted of acetonitrile with 0.1% formic acid. The method ran 60% mobile phase A and 40% mobile phase B initially; then at 30 minutes decreased the mobile phase A to 55% and increased the mobile phase B to 45%; and, finally, gradually decreased the percentage of mobile phase A and increased the percentage of mobile phase B until it reached 25% mobile phase A and 75% mobile phase B at 60 minutes. The flow rate was 200 $\mu\text{L}/\text{min}$. The products were ionized by electrospray ionization. MS/MS was performed in a targeted manner with a mass of 319.5 (for HETE detection). The reaction products were identified by matching their retention times, MS/MS (fragmentation) spectra, and UV spectra to known standards.

***In silico* modeling of human h12-LOX dimer.**

The ZDock protein-protein docking server³⁷ was used to predict the dimeric structure of h12-LOX. The top 10 most favorable complexes were analyzed, and the lowest energy docking pose was chosen for further analysis.

HDX-MS sample preparation.

Aliquots of h12-LOX monomer or dimer (3 mg/mL) were thawed and were diluted 10-fold (5 μ L into 45 μ L) in 10 mM HEPES, 150 mM NaCl, 5 mM DTT, pD 7.4 D₂O (99% D) buffer (corrected; pD = pH_{read} + 0.4). Samples were incubated randomly at 10 time points (0, 10, 20, 45, 60, 180, 600, 1800, 3600, and 7200 s) at 25 °C using a water bath. For each h12-LOX variant, the HDX samples were prepared over the course of three days and the time points were randomized to reduce systematic error. Each time point was prepared and processed once. At the designated incubation time, all samples were then treated identically; the samples were rapidly cooled (5-6 seconds in a -20 °C bath) and acid quenched (to pH 2.4, confirmed with pH electrode, with 0.32 M citric acid stock solution to 90 mM final concentration). Procedures from this point were conducted near 4°C. Prior to pepsin digestion, guanidine HCl (in citric acid, pH 2.4) was mixed with the samples to a final concentration of 0.5 M. h12-LOX HDX samples were digested with pre-equilibrated (10 mM citrate buffer, pH 2.4), immobilized pepsin for 2.5 min. The peptide

fragments were filtered, removing the pepsin, using spin cups (cellulose acetate) and by centrifugation for 10 seconds at 4°C. Samples were flash frozen immediately in liquid nitrogen and stored at -80°C until data collection.

Liquid chromatography-tandem mass spectrometry for h12-LOX peptide identification.

To identify peptide fragments of h12-LOX resulting from pepsin digestion, samples of pepsin-digested h12-LOX at time = 0 s (H₂O buffer) were analyzed using a Thermo Dionex UltiMate3000 RSLCnano liquid chromatography system (LC) that was connected in-line with an LTQ Orbitrap XL mass spectrometer equipped with an electrospray ionization (ESI) source (Thermo Fisher Scientific, Waltham, MA). The LC was equipped with a C18 analytical column (Acclaim® PepMap 100, length: 150 mm, inner diameter: 0.075 mm, particle size: 3 µm, Thermo). Solvent A was 99.9% water/0.1% formic acid and solvent B was 99.9% acetonitrile/0.1% formic acid (volume/volume). The elution program consisted of isocratic flow at 2% B for 4 min, a linear gradient to 30% B over 38 min, isocratic flow at 95% B for 6 min, and

isocratic flow at 2% B for 12 min, at a flow rate of 300 nL/min. The column exit was connected to the ESI source of the mass spectrometer using polyimide-coated, fused-silica tubing (inner diameter: 20 μm , outer diameter: 280 μm , Thermo). Full-scan mass spectra were acquired in the positive ion mode over the range $m/z = 350$ to 1800 using the Orbitrap mass analyzer, in profile format, with a mass resolution setting of 60,000 (at $m/z = 400$, measured at full width at half-maximum peak height).

In the data-dependent mode, the eight most intense ions exceeding an intensity threshold of 30,000 counts were selected from each full-scan mass spectrum for tandem mass spectrometry (MS/MS) analysis using collision-induced dissociation (CID). Real-time dynamic exclusion was enabled to preclude re-selection of previously analyzed precursor ions. Data acquisition was controlled using Xcalibur software (version 2.0.7, Thermo). Raw data were searched against the amino acid sequence of h12-LOX using Proteome Discoverer software (version 1.3, SEQUEST, Thermo) to identify peptides from MS/MS spectra.

Liquid chromatography-mass spectrometry for hydrogen/deuterium exchange measurements.

Deuterated, pepsin-digested samples of h12-LOX monomer and dimer were analyzed using a 1200 series LC (Agilent, Santa Clara, CA) that was connected in-line with the LTQ Orbitrap XL mass spectrometer (Thermo). The LC was equipped with a reversed-phase analytical column (Viva C8, length: 30 mm, inner diameter: 1.0 mm, particle size: 5 μ m, Restek, Bellefonte, PA) and guard pre-column (C8, Restek). Solvent A was 99.9% water/0.1% formic acid and solvent B was 99.9% acetonitrile/0.1% formic acid (volume/volume). Each sample was thawed immediately prior to injection onto the column. The elution program consisted of a linear gradient from 5% to 10% B over 1 min, a linear gradient to 40% B over 5 min, a linear gradient to 100% B over 4 min, isocratic conditions at 100% B for 3 min, a linear gradient to 5% B over 0.5 min, and isocratic conditions at 5% B for 5.5 min, at a flow rate of 300 μ L/min. The column compartment was maintained at 4 °C and lined with towels to absorb atmospheric moisture condensation. The column exit was

connected to the ESI source of the mass spectrometer using PEEK tubing (inner diameter: 0.005 inch, outer diameter: 1/16 inch, Agilent). Mass spectra were acquired in the positive ion mode over the range $m/z = 350$ to 1800 using the Orbitrap mass analyzer, in profile format, with a mass resolution setting of 100,000 (at $m/z = 400$). Data acquisition was controlled using Xcalibur software (version 2.0.7, Thermo).

Mass spectral data acquired for HDX measurements were analyzed using the software, HDX Workbench.³⁸ The percent deuterium incorporation was calculated for each of these peptides, taking into account the number of amide linkages (excluding proline residues) and the calculated number of deuterons incorporated. The values were normalized for 100% D₂O and corrected for peptide-specific back-exchange,
$$\text{HDX}\% = (\text{observed, normalized extent of deuterium incorporation \{in percent\}}) / (1 - \{\text{BE}/100\}).$$
³⁹

Peptide-specific back-exchange was determined by fully exchanging the h12-LOX-derived peptides in 100% D₂O, quenching with deuterated acid and performing HDX-MS measurement to determine the extent of the reverse exchange

(N-D→N-H). Peptides of h12-LOX were generated from pepsin digestion as described above, but in H₂O buffer. Water was subsequently removed by lyophilization. The peptide mixture was dissolved in buffered D₂O, pD 9 and incubated at 90 °C for 2 h in a sealed microcentrifuge tube and then quenched to pD 2.5 using dilute DCl (Cambridge Isotope Laboratories). The sample was frozen in liquid nitrogen and stored at -80 °C until HDX analysis. The extent of deuterium incorporation in this sample was analyzed via LC-MS as described above for HDX. Back-exchange values ranged from 2 to 50%, for an average value of 20% (see **SI HDX Table**). The resulting data were plotted as deuterium exchange versus time using Igor Pro software (See **SI HDX traces**).

4.4 Results and Discussion

TOP-to-TOP model of dimerization in h12-LOX.

Previously, it was demonstrated that h12-LOX existed as a dimer, which was easily converted to larger aggregates.³⁰ This could be controlled by mutating surface-exposed Cys residues to Ser, but not totally eliminated.^{30, 32} Furthermore, following SAXS analysis and modeling, Shang and co-workers predicted a TOP-to-TOP model of dimerization of h12-LOX (**Figure 1B**). It should be noted that the TOP is a subdomain region of h12-LOX (residues 163-222), as depicted in **Figure 1**. This region has many leucines (L172, L178, L183, L187, L193, L194) that could provide hydrophobic interactions between the monomers. Also present in this region are aromatic amino acids, F174, W176, and Y191, that could form $\pi - \pi$ interactions at the dimer interface. To test this model, a mutant was made in which the leucines at position 183 and 187 were replaced by negatively charged glutamates and the neighboring aromatic residues were replaced with alanine residues

(F174A/W176A/L183E/L187E/Y191A), to disrupt both the hydrophobic and $\pi - \pi$ interactions. Size exclusion chromatography was performed, and the mutant protein eluted as a monomer (**Figure 2**), supporting our hypothesis that h12-LOX dimerizes in TOP-to-TOP fashion.

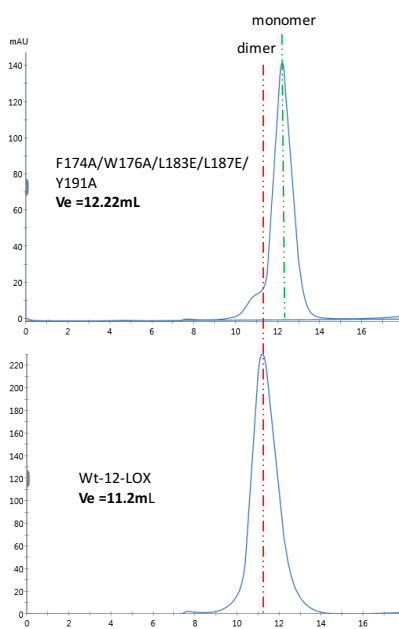


Figure 2. Size exclusion chromatogram of wt-h12-LOX and the F174A/W176A/L183E/L187E/Y191A mutant protein. V_e is elution volume.

Leucine interactions responsible for dimerization.

Having successfully disrupted the h12-LOX dimer using 5 mutations, we further investigated specific interactions of the dimer interface. In the r15-LOX-1 crystallographic dimer, leucines at positions 179, 183, 188 and 192 form a

hydrophobic cluster, contributing to the dimer interface (L179A \longleftrightarrow L192B and L183A \longleftrightarrow L188B, where A and B stand for monomer A and monomer B). Introduction of negatively charged residues (W181E + H585E and L183E + L192E) at the inter-monomer interface disturbed the hydrophobic dimer interaction of r15-LOX-1. In h12-LOX, only two of these leucines are conserved (L178 and L187, corresponding to L179 and L188 in the rabbit sequence), however, other leucines are present in the vicinity, namely L183, L193 and L194 that might contribute to this network of hydrophobic interactions. Therefore, the L183E/L187E mutant was made and characterized by SEC to determine the shift of monomer-dimer equilibrium. As shown in **Figure 3** and confirmed by protein standards (**Supporting information, Figure S3**), L183E/L187E shifted the equilibrium mostly towards monomer, confirming that exchanging the two leucines of the same polypeptide with glutamates, L183 and L187, disrupt the dimer and indicate that they form a leucine A:B pairs at the dimer interface.

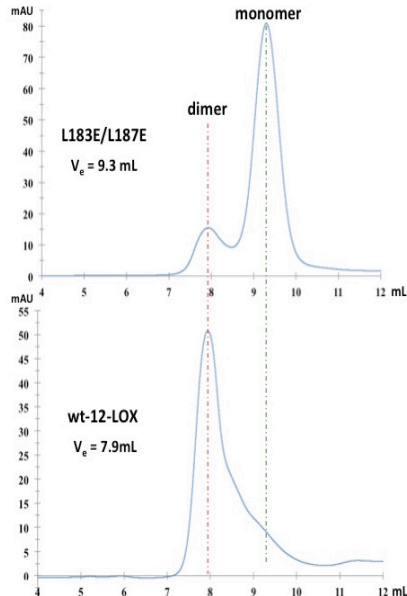


Figure 3. Size exclusion chromatogram of wt-h12-LOX and L183E/L187E monomer mutant.

***In silico* modeling of human h12-LOX dimers.**

In this work, we created a homology model of the h12-LOX monomer structure and then performed protein-protein docking to create models of the dimeric complex. Nine out of the top 10 most energetically favorable docking models (**Supporting Information, Figure S2**) predict a TOP-to-TOP dimeric arrangement of h12-LOX, with the α -helices containing a Leu-rich region (L172, L187, L183 and L194) of the different monomeric units interacting with each other by hydrophobic interactions. Although no symmetry was enforced, most of the models could be described

approximately as either anti-symmetric (head to tail) or symmetric (head to head). Based on the mutagenesis alone, we cannot distinguish which arrangement is more likely to be correct, although the previously proposed h12-LOX dimer is anti-symmetric. In addition, the lowest energy predicted dimer demonstrates $-CH-\pi$ interactions between the side chains of L187 and W176, which may contribute to the stability of the complex. This h12-LOX TOP-to-TOP conformation being stabilized by a network of Leu residues has been previously suggested by SAXS data.³⁰ It is worth noting, however, that the lowest energy docking conformation presented an interface with a higher degree of surface complementarity when compared to the dimeric conformation proposed by SAXS data in our previous work, and therefore these models are not superimposable (**Figure 4**).

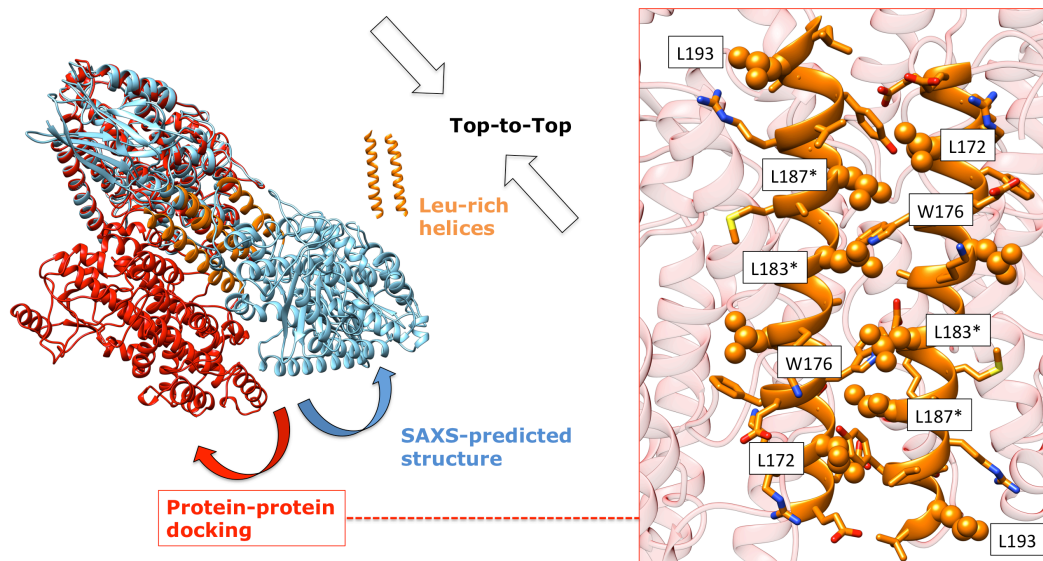


Figure 4. Superimposition of the predicted TOP-to-TOP models of the dimeric structure of h12-LOX from protein-protein docking (red) and SAXS data (blue). In spite of both models showing Leu-rich alpha-helices (orange) at the interface of the dimerization domain, differences in the overall conformation of the predicted structures are observed, with the protein-protein docking predicted model presenting a higher degree of surface complementarity. Leucine residues are shown as balls and sticks representation, while other residues in the helices are shown as sticks. *Mutation sites in this current manuscript.

Comparison of Biochemical Properties of Native Dimer (wt-h12-LOX) vs Mutant Monomer (L183E/L187E).

After identifying L183 and L187 as critical residues for dimerization, the biochemical differences between the dimer (wt-h12-LOX) and monomer (L183E/L187E) were investigated in order to determine if dimerization affected the

biochemistry of h12-LOX. First, the inhibitory potency of wt-h12-LOX (dimer) and L183E/L187E (monomer) by the potent/selective h12-LOX inhibitor, ML355,⁴⁰ was investigated. The results revealed that the inhibitory effect of ML355 against wt-h12-LOX (dimer) was consistent with previous work, with $IC_{50} 0.43 \pm 0.04 \mu M$,³⁶ however, the inhibitory effect of ML355 against the L183E/L187E mutant monomer was almost completely absent (**Table 1**). This discovery suggests that the conformational changes related to oligomerization could translate to active site residues and affect the inhibitor binding. Subsequently, the steady-state kinetics were determined for both wt-h12-LOX (dimer) and L183E/L187E (monomer) and it was observed that the kinetics of L183E/L187E were dramatically slower than that of wt-h12-LOX, with the k_{cat}/K_M being $0.2 \pm 0.02 s^{-1}\mu M^{-1}$ and k_{cat} being $2.4 \pm 0.5 s^{-1}$, which are 13.5-fold and 2.9-fold, respectively, slower than that of wt-h12-LOX (dimer) (**Table 1**). The product profile with AA as the substrate was also examined and for wt-h12-LOX (dimer), 100 % 12S-HETE was detected as the only product, however, for L183E/L187E (monomer) both 12S-HETE ($78 \pm 1 \%$) and 15S-HETE

(22 ± 1 %) were detected (**Table 1**). In previous work, it has shown that r15-LOX-1 dimerization protects the enzyme from kinetic substrate inhibition by shielding the hydrophobic $\alpha 2$ helices.²⁵ However, for h12-LOX, both the dimer and monomer were inactivated at the same level of substrate concentration (**Supporting information, Figure S4**). This observation is contrary to the r15-LOX-1 results where only the mutant monomers revealed substrate/product inactivation above 5-15 μM but not the dimer. In total, these data indicate that the disruption of the dimeric state of h12-LOX translates into an allosteric effect, either through structural or dynamic changes in the active site, ultimately affecting inhibition, catalysis, and the product profile.

Protein	K_M (μM)	k_{cat} (s^{-1})	k_{cat}/K_M ($\mu\text{M})^{-1}\text{s}^{-1}$	Product profile 12S-HETE:15S-HETE	ML355 IC_{50} (μM)
wt-h12-LOX	2.6 ± 0.4	7.0 ± 0.4	2.7 ± 0.3	100:0	0.43 ± 0.04
L183E/L187E	11.2 ± 4	2.4 ± 0.5	0.2 ± 0.02	78:22	>100

Table 1. Steady-state kinetic, AA product profile and ML355 IC_{50} comparison of wt-h12-LOX and L183E/L187E mutant monomer.

Structural stability of the h12-LOX variants assessed by circular dichroism (CD) spectroscopy

The CD spectrum of the wt-h12-LOX dimer variant (**Figure 6**, red trace) shows the characteristic line shape for a lipoxygenase fold that is predominantly α helical. The L183E/L187E mutant has a similar CD spectrum (**Figure 5**, green trace). The thermal stabilities of these variants were measured from CD variable temperature mode collected at 220 nm (**Figure 5**, inset). The resulting melting temperatures, T_{ms} , were virtually identical (50.0 ± 0.7 °C for WT and 48.9 ± 0.6 C for L183E/L187E). These data dismiss any significant protein unfolding or destabilization as the origins of the kinetic properties emerging from the substitution of aliphatic leucine for the charged glutamate residues.

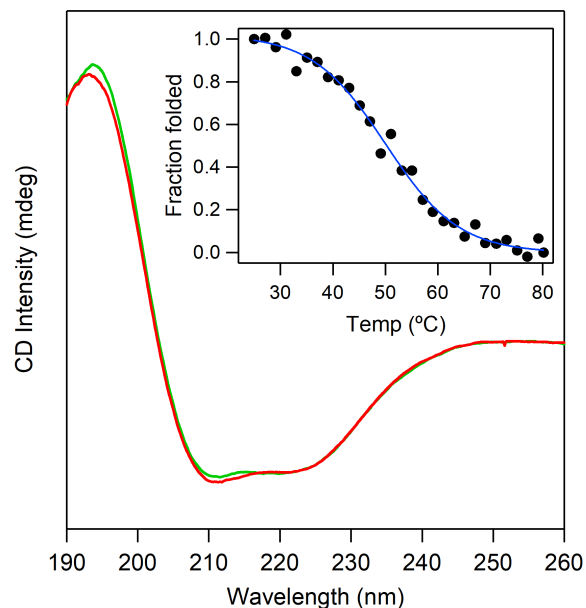


Figure 5. CD spectra of wt-h12-LOX dimer (green trace) and L183E/L187E monomer (red trace), collected at 25 °C. The h12-LOX samples were prepared at 1 μ M concentrations in 25 mM sodium phosphate, pH 7.5 buffer. The inset shows a representative temperature-dependent CD melting curve for wt-h12-LOX.

HDX-MS of wild-type h12-LOX

In this report, to provide a physical basis for the impact of the L183E/L187E mutation on the protein structure and flexibility that could be linked to the empirical differences in catalytic proficiency, we present comparative HDX-MS performed on wt-h12-LOX (dimer) and the mutant monomer variants. HDX-MS is a powerful tool to investigate protein structure, allostery, and protein-ligand and protein-protein interactions.^{39, 41-43} Amide backbone N-H bonds that become protected through

protein-protein (or dimer) interactions typically undergo slower exchange in the presence of deuterium oxide than solvent-exposed sites. Thus, we anticipated reduced HDX-MS exchange rates at the dimer interface of wt-h12-LOX compared to the mutant monomer.

Tandem MS analysis of pepsin-generated peptides of wt-h12-LOX identified 181 peptides corresponding to 90% coverage of the primary sequence. For data reduction purposes, 50 non-overlapping peptides, ranging in length from 5 to 28 amino acid residues (average length, 13 residues), were selected for HDX-MS analysis (**Supporting Information, Figure S5**). The peptide list was well covered over all 10 time points, ranging from 10 seconds to 2 hours, and identical for monomeric form (see below). The percent HDX at three time points was mapped onto the *in silico* model of human 12-LOX (**Figure 6**). These data provide an important, spatially resolved glimpse into structure and protein flexibility of wt-h12-LOX. While HDX-MS and an X-ray crystal structure of another human LOX, human epithelial 15-LOX-2, have been reported,^{29, 44} the pairwise sequence homology between the

isozymes is low (37% identity). It is also important to note that h15-LOX-2 functions as a soluble monomer.

Despite the poor sequence identity, the overall exchange pattern for wt-h12-LOX is similar to that reported for h15-LOX-2 (*cf.* **Supporting Information, Figure S6**),⁴⁴ with one notable and significant distinction in the exchange behavior of helix $\alpha 2$, the central helix in the TOP domain. In h15-LOX-2, the percent exchange is 40-50% at 10 seconds, 70-80% at 3 minutes, and is nearly complete (80-90%) at 2 hours. The exchange pattern for the $\alpha 2$ helix in the wild-type (dimeric) h12-LOX exhibits a decreased extent of exchange accompanied by a more sluggish apparent rate of exchange. More specifically, the percent exchange values are 20-25, 30-40, and 55-65% at 10 seconds, 3 minutes, and 2 hours, respectively. This difference is functionally relevant as helix $\alpha 2$ lines the putative substrate binding channel and has been proposed to be involved in the allosteric control of substrate binding in 15-LOXs from both plants and mammals.⁴⁵ Relevant to the h12-LOX model, proposed herein, it is anticipated that this helix serves as the dimer interface in the

wild-type enzyme. The reduced exchange of helix $\alpha 2$ in wt-h12-LOX (**Figure 7**), relative to h15-LOX-2, is consistent with dampened protein flexibility at this helix and with the assignment of the dimer interface (**Figure 4**).

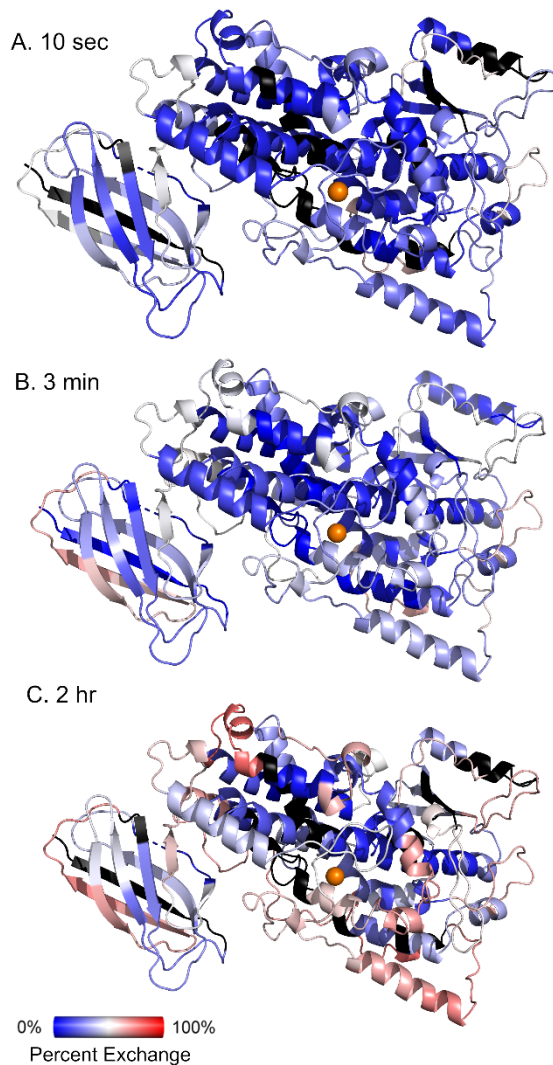


Figure 6. HDX-MS properties of wt-h12-LOX which exists as a dimer in solution. The coloring is defined by the spectrum bar. Black colored peptides represent uncovered regions in the mass spectra. All HDX-MS traces can be found in the supplemental information.

Identification of h12-LOX dimer interface by HDX-MS: Comparison of the wild-type dimer and mutant monomer

Of the non-overlapping peptides (**Figure S5**), 11 exhibited at least a six percent difference in hydrogen exchange extent for at least three time points when the wt-h12-LOX dimer and mutant monomer were compared. Representative peptides illustrating these changes are displayed in **Figure 7**. The differences were found to be localized at two primary sites, helix $\alpha 2$ of the TOP domain and the active site (**Figure 8**). In all altered peptides, the mutant monomer (L183E/L187E) exhibited increased exchange in the form of apparent rates and/or extents of HDX.

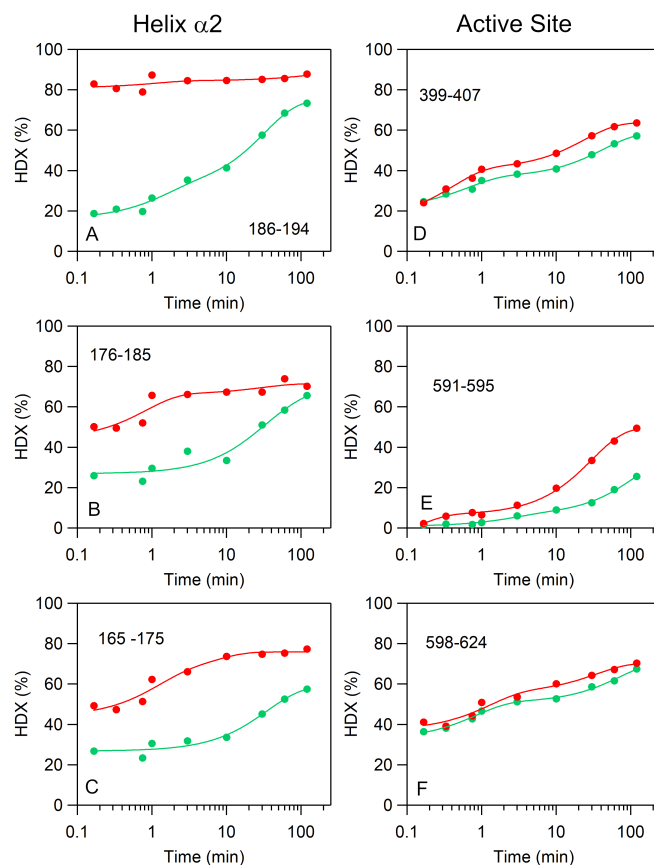


Figure 7. Representative HDX-MS traces that show differences in exchange between the h12-LOX mutant monomer (red trace) and WT dimer (green trace) at the (*left*) helix $\alpha 2$ (site of mutations) and (*right*) active site.

The most dramatic effect in the HDX-MS is seen at the site of the L187→E mutation (**Figure 7A**, peptide 186-194). At 10 seconds, the exchange was 18% for dimeric wt-h12-LOX and increased to 83 % for the monomeric L183E/L187E mutant. This corresponds to *ca.* 65% difference in the extents of exchange at this time point; this percent exchange variance is represented as red coloring on the protein model in **Figure 8**. As the exchange time reaches 2 hours, the HDX percent of the dimer

increases to 74%, while the HDX of the mutant monomer increases only slightly. The near complete exchange of this peptide for the monomer at all time points precludes a quantitative analysis for the apparent exchange rates. In addition to this peptide, the adjacent peptide, 176-185, which harbors another mutation (L183E), also showed an enhanced exchange behavior for the mutant monomer. From the multi-exponential fits to the data (**Figure 7B**), the apparent averaged rate of exchange for the mutant was 30-fold faster than wt-h12-LOX. Note that mutations, especially non-conserved mutations, can shift the LC retention times that can alter the intrinsic HDX back-exchange values. Indeed, the L→E mutation shifts the LC elution for both peptides, 176-185 and 186-195, from *ca.* 8.4 and 7.9 min to 7.6 and 7.7 min, respectively. To correct for these retention time shifts, back-exchange values were corrected for individual peptides and measured for both wt-h12-LOX and L183E/L187E variants (see **Supporting Information Excel File**). The 176-185 peptide exhibited the largest perturbation in the back-exchange value, from 11.4% in the WT to 21.4% in the mutant, despite comparable LC retention times.

Importantly, there are two additional peptides (155-164 and 165-175), connected at the N-terminus of peptide 176-185, that do not contain a mutation and yet the HDX-MS behavior between dimer and monomer h12-LOX follows that seen for peptide 176-185. These peptides are represented by green and orange coloring, respectively, in **Figure 8**. Additional overlapping peptides further support these trends (**Supporting Information, Figure S7**). Together, these HDX-MS properties are consistent with enhanced peptide flexibility resulting from loss of dimerization.

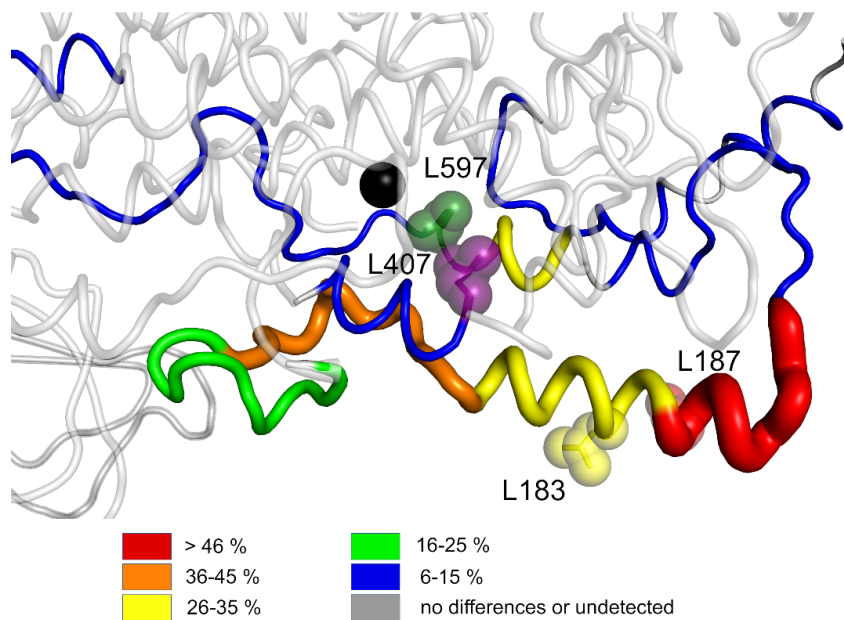


Figure 8. HDX-MS differences between the h12-LOX mutant monomer and wild-type dimer, mapped onto the *in silico* model. The largest degree of HDX differences (in %) for a given peptide and time is color coded on the structure by the legend and represented by changes in cartoon putty radii. The residues that mark the

site of mutation (L183→E, L187→E) are represented as spheres. Conserved active site leucine residues, L407 and L597, are shown as purple and forest spheres, respectively.

In addition to helix $\alpha 2$, the HDX-MS properties of peptides at the active site were also affected (*cf.* **Figure 7D-F**). These peptides (396-417, 591-595, and 598-624) are predicted to make direct contact with the $\alpha 2$ helix, and their backbone flexibility is greatly influenced (i.e. loosened up) by the change in oligomerization. The first example, peptide 396-417, represents the arched helix, which runs parallel to helix $\alpha 2$ and covers the active site pocket. It contains the invariant leucine, L407 (**Figure 8**, purple spheres), that is located at the hinge region of the U-shaped substrate binding channel. Mutation of this residue to alanine was previously shown to increase the substrate cavity volume and linked to a 100-fold reduction in both the first- and second-order rate constants and a slight shift in AA product distribution.⁴⁶ The latter two peptides flank L597 that is located across the binding channel from and proximal to L407. Mutational studies of L597 have not been performed, but the alanine mutation of the orthologous residue in the model 15-LOX from plants (SLO-1), L754A, leads to a 1,000-fold decreased k_{cat} .⁴⁷ It has been concluded that these two

residues are critical for the proper positioning of the substrate with respect to the metallocofactor.⁴⁸ While the enzyme activity of these mutations is more compromised than that from the change in oligomerization reported herein, it illustrates how even subtle alterations to the positioning and/or conformational motions of these side chains can be linked to impaired catalytic proficiency. The results further implicate a role for allostery stemming from helix $\alpha 2$ and induced by oligomerization changes that likely accounts for the decreased catalytic proficiency, altered product distribution, and loss of wt-h12-LOX (dimer)-selective inhibitor effects in the case of the monomer.

Note that there are no significant HDX-MS differences observed for peptides located in the h12-LOX PDZ or PLAT domains. The PDZ domain was previously proposed to mediate the dimerization in the coral 11R-LOX.³¹ However, from our data, HDX traces for peptides covering the PDZ domain were identical when the wt-h12-LOX dimer and mutant monomer were compared (for example, see peptides 241-251, 265-273, and 300-315 in **Supporting Information HDX traces pdf**). Thus,

we can rule out the PDZ domain as the site for the dimer interface in wt-h12-LOX. Likewise, HDX-MS properties of peptides in the PLAT domain (residues 1-110), which serves to interact with the phospholipid membrane, are largely unchanged upon mutation of L183 and L187. These data combined with the previously reported SAXS data and our *in silico* model provide compelling support for the anti-parallel arrangement for wt-h12-LOX dimerization, in which the contacts are made along helix $\alpha 2$ of the TOP domain.

We cannot eliminate the possibility that the nonconservative mutations of leucine to glutamate do not contribute to the enhanced flexibility of helix $\alpha 2$. For example, a catalytically impairing mutant, I553G, of SLO-1 has been shown to influence the flexibility of helix $\alpha 2$ by HDX-MS;⁴⁹ however, these effects are relatively modest compared to the drastic effects in HDX that are presented in **Figure 7**. In addition, the L183E/L187E mutation, presented herein, clearly shifts the oligomerization state from dimer (WT) to a soluble monomer. The variable temperature CD measurements also support the conclusion that the mutant does not

greatly perturb the protein structure and stability. Together with the lack of any observed HDX differences at the protein surface (other than helix $\alpha 2$), the data support the model presented in **Figure 4** in which the dimer interface is formed between the TOP domains and along helix $\alpha 2$.

4.5 Conclusion

There is experimental data that indicates that h12-LOX exists as a dimer in solution, but since there is no crystal structure of an active, full-length h12-LOX, there is little molecular information about its dimeric interactions. In the current work, we demonstrate that mutations of Leu183 and Leu187 to Glu have successfully disrupted the h12-LOX wt-dimer, which suggests dimerization is favored by Leu-zippers involving both monomeric units. Recent findings for coral 11R-LOX show that leucines in that upper helix impact its stereo- and regio-specificity,⁵⁰ which suggests that these hydrophobic residues may have importance in other LOX isozymes as well. In addition, our protein-protein docking results predict the dimerization of h12-LOX in a TOP-to-TOP orientation, corroborating previous results based on SAXS analysis and *in silico* modeling, with this network of α -helix Leu residues in the dimeric interface.²⁹ The dimer interaction at the $\alpha 2$ helix within the TOP subdomain was validated through HDX-MS results in which enormous enhancements were observed

in the apparent rates and the extent of exchange that accompany mutant-induced loss of dimerization. Interestingly, the *in vitro* kinetics and inhibitor profile of the monomer h12-LOX was distinct from the dimer, indicating a significant allosteric effect on the active site structure due to dimerization. These observations were supported by our HDX investigations where enhanced flexibility of helix $\alpha 2$ was accompanied by enhanced flexibility of spatially adjacent active site peptides that are expected to alter the proper positioning of substrate and inhibitor within the binding pocket.

These data raise the obvious question, what is the biological role of the h12-LOX dimer in the cell? It is not unusual to observe a conformational change upon protein dimerization and that conformational interconversion could depend on concentration.⁵¹ Therefore, the dimer could present a structurally distinct species in the cell, affecting protein:protein interactions of h12-LOX, as has been previously postulated with respect to platelet activation.⁵² It is also possible that having two membrane association domains in close proximity, which occurs in the dimer, could

enhance membrane association of h12-LOX in the cell. Finally, the biological activity of the h12-LOX dimer could depend on its ability to form a heterodimer. The iron content in h12-LOX samples is not always tested and is very seldom mentioned. Our own results and the results reported by others,^{35, 53, 54} show that the iron content varies from 0.01 to 0.67 iron atoms per molecule of h12-LOX. This means there is always a mixture of catalytically active molecules (E_{cat}) and inactive molecules that do not contain iron (E_{apo}), which could form a heterodimer ($E_{\text{cat}}:E_{\text{apo}}$). Heterodimers have been observed in the COX isozymes,²¹ where the E_{apo} acts as an allosteric domain and therefore h12-LOX may also function as a heterodimer in a similar manner. We are currently investigating all of these possibilities with h12-LOX, in the hopes of understanding the biological role of the dimer further and possibly developing inhibitors against this function.

4.6 Abbreviations

LOX, lipoxygenase; h12-LOX, human platelet 12S-lipoxygenase; r15-LOX-1 or r12/15-LOX or rALOX15, rabbit 15S-LOX-1; c11-LOX, coral 11R-LOX; AA, arachidonic acid; 12(S)-HpETE, 12(S)-hydroperoxyeicosatetraenoic acid; 12(S)-HETE, 12(S)-hydroxyeicosatetraenoic acid; COX, cyclooxygenase; ML355, h12-LOX specific inhibitor; NSAIDs, nonsteroidal anti-inflammatory drugs; coxibs, COX-2 selective inhibitors; 13-HpODE, 13S-hydroperoxyoctadeca-9Z,11E-dienoic acid; 13-HODE, 13S-hydroxyoctadeca-9Z,11E-dienoic acid; TOP, a subdomain region in the helical bundle of the catalytic domain (residues 163-222); PLAT domain, Polycystin-1, Lipoxygenase, Alpha-Toxin: PDZ domain, PSD95, Dig1, Zo-1 domain; E_{cat}, catalytically active enzyme; E_{apo}, inactive Fe-free enzyme; SAXS, Small angle X-ray scattering; ICP-MS, inductively coupled plasma mass spectrometer; SEC, size exclusion chromatography; BSA, bovine serum albumin; DCM, dichloromethane; HDX-MS, hydrogen deuterium exchange-mass spectrometry; wt-h12-LOX, wild-type

human platelet 12S-lipoxygenase; h15-LOX-2, human epithelial 15-lipoxygenase;

SLO-1, soybean lipoxygenase-1.

References:

- [1] Brash, A. R. (1999) Lipoxygenases: Occurrence, Functions, Catalysis and Acquisition of Substrate, *J. Biol. Chem.* 274, 23679-23682.
- [2] Kuhn, H., Saam, J., Eibach, S., Holzhutter, H. G., Ivanov, I., and Walther, M. (2005) Structural biology of mammalian lipoxygenases: enzymatic consequences of targeted alterations of the protein structure, *Biochem Biophys Res Commun* 338, 93-101.
- [3] Newcomer, M. E., and Brash, A. R. (2015) The structural basis for specificity in lipoxygenase catalysis, *Protein Sci* 24, 298-309.
- [4] Kagan, V. E., Mao, G., Qu, F., Angeli, J. P., Doll, S., Croix, C. S., Dar, H. H., Liu, B., Tyurin, V. A., Ritov, V. B., Kapralov, A. A., Amoscato, A. A., Jiang, J., Anthonymuthu, T., Mohammadyani, D., Yang, Q., Proneth, B., Klein-Seetharaman, J., Watkins, S., Bahar, I., Greenberger, J., Mallampalli, R. K., Stockwell, B. R., Tyurina, Y. Y., Conrad, M., and Bayir, H. (2017) Oxidized arachidonic and adrenic PEs navigate cells to ferroptosis, *Nat Chem Biol* 13, 81-90.
- [5] Drefs, M., Thomas, M. N., Guba, M., Angele, M. K., Werner, J., Conrad, M., Steib, C. J., Holdt, L. M., Andrassy, J., Khandoga, A., and Rentsch, M. (2017) Modulation of Glutathione Hemostasis by Inhibition of 12/15-Lipoxygenase Prevents ROS-Mediated Cell Death after Hepatic Ischemia and Reperfusion, *Oxid Med Cell Longev* 2017, 8325754.
- [6] Friedmann Angeli, J. P., Schneider, M., Proneth, B., Tyurina, Y. Y., Tyurin, V. A., Hammond, V. J., Herbach, N., Aichler, M., Walch, A., Eggenhofer, E., Basavarajappa, D., Radmark, O., Kobayashi, S., Seibt, T., Beck, H., Neff, F., Esposito, I., Wanke, R., Forster, H., Yefremova, O., Heinrichmeyer, M., Bornkamm, G. W., Geissler, E. K., Thomas, S. B., Stockwell, B. R., O'Donnell, V. B., Kagan, V. E., Schick, J. A., and Conrad, M. (2014) Inactivation of the ferroptosis regulator Gpx4 triggers acute renal failure in mice, *Nat Cell Biol* 16, 1180-1191.
- [7] Toppo, S., Flohe, L., Ursini, F., Vanin, S., and Maiorino, M. (2009) Catalytic

mechanisms and specificities of glutathione peroxidases: variations of a basic scheme, *Biochim Biophys Acta* 1790, 1486-1500.

- [8] Tourdot, B. E., and Holinstat, M. (2017) Targeting 12-Lipoxygenase as a Potential Novel Antiplatelet Therapy, *Trends Pharmacol Sci* 38, 1006-1015.
- [9] Hussain, H., Shornick, L. P., Shannon, V. R., Wilson, J. D., Funk, C. D., Pentland, A. P., and Holtzman, M. J. (1994) Epidermis Contains Platelet-Type 12-Lipoxygenase that is Overexpressed in Germinal Layer Keratinocytes in Psoriasis, *Am. J. Physiol.* 266, C243-C253.
- [10] Ma, K., Nunemaker, C. S., Wu, R., Chakrabarti, S. K., Taylor-Fishwick, D. A., and Nadler, J. L. (2010) 12-Lipoxygenase Products Reduce Insulin Secretion and β -Cell Viability in Human Islets, *J Clin Endocrinol Metab* 95, 887-893.
- [11] Tersey, S. A., Bolanis, E., Holman, T. R., Maloney, D. J., Nadler, J. L., and Mirmira, R. G. (2015) Minireview: 12-Lipoxygenase and Islet β -Cell Dysfunction in Diabetes, *Mol Endocrinol* 29, 791-800.
- [12] Semeraro, M. L., Glenn, L. M., and Morris, M. A. (2017) The Four-Way Stop Sign: Viruses, 12-Lipoxygenase, Islets, and Natural Killer Cells in Type 1 Diabetes Progression, *Front Endocrinol (Lausanne)* 8, 246.
- [13] Connolly, J. M., and Rose, D. P. (1998) Enhanced angiogenesis and growth of 12-lipoxygenase gene-transfected MCF-7 human breast cancer cells in athymic nude mice, *Cancer Lett* 132, 107-112.
- [14] Natarajan, R., and Nadler, J. (1998) Role of lipoxygenases in breast cancer., *Front. Biosci.* 3, E81-88.
- [15] Ding, X. Z., Iversen, P., Cluck, M. W., Knezetic, J. A., and Adrian, T. E. (1999) Lipoxygenase inhibitors abolish proliferation of human pancreatic cancer cells., *Biochemical and Biophysical Research Communications* 261, 218-223.
- [16] Shappell, S. B., Olson, S. J., Hannah, S. E., Manning, S., Roberts, R. L., Masumori, N., Jisaka, M., Boeglin, W. E., Vader, V., Dave, D. S., Shook, M. F., Thomas, T. Z., Funk, C. D., Brash, A. R., and Matusik, R. J. (2003) Elevated expression of 12/15-lipoxygenase and cyclooxygenase-2 in a

- transgenic mouse model of prostate carcinoma, *Cancer Res* 63, 2256-2267.
- [17] Guo, A. M., Liu, X., Al-Wahab, Z., Maddipati, K. R., Ali-Fehmi, R., Scicli, A. G., and Munkarah, A. R. (2011) Role of 12-lipoxygenase in regulation of ovarian cancer cell proliferation and survival, *Cancer Chemother Pharmacol* 68, 1273-1283.
- [18] Prasad, V. V., Kolli, P., and Moganti, D. (2011) Association of a functional polymorphism (Gln261Arg) in 12-lipoxygenase with breast cancer, *Exp Ther Med* 2, 317-323.
- [19] Dailey, L. A., and Imming, P. (1999) 12-Lipoxygenase: Classification, Possible Therapeutic Benefits from Inhibition and Inhibitors, *Curr. Med. Chem.* 6, 389-398.
- [20] Berglund, L., Bjorling, E., Oksvold, P., Fagerberg, L., Asplund, A., Szigartyo, C. A., Persson, A., Ottosson, J., Wernerus, H., Nilsson, P., Lundberg, E., Sivertsson, A., Navani, S., Wester, K., Kampf, C., Hober, S., Ponten, F., and Uhlen, M. (2008) A genecentric Human Protein Atlas for expression profiles based on antibodies, *Mol Cell Proteomics* 7, 2019-2027.
- [21] Sidhu, R. S., Lee, J. Y., Yuan, C., and Smith, W. L. (2010) Comparison of cyclooxygenase-1 crystal structures: cross-talk between monomers comprising cyclooxygenase-1 homodimers, *Biochemistry* 49, 7069-7079.
- [22] Dong, L., Vecchio, A. J., Sharma, N. P., Jurban, B. J., Malkowski, M. G., and Smith, W. L. (2011) Human cyclooxygenase-2 is a sequence homodimer that functions as a conformational heterodimer, *J Biol Chem* 286, 19035-19046.
- [23] Gillmor, S. A., Villasenor, A., Fletterick, R., Sigal, E., and Browner, M. (1997) The structure of mammalian 15-lipoxygenase reveals similarity to the lipases and the determinants of substrate specificity., *Nature Struct. Biol.* 4, 1003-1009.
- [24] Choi, J., Chon, J. K., Kim, S., and Shin, W. (2008) Conformational flexibility in mammalian 15S-lipoxygenase: Reinterpretation of the crystallographic data, *Proteins* 70, 1023-1032.
- [25] Ivanov, I., Shang, W., Toledo, L., Masgrau, L., Svergun, D. I., Stehling, S.,

- Gómez, H., Di Venere, A., Mei, G., Lluch, J. M., Skrzypczak-Jankun, E., González-Lafont, À., and Kühn, H. (2012) Ligand-induced formation of transient dimers of mammalian 12/15-lipoxygenase: A key to allosteric behavior of this class of enzymes?, *Proteins: Structure, Function, and Bioinformatics* 80, 703-712.
- [26] Neau, D. B., Gilbert, N. C., Bartlett, S. G., Boeglin, W., Brash, A. R., and Newcomer, M. E. (2009) The 1.85 Å structure of an 8R-lipoxygenase suggests a general model for lipoxygenase product specificity, *Biochemistry* 48, 7906-7915.
- [27] Gilbert, N. C., Bartlett, S. G., Waight, M. T., Neau, D. B., Boeglin, W. E., Brash, A. R., and Newcomer, M. E. (2011) The structure of human 5-lipoxygenase, *Science* 331, 217-219.
- [28] Oldham, M. L., Brash, A. R., and Newcomer, M. E. (2005) Insights from the X-ray crystal structure of coral 8R-lipoxygenase: calcium activation via a C2-like domain and a structural basis of product chirality, *J Biol Chem* 280, 39545-39552.
- [29] Kobe, M. J., Neau, D. B., Mitchell, C. E., Bartlett, S. G., and Newcomer, M. E. (2014) The structure of human 15-lipoxygenase-2 with a substrate mimic, *J Biol Chem* 289, 8562-8569.
- [30] Aleem, A. M., Jankun, J., Dignam, J. D., Walther, M., Kuhn, H., Svergun, D. I., and Skrzypczak-Jankun, E. (2008) Human platelet 12-lipoxygenase, new findings about its activity, membrane binding and low-resolution structure, *J Mol Biol* 376, 193-209.
- [31] Eek, P., Poldemaa, K., Kasvandik, S., Jarving, I., and Samel, N. (2017) A PDZ-like domain mediates the dimerization of 11R-lipoxygenase, *Biochim Biophys Acta Mol Cell Biol Lipids* 1862, 1121-1128.
- [32] Aleem, A. M., Wells, L., Jankun, J., Walther, M., Kuhn, H., Reinartz, J., and Skrzypczak-Jankun, E. (2009) Human platelet 12-lipoxygenase: naturally occurring Q261/R261 variants and N544L mutant show altered activity but unaffected substrate binding and membrane association behavior, *Int J Mol*

Med 24, 759-764.

- [33] Shang, W., Ivanov, I., Svergun, D. I., Borbulevych, O. Y., Aleem, A. M., Stehling, S., Jankun, J., Kuhn, H., and Skrzypczak-Jankun, E. (2011) Probing dimerization and structural flexibility of mammalian lipoxygenases by small-angle X-ray scattering, *J Mol Biol* 409, 654-668.
- [34] Amagata, T., Whitman, S., Johnson, T. A., Stessman, C. C., Loo, C. P., Lobkovsky, E., Clardy, J., Crews, P., and Holman, T. R. (2003) Exploring sponge-derived terpenoids for their potency and selectivity against 12-human, 15-human, and 15-soybean lipoxygenases, *J Nat Prod* 66, 230-235.
- [35] Segraves, E. N., and Holman, T. R. (2003) Kinetic investigations of the rate-limiting step in human 12- and 15-lipoxygenase, *Biochemistry* 42, 5236-5243.
- [36] Luci, D. K., Jameson, J. B., Yasgar, A., Diaz, G., Joshi, N., Kantz, A., Markham, K., Perry, S., Kuhn, N., Yeung, J., Kerns, E. H., Schultz, L., Holinstat, M., Nadler, J. L., Taylor-Fishwick, D. A., Jadhav, A., Simeonov, A., Holman, T. R., and Maloney, D. J. (2014) Synthesis and Structure-Activity Relationship Studies of 4-((2-Hydroxy-3-methoxybenzyl)amino)benzenesulfonamide Derivatives as Potent and Selective Inhibitors of 12-Lipoxygenase, *J Med Chem* 57, 495-506.
- [37] Pierce, B. G., Wiehe, K., Hwang, H., Kim, B. H., Vreven, T., and Weng, Z. (2014) ZDOCK server: interactive docking prediction of protein-protein complexes and symmetric multimers, *Bioinformatics* 30, 1771-1773.
- [38] Pascal, B. D., Willis, S., Lauer, J. L., Landgraf, R. R., West, G. M., Marciano, D., Novick, S., Goswami, D., Chalmers, M. J., and Griffin, P. R. (2012) HDX Workbench: software for the analysis of H/D exchange MS data, *J. Am. Soc. Mass Spectrom.* 23, 1512-1521.
- [39] Hoofnagle, A. N., Resing, K. A., and Ahn, N. G. (2003) Protein analysis by hydrogen exchange mass spectrometry, *Annu. Rev. Biophys. Biomol. Struct.* 32, 1-25.
- [40] Luci, D. K., Jameson, J. B., Yasgar, A., Diaz, G., Joshi, N., Kantz, A., Markham,

- K., Perry, S., Kuhn, N., Yeung, J., Kerns, E. H., Schultz, L., Holinstat, M., Nadler, J. L., Taylor-Fishwick, D. A., Jadhav, A., Simeonov, A., Holman, T. R., and Maloney, D. J. (2014) Synthesis and Structure-Activity Relationship Studies of 4-((2-Hydroxy-3-methoxybenzyl)amino)benzenesulfonamide Derivatives as Potent and Selective Inhibitors of 12-Lipoxygenase, *Journal of Medicinal Chemistry* 57, 495-506.
- [41] Englander, S. W. (2006) Hydrogen exchange and mass spectrometry: a historical perspective, *J. Am. Soc. Mass Spectrom.* 17, 1481-1489.
- [42] Konermann, L., Pan, J., and Liu, Y.-H. (2011) Hydrogen exchange mass spectrometry for studying protein structure and dynamics, *Chem. Soc. Rev.* 40, 1224-1234.
- [43] Pirrone, G. F., Iacob, R. E., and Engen, J. R. (2015) Applications of hydrogen/deuterium exchange MS from 2012 to 2014, *Anal. Chem.* 87, 99-118.
- [44] Droege, K. D., Keithly, M. E., Sanders, C. R., Armstrong, R. N., and Thompson, M. K. (2017) Structural dynamics of 15-lipoxygenase-2 via hydrogen-deuterium exchange, *Biochemistry* 56, 5065-5074.
- [45] Offenbacher, A. R., and Holman, T. R. (2020) Fatty acid allosteric regulation of C-H activation in plant and animal lipoxygenases, *Molecules* 25, 3374.
- [46] Aleem, A. M., Tsai, W.-C., Tena, J., Alvarez, G., Deschamps, J., Kalyanaraman, C., Jacobson, M. P., and Holman, T. R. (2019) Probing the electrostatic and steric requirements for substrate binding in human platelet-type 12-lipoxygenase, *Biochemistry* 58, 848-857.
- [47] Knapp, M. J., Rickert, K., and Klinman, J. P. (2002) Temperature-dependent isotope effects in soybean lipoxygenase-1: correlating hydrogen tunneling with protein dynamics, *J. Am. Chem. Soc.* 124, 3865-3874.
- [48] Hu, S., Offenbacher, A. R., Thompson, E. M., Gee, C. L., Wilcoxon, J., Carr, C. A. M., Prigozhin, D. M., Yang, V., Alber, T., Britt, R. D., Fraser, J. S., and Klinman, J. P. (2019) Biophysical characterization of a disabled double mutant of soybean lipoxygenase: the 'undoing' of precise substrate positioning

- relative to metal cofactor and an identified dynamical network, *J. Am. Chem. Soc.* *141*, 1555-1567.
- [49] Offenbacher, A. R., Hu, S., Poss, E. M., Carr, C. A. M., Scouras, A. D., Prigozhin, D. M., Iavarone, A. T., Palla, A., Alber, T., Fraser, J. S., and Klinman, J. P. (2017) Hydrogen-deuterium exchange of lipoxygenase uncovers a relationship between distal, solvent exposed protein motions and the thermal activation barrier for catalytic proton-coupled electron tunneling, *ACS Cent. Sci.* *3*, 570-579.
- [50] Newie, J., Neumann, P., Werner, M., Mata, R. A., Ficner, R., and Feussner, I. (2017) Lipoxygenase 2 from *Cyanotheca* sp. controls dioxygen insertion by steric shielding and substrate fixation, *Sci Rep* *7*, 2069.
- [51] Lella, M., and Mahalakshmi, R. (2017) Metamorphic Proteins: Emergence of Dual Protein Folds from One Primary Sequence, *Biochemistry* *56*, 2971-2984.
- [52] Yeung, J., Tourdot, B. E., Fernandez-Perez, P., Vesci, J., Ren, J., Smyrniotis, C. J., Luci, D. K., Jadhav, A., Simeonov, A., Maloney, D. J., Holman, T. R., McKenzie, S. E., and Holinstat, M. (2014) Platelet 12-LOX is essential for FcγRIIa-mediated platelet activation, *Blood* *124*, 2271-2279.
- [53] Deschamps, J. D., Gautschi, J. T., Whitman, S., Johnson, T. A., Gassner, N. C., Crews, P., and Holman, T. R. (2007) Discovery of platelet-type 12-human lipoxygenase selective inhibitors by high-throughput screening of structurally diverse libraries, *Bioorganic & Medicinal Chemistry* *15*, 6900-6908.
- [54] Suzuki, H., Kishimoto, K., Yoshimoto, T., Yamamoto, S., Kanai, F., Ebina, Y., Miyatake, A., and Tanabe, T. (1994) Site-directed mutagenesis studies on the iron-binding domain and the determinant for the substrate oxygenation site of porcine leukocyte arachidonate 12-lipoxygenase, *Biochim Biophys Acta* *1210*, 308-316.

Chapter 5

Docking and Mutagenesis Studies Lead to Improved Inhibitor Development of ML355 for Human Platelet 12-lipoxygenase

5.1 Abstract

Human platelet 12-(S)-Lipoxygenase (12-LOX) is a fatty acid metabolizing oxygenase that plays an important role in platelet activation. Uncontrolled platelet activation is a hallmark of cardiovascular diseases, which remain the leading cause of death worldwide. Side effects associated with current anti-platelet therapies motivate the search for new drugs. Several studies implicate 12-LOX as a potential novel target for antiplatelet therapeutics. ML355 is a specific 12-LOX inhibitor that has been shown to decrease thrombosis without prolonging hemostasis. It has an amenable drug-like scaffold with nM potency and encouraging ADME and PK profiles. The current study is an attempt to gain insight into the binding of ML355 to 12-LOX in order to improve its binding potency and drug-like qualities.

5.2 Introduction

Human Platelet-type 12-(S)-lipoxygenase (12-LOX) is a non-heme iron-containing oxygenase that catalyzes the regio- and stereo-specific addition of molecular oxygen to polyunsaturated fatty acids (PUFA).[1] 12-LOX belongs to a family of enzymes that also include 5-LOX and 15-LOX, which oxygenate arachidonic acid (AA) at their corresponding carbon positions. The hydroperoxyeicosatetraenoic acid (HPETE) product is subsequently reduced by cellular peroxidases to form the hydroxyeicosatetraenoic acid (HETE), which in the case of 12-LOX is 12-(S)-HETE.[2]

Although 12-LOX expression is predominantly restricted to platelets (~14,000 molecules per platelet), it is also expressed in some hematopoietic and solid tumors[3, 4] To date, 12-LOX is the only LOX isoform identified to be present in platelets, and its activity is crucial for a number of platelet functions, including granule secretion, platelet aggregation, and normal adhesion through specific agonist-mediated

pathways, such as collagen and the thrombin receptor, PAR4.[5] Normal platelet activation plays a central role in the regulation of hemostasis, but uncontrolled activation can lead to pathologic thrombotic events, such as ischemic coronary heart disease.[6-12] Although currently approved antiplatelet drugs, such as Ticlopidine , Clopidogrel, Prasugrel , Abciximab , Eptifibatide , Tirofiban and Dipyridamole have significantly decreased the morbidity and mortality of ischemic heart disease, their efficacy is limited by the subsequent increased risk of severe bleeding.[13] This limitation has motivated the development of new approaches for limiting platelet activation, and a number of new platelet targets are currently being investigated for their potential to limit clot formation, such as thrombin receptor (PAR1), α IIB β 3 and GPVI antagonists (reviewed by Holinstat and coworkers).[13] In addition to these new platelet targets, we propose that since 12-LOX is one of the key pro-thrombotic enzymes within the platelet, it may also be an effective approach to anti-platelet therapy.[5, 14, 15]

Few potent and selective 12-LOX inhibitors have been reported in the literature.

Initially, selective 12-LOX inhibitors were found in natural sources, such as hinokitiol, bromophenols and isoflavanones, however, their drug-like properties were marginal. High-throughput screening produced a number of selective inhibitors, but like with the natural products, the drug-like properties of most of them were not optimal for drug development, except for one, ML355. ML355 ((N-benzo[d]thiazol-2-yl)-4((2-hydroxy-3 methoxybenzyl) amino) benzenesulfonamide) is a non-reductive, reversible, mixed-type 12-LOX inhibitor with nM potency and excellent selectivity over related enzymes, including 5-LOX, 15-LOX-1, 15-LOX-2, COX1, and COX2.[16] ML355 has a drug-like scaffold, with encouraging *in vitro* absorption, distribution, metabolism and excretion (ADME) and *in vivo* pharmacokinetic (PK) profiles. *In vitro* studies have shown that ML355 reduces platelet aggregation in response to low dose platelet activators[17] and oral administration of ML355 in mice limits thrombosis formation without significant prolongation of hemostasis.[18] ML355 also inhibits platelet activation mediated by the immune receptor, FcγRIIa,[17] which is required for immune-mediated

thrombocytopenia, such as heparin-induced thrombocytopenia (HIT). ML355 has been used to delineate the role of 12-LOX in hemostasis,[17] and improves human islet function after cytokine treatment in vitro.[19] These studies indicate that ML355 could represent a viable approach to decrease platelet reactivity following vascular insult or injury, while minimizing the increased risk of bleeding that is concomitant with antiplatelet therapy.[20] Nonetheless, there is limited information on the molecular nature of ML355 binding to 12-LOX. In the current work, we employ site-directed mutagenesis and molecular modeling to elucidate a binding model of ML355 to its target 12-LOX, and utilize that information to guide the synthesis of a novel 12-LOX inhibitor. This novel inhibitor has 8-fold improved potency and equivalent cellular activity in human islets relative to ML355, and indicates possible avenues for improved analogues to ML355.

5.3 Materials and Methods

Chemicals.

Fatty acids used in this study were purchased from Nu Chek Prep, Inc. (MN, USA). All other solvents and chemicals were reagent grade or better and were used as purchased without further purification.

Molecular Modeling

A homology model of the human platelet 12-LOX catalytic domain (Uniprot accession P18054) was built based on the porcine leukocyte 12(S)-LOX structure (PDB ID: 3RDE, sequence identity 65%), using the software Prime (version 6.0, Schrodinger Inc.). During homology modeling, the metal ion (Fe^{3+}), the iron coordinated hydroxide ion and the co-crystallized ligand, 3-{4-[(tridec-2-yn-1-yloxy)methyl] phenyl} propanoic acid, from the porcine 12(S)-LOX structure were retained. In the published structure, a water is shown coordinating the metal ion; for our modeling purposes, we assigned iron to the ferric (Fe^{3+}) oxidation state, with a

coordinating hydroxide to mimic the catalytically-competent state and complete the octahedral symmetry [21]. The human 12-LOX model was subsequently energy minimized using Protein Preparation Wizard (Schrodinger Inc). During this step, hydrogen atoms were added and optimized to make better hydrogen bonding interactions, and all heavy atoms were energy minimized with a restraint such that they did not move beyond 0.3 Å from their starting positions. The structure of **ML355** was prepared using Edit/Build panel of Maestro software (version 12.4, Schrodinger Inc.) and energy minimized using LigPrep software (Schrodinger Software Suite 2020-2).

Initially, we docked **ML355** to the wild-type (wt) protein using the docking software Glide (version 8.7, Schrodinger Inc.), consisting of grid preparation and virtual screening. We used the coordinates of the co-crystallized ligand from the porcine 12-LOX homolog to define the grid center. Following grid preparation, we docked **ML355** to the h12-LOX active site using standard-precision (SP) scoring function. Only the ligand was treated flexibly during docking.

Starting from the wt protein structural model, we made each mutant protein using the *Mutate Residue* option in the Build panel of the Maestro software. After making the virtual mutation, we predicted sidechain conformation of the mutated residue using the software Prime (version 6.0, Schrodinger Inc.). During the sidechain prediction step, except for the metal and the hydroxide ions, all the other modeled compounds were removed from the active site. The protein was held rigid and only the conformation of the mutated residue was optimized. We then used the coordinates of ML355 docked to the wt protein to define the docking grid center for each mutant protein. After the grid preparation step, ML355 was docked to the mutant proteins using Glide with the SP scoring function.

Site-Directed Mutagenesis

Based on the ML355 binding mode predicted by the modeling, we selected all residues within 5 Å of any atom of ML355 for experimental mutagenesis. The selected residues were replaced with amino acids with either bulkier or smaller side chains in order to determine what specific interactions play a role in inhibitor binding.

The following mutations were made: F352L, I399L, I399M, E356A, E356K, L361M, R402L, A403S, L407A, L407G, I413A, F414L, A417I, V418M, A417I/V418M, Q547L, and L597M. The numbering refers to the UniProt accession number P18054 sequence, with the N-terminal methionine assigned as amino acid number one. The primers for all mutants were designed using the online QuikChange Primer Design tool (<http://www.genomics.agilent.com/primerDesignProgram.jsp>) from Agilent Technologies (CA, USA). The mutations were introduced by using the QuikChange[®] II XL site-directed mutagenesis kit from Agilent, following the instructions in the protocol provided. The mutations were confirmed by sequencing the 12-LOX insert in the pFastBac1 shuttle vector (Eurofins Genomics, KY, USA).

Protein Expression and Purification

The expression and purification of 12-LOX (UniProt entry P18054) and all mutants used in this study were performed as described previously[22]. Briefly, the wild type 12-LOX (wt-12-LOX) enzyme and its mutants were expressed as fusion

proteins, with an N-terminal 6xHis tag, and were affinity purified by nickel-iminodiacetic acid agarose using FPLC (Biorad). For inhibitor selectivity, human 5-LOX (h5-LOX, UniProt entry P09917), human reticulocyte 15-LOX-1 (h15-LOX-1, UniProt entry P16050) and human epithelial 15-LOX-2 (h15-LOX-2, UniProt entry O15296) were also isolated, as previously described.[23, 24]. The purity of all the proteins, except h5-LOX, was greater than 90% as determined by SDS-PAGE analysis. h5-LOX was an ammonium sulfate fraction due to the extensive loss of activity upon purification.[25]

Determination of Iron Content using ICP-MS

The iron content of wt12-LOX and the mutant enzymes that exhibited a significant change in their IC_{50} values was determined by a Thermo Element XR inductively-coupled plasma mass spectrometer (ICP-MS), using cobalt (EDTA) as an internal standard. Iron concentrations were compared with standardized iron solutions and all kinetic data were normalized to the iron content. The Bradford assay, with bovine serum albumin (BSA) as the protein standard, was used to determine the

protein concentration.

Steady-State Kinetics

The kinetic rates of wt12-LOX and mutant enzymes that exhibited more than 3.5-fold increase in the IC_{50} values were determined by monitoring the formation of the conjugated diene product, 12(S)-HpETE ($\epsilon = 25,000 \text{ M}^{-1}\text{cm}^{-1}$) at 234 nm, with a Perkin-Elmer Lambda 40 UV/Vis spectrophotometer. The reactions were initiated by adding the appropriate amount of enzyme to a 2 mL reaction mixture containing 1-20 mM AA, 25 mM HEPES buffer (pH 8.0), 0.01% Triton X-100, at 23°C, with constant stirring using a magnetic bar. Kinetic data were obtained by recording initial enzymatic rates at each substrate concentration and then fitting them to the Michaelis-Menten equation using KaleidaGraph (Synergy) to determine the k_{cat} and k_{cat}/K_M values.

UV-Vis-based IC_{50} Assay

IC_{50} values of **ML355** against 12-LOX and its mutants were determined in a similar manner as the steady state kinetic values. The percent inhibition was

determined by comparing the enzyme rates of the control (DMSO solvent) and the inhibitor sample by following the formation of the conjugated diene product at 234 nm ($\epsilon = 25,000 \text{ M}^{-1}\text{cm}^{-1}$). The reactions were initiated by adding 200 nM 15-LOX-2, 30 nM 12-LOX, 40 nM 15-LOX-1, or approximately 100 - 300 nM (total protein) of 5-LOX ammonium sulfate fraction to a cuvette with 2 mL reaction buffer, constantly stirred using a magnetic stir bar at room temperature (22 °C). Reaction buffers used for various LOX isozymes were as follows: 25 mM HEPES (pH 7.3), 0.3 mM CaCl_2 , 0.1 mM EDTA, 0.2 mM ATP, 0.01% Triton X-100, 10 μM AA for the crude, ammonium sulfate precipitated 5-LOX; and 25 mM HEPES (pH 7.5), 0.01% Triton X-100, 10 μM AA for 15-LOX-2, 15-LOX-1, and 12-LOX. The substrate concentration was quantitatively determined by allowing the enzymatic reaction to go to completion in the presence of soybean LOX-1. IC_{50} values were obtained by determining the % inhibition, relative to solvent vehicle only, at various inhibitor concentrations. The data were then plotted against inhibitor concentration, followed by a hyperbolic saturation curve fit (assuming total enzyme concentration $[\text{E}] \ll$

IC₅₀). It should be noted that all of the potent inhibitors displayed greater than 80% maximal inhibition, unless otherwise stated in the tables. All inhibitors were stored at -20 °C in DMSO.

Synthesis of

4-((2-hydroxy-3-methoxybenzyl)amino)-N-(naphtho[1,2-d]thiazol-2-yl)benzenesu

lfonamide (Lox12Slug001)

General Methods for Chemistry.

All air or moisture sensitive reactions were performed under positive pressure of nitrogen with oven-dried glassware. Chemical reagents and anhydrous solvents were obtained from commercial sources and used as-is. The analog for assay has purity greater than 95% and ¹H and ¹³C NMR spectra were recorded on **Bruker Avance III**

HD 500MHz NMR spectrometer.

General Synthetic Procedures

The synthesis of the ML355 derivatives were achieved with the following steps

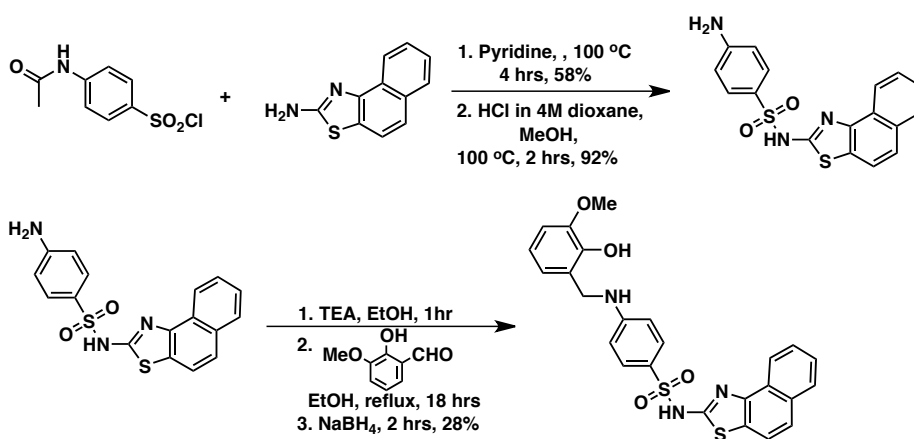
(Scheme 1).

Step 1. To a stirred solution of naphtho[1,2-d]thiazol-2-amine (1eq.) in pyridine (6 eq.) was added N-acetylsulfanilyl chloride (1.1 eq.) in three equal parts. The reaction mixture was heated for 4 hrs at 100 °C and allowed to cool to room temperature. The reaction mixture was then allowed to sit at room temperature for 2 hrs, and afterwards was poured into EtOAc and 1N HCl_(aq.) in a separation funnel. A white solid was formed in the EtOAc layer, which was collected by filtration, washed with cold ethanol, and dried under reduced pressure overnight to give the desired acetamide product (yield: 58 %).

Step 2. To a stirred solution of the acetamide product (1 eq.) in MeOH (2 mL) was added 4M HCl in dioxane (1.5 eq.). The reaction was heated for 2 hrs at 100 °C and then cooled to room temperature. The reaction mixture was then concentrated with a rotavap to get the white solid amine product (yield: 92 %).

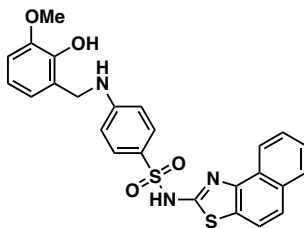
Step 3. The amine product (1 eq.) in anhydrous ethanol (1mmol of amine product in 5 mL) was added to TEA (2eq.) and stirred for 1 hr at room temperature.

2-hydroxy-3-methoxybenzaldehyde (1.2 eq.) was then added to the reaction mixture and refluxed overnight. The reaction mixture was then cooled to room temperature before sodium borohydride (3 eq.) was added and stirred for 2hrs. The reaction was quenched with MeOH and water until it stopped bubbling. The white solid was collected by filtration, washed with cold EtOH and then dried under vacuum. The crude solid was purified by RP-18 column chromatography (3 column volumes of 20 % MeOH w/0.1 % NH₄OH in water to wash out the impurity then elute out the product with 50 % MeOH w/0.1 % NH₄OH in water) to give the desired final product (yield: 28 %).



Scheme 1. Synthesis of

4-((2-hydroxy-3-methoxybenzyl)amino)-N-(naphtho[1,2-d]thiazol-2-yl)benzenesulfonamide (**Lox12Slug001**).



4-((2-hydroxy-3-methoxybenzyl)amino)-N-(naphtho[1,2-*d*]thiazol-2-yl)benzenesulfonamide

^1H NMR (500 MHz, DMSO- d_6) δ 8.69 (s, 1H), 8.34 (d, $J = 5$ Hz, 1H), 7.93 (s, 1H), 7.77 (s, 1H), 7.53 (d, $J = 10$ Hz, 4H), 6.81 (d, $J = 10$ Hz, 1H), 6.73 (d, $J = 10$ Hz, 1H), 6.66 (t, $J = 5$ Hz, 1H), 6.57 (d, $J = 5$ Hz, 2H), 4.21 (d, $J = 10$ Hz, 2H), 3.77 (s, 3H).

^{13}C NMR (500 MHz, DMSO- d_6) δ 147.1, 143.5, 131.3, 127.6, 127.5, 127.3, 125.6, 119.8, 119.1, 118.4, 110.3, 110.1, 55.6, 40.6.

Culture of Human Islets

Human islets from nondiabetic donors were received from the Integrated Islet Distribution Program or Prodo Laboratories (Aliso Viejo, CA) with approval from the institutional review board at New York Medical College (**Table 1**). Characteristics of islets and donors are summarized in the below table. Islets were incubated in CMRL-1066 medium supplemented with 10% fetal bovine serum and 1% Pen-Strept overnight at 37°C in 5% CO₂ for recovery from shipment. On the next day, islets

were transferred to CMRL-1066 supplemented with 5% fetal bovine serum and 1% Pen-Strept. A portion of the islets were randomly selected and incubated with a mixture of human PICs, 0.57 mmol/L tumor necrosis factor α , 5.9 mmol/L interferon- γ , and 0.29 mmol/L IL-1 β (all from BD Biosciences, San Jose, CA) in the presence or absence of 1 μ mol/L **Lox12Slug001**. The **Lox12Slug001** was added 30 minutes before the addition of PIC[19].

Sex	Age (y)	BMI (kg/m ²)	Race	Cause of Death, A1c Value if Reported	Study Done	Source
F	60	44.4	Wh	Head Trauma	Nondiabetic donors	IIDP
F	53	32.5	Caucasian	Anoxic event, HbA1c 5.2%	Nondiabetic donors	Prodo
M	34	28.1	Hispanic	Head trauma	Nondiabetic donors	IIDP

Table 1. Characteristics of Human Islet Donors

Glucose Stimulated Insulin Secretion

Use of Krebs-Ringer buffer (KRB) for glucose-stimulated insulin secretion (GSIS) was previously published. For batch assays, islets treated with PIC in the presence or absence of Lox12Slug001 for 24 hours were transferred to KRB without glucose and were incubated for 1 hour at 37°C in 5% CO₂ in the absence of PIC and Lox12Slug001. Thereafter, 50 islet equivalents (IEQs) per well were transferred to six-well plates filled with 1 mL of KRB containing 3 mmol/L or 18 mmol/L of glucose and were incubated for 1 hour at 37°C in 5% CO₂. Each condition was performed in triplicate. After incubation, supernatant was collected for determination of insulin secretion by human insulin enzyme-linked immunosorbent assay (Merckodia, Winston-Salem, NC) [19].

Statistics

Data are presented as mean \pm standard error of the mean and were analyzed using Two-way Anova analysis of variance Sidak's multiple comparison test (Prism software, Irvine, CA) as indicated in each figure. $P < 0.05$ was considered significant.

5.4 Results and Discussion

Computational Modeling of ML355 Interactions with wt12-LOX and its mutants

ML355 is a potent/selective inhibitor of h12-LOX, however little is known regarding its specific molecular interactions in the active site of h12-LOX. In order to rectify this deficiency, a homology model of the h12-LOX catalytic domain was constructed and **ML355** was docked into the catalytic site. Our model predicted **ML355** to bind tightly in the active site with a standard-precision (SP) docking score of -10.37. The docking pose (**Figure 1**) shows the following interactions between **ML355** and h12-LOX. The amidine hydrogen forms a hydrogen bond with the backbone carbonyl oxygen of I399, the bridging aromatic ring forms a pi-stacking interaction with the metal coordinated H365, the epsilon nitrogen of H596 is 3.6 Å to the oxygen atom of the hydroxyl group on the p-methoxy catechol moiety [26], **ML355** wraps around L407 and the **ML355** benzothiazole ring is buried in a hydrophobic pocket, whose base is defined by A417/V418 and whose sides are defined by the aromatic residues, F352 and F414. Based on this docking model,

homology models for each mutation were constructed and docking calculations were performed for **ML355** binding (**Table 2**). In parallel, the h12-LOX mutants were purified and their IC₅₀ values determined to assess the validity of the docking model. Gratifyingly, the docking scores show a positive correlation with the experimental IC₅₀ values (**Figure 2**), which lend support to our docking model of **ML355** in the h12-LOX active site, and the specific interactions are discussed (*vide infra*).

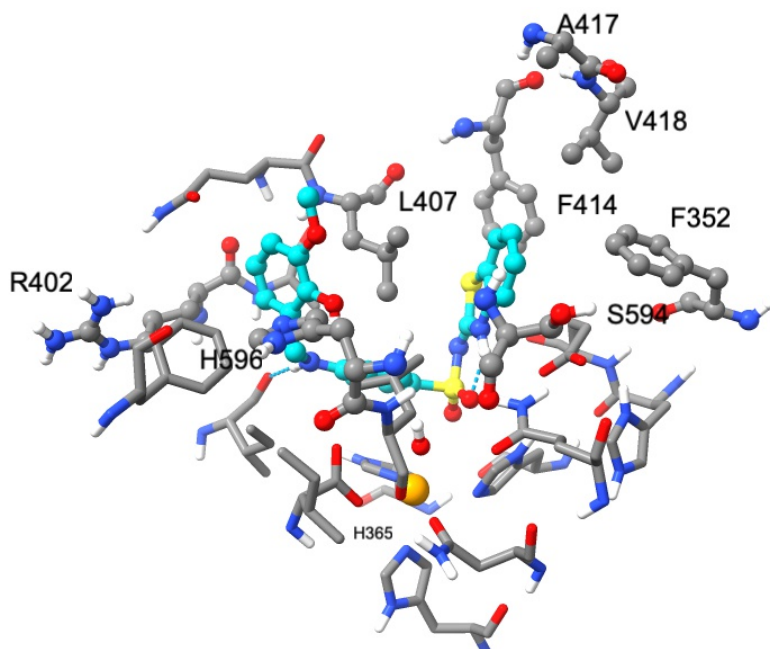


Figure 1. Predicted binding mode of **ML355** with wt12-LOX. Carbon atoms of **ML355** are shown in turquoise, whereas carbon atoms of the protein are shown in gray color. Nitrogen, oxygen, hydrogen and sulfur atoms are shown in blue, red, white and yellow colors respectively. Residues interacting with **ML355** and the metal ion are also shown. Residues that were mutated in this study are shown in

ball-and-stick representation and labelled, whereas other residues are shown in stick representation. A hydroxide ion interacting with Fe³⁺ is also shown in ball-and-stick representation. Fe³⁺ ion is shown as an orange sphere. Hydrogen bonds are shown in cyan color.

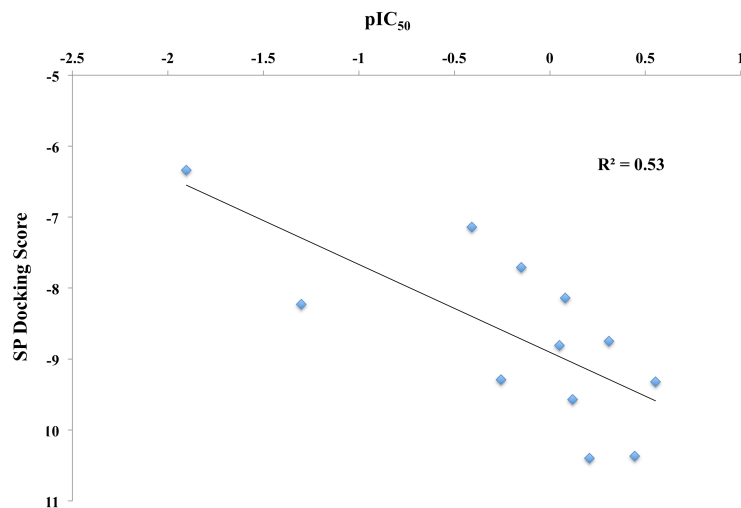


Figure 2. Correlation of pIC₅₀ values of **ML355** against human 12-LOX mutants to the docking scores.

Enzyme	ML355 IC ₅₀ (μM)	SP Docking Score
wt12-LOX	0.36 ± 0.02	-10.37
R402L	0.28 ± 0.06	-9.32
H596L	1.8 ± 0.4	-9.29
L407A	1.41 ± 0.18	-7.71
L407G	2.56 ± 0.86	-7.14
A417I	0.62 ± 0.08	-10.4
V418M	0.76 ± 0.07	-9.57

A417I/V418M	0.83 ± 0.2	-8.14
A417I/V418M/S594T	>20	-8.23
A417I/V418M/L407G	>80	-6.34
F414L	0.49 ± 0.03	-8.75
F352L	0.89 ± 0.08	-8.81

Table 2. ML355 IC₅₀ values and XP docking scores of the wt12-LOX and the mutant enzymes

Critical Role of L407 in ML355 Positioning

On the basis of the computational model of **ML355** in the active site, the importance of the bulky hydrophobic residue, L407, was investigated. Our **ML355** docking model indicated that **ML355** wrapped around L407 and gratifyingly, replacement of L407 with a smaller alanine residue caused a 3.9-fold decrease in inhibitory potency compared to wt12-LOX, $1.4 \pm 0.18 \mu\text{M}$ and $0.36 \pm 0.02 \mu\text{M}$, respectively. This change in inhibitory potency decreased even more when the cavity was made larger with the L407G mutant enzyme, with a 7.1-fold decrease in IC₅₀ relative to wt12-LOX, $2.6 \pm 0.9 \mu\text{M}$ and $0.36 \pm 0.02 \mu\text{M}$, respectively (**Table 3**). The side chain of L407, along with I399, A403, L597, form a narrow hydrophobic channel for the substrate. As shown in **Figure 1**, the phenyl ring linker of **ML355**

fills the hydrophobic channel in the wt-12-LOX binding pose. Mutation of L407 to a smaller hydrophobic residue, such as Ala or Gly, greatly widens the hydrophobic channel, reducing favorable hydrophobic contacts with **ML355** (**Figure 3**).

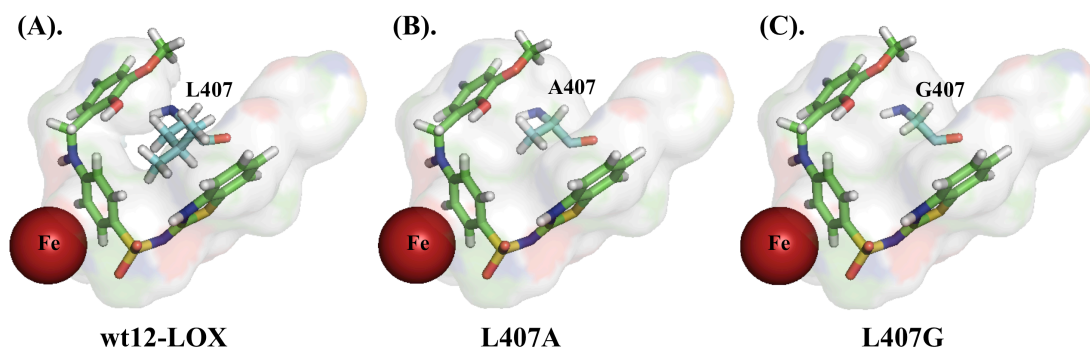


Figure 3. Relative cavity shapes and sizes of **ML355** binding in the active site of (A). wt12-LOX (B). L407A and (C). L407G

Enzyme	ML355 IC ₅₀ (μM)	Relative ML355 IC ₅₀
wt12-LOX	0.36 ± 0.02	1
L407A	1.4 ± 0.2	3.9
L407G	2.6 ± 0.9	7.1

Table 3. ML355 IC₅₀ values and relative IC₅₀ values of the wt12-LOX and its two mutants to determine the role of L407 in ML355 binding with human 12-LOX

Role of A417, V418 and S594 in ML355 binding and the Development of More

Potent Derivative, Lox12Slug001

Residues A417 and V418 (**Figure 1**), known as the Sloane determinants, form the bottom of the active site cavity and play a major role in the substrate positional specificity of 12-LOX [26]. However, our ML355 docking model did not indicate a structural interaction between these two residues and the inhibitor (**Figure 4A & 4B**). The benzothiazole of ML355 was positioned 6.9Å away from A417 and 4.2Å away from V418 and therefore the mutants, A417I, V418M, and A417I/V418M, were tested to determine if the depth of the active site would affect ML355 potency. As predicted by our docking model, mutating these two residues to bulkier amino acids showed only a modest change of the IC₅₀ value compared to the wt-12LOX, with only a 2.3-fold decrease in potency in the double mutant (A417I/V418M) (**Table 1**). This result indicated that bulkier substituents on the benzothiazole ring of ML355 could be tolerated and possibly increase the inhibitor potency by hydrophobic interactions in the active site. Therefore, the ML355 derivative, 4-((2-hydroxy-3-methoxybenzyl)amino)-N-(naphtho[1,2-d]thiazol-2-yl)benzenesulfo

namide (Lox12Slug001) was docked to the active site and found to have a favorable binding score (-11.40) (**Table 5**). The molecule was subsequently synthesized (**Lox12Slug001**, **Scheme 1**) and its potency was observed to increase by 7.2-fold ($IC_{50} = 0.050 \pm 0.02 \text{ uM}$) (**Table 5**) against the wt12-LOX, thus supporting our binding model for **ML355** docking to the active site of 12-LOX.

Surprisingly, when Lox12Slug001 was screened against the A417I/V418M mutant, the potency only decreased 2.4-fold, similar to that seen with **ML355**, indicating additional cavity area near the (naphthyl)thiazole moiety of **Lox12Slug001**. Previously, we observed with AA catalysis that to affect substrate binding, it was necessary to not only shorten the active site cavity (A417I and V418M) but to also make it narrower (S594T). The triple mutant, A417I/V418M/S594T, restricted the methyl tail of AA sufficiently to increase 15-HETE production significantly [26]. Therefore, we tested both **ML355** and Lox12Slug001 against A417I/V418M/S594T and observed a dramatic decrease in potency for both inhibitors (greater than 20 μM IC_{50} values for both **ML355** and **Lox12Slug001** (**Table 4A & 4B**)). These results

indicate that by reducing the active site size by both depth and width, the inhibitor potency is reduced, supporting our inhibitor docking model.

As discussed above, L407 plays a role in **ML355** binding by interacting with its phenyl ring linker and positioning the ends of **ML355** properly in the “U” shaped cavity. It was therefore postulated that mutating L407 could have an additive effect with other mutants and thus the triple mutant, L407G/A417I/V418M, was designed to investigate the effect of both widening and reducing the length of the active site cavity on **ML355** positioning. Amazingly, this triple mutant lowered the inhibitor potency dramatically for both **ML355** and **Lox12Slug001** with IC₅₀ values of greater than 80 and 15 uM, respectively (**Table 4A & 4B**), indicating that without the bulk of L407, a more shallow active site impedes ML355 binding. Finally, it should be noted that the IC₅₀ value trend of Lox12Slug001 against the mutants, A417I/418M, A417I/V418M/S594T and L407G/A417I/V418M (**Table 4B**), are similar to the IC₅₀ value trend of **ML355**, suggesting a similar binding mode between **Lox12Slug001** and **ML355**.

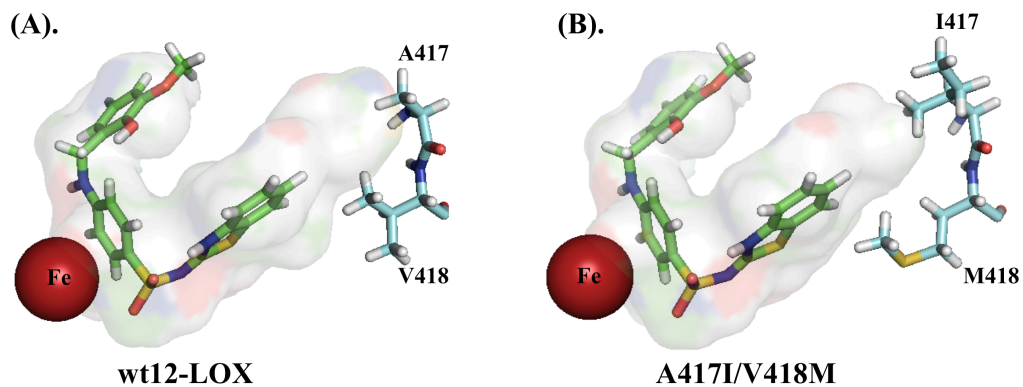


Figure 4. Relative cavity sizes of **ML355** binding in the active site of (A). wt12-LOX and (B). A417I/V418M (Sloane determinants)

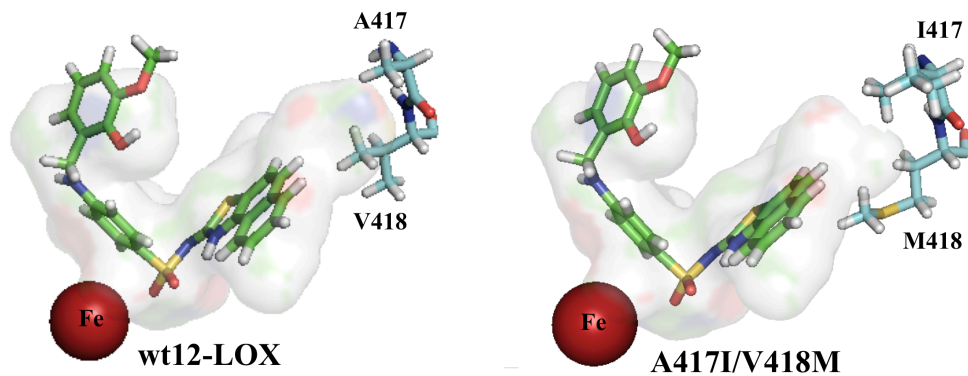


Figure 5. Relative cavity sizes of **Lox12Slug001** binding in the active site of (A). wt12-LOX and (B). A417I/V418M (Sloane determinants)

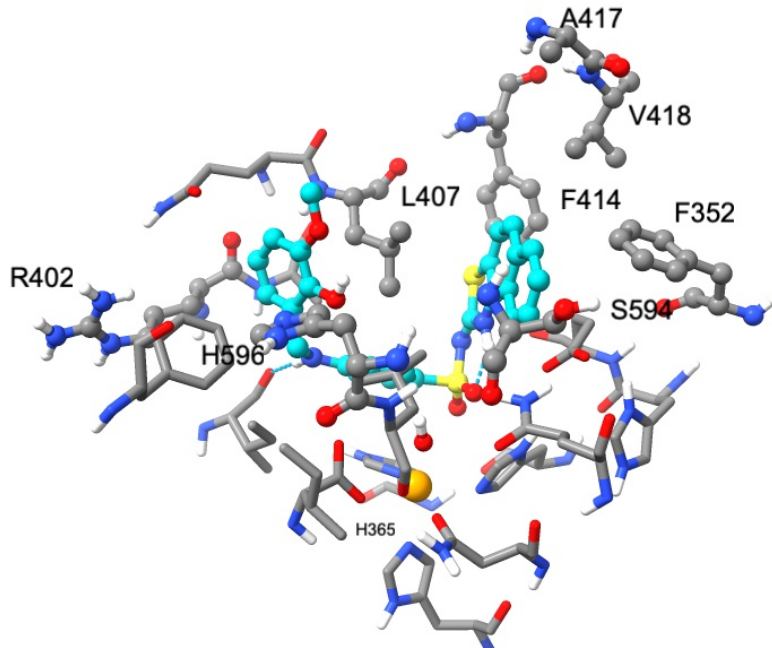


Figure 6. Predicted binding mode of **Lox12Slug001** with wt12-LOX. Residues that interact with the inhibitor are shown. Residues that mutated in the present study are shown in ball-and-stick representation and they are labelled. Carbon atoms of 12Slug001 are shown in turquoise color, whereas carbon atoms of wt12-LOX are shown in gray color. Oxygen, nitrogen, hydrogen and sulfur atoms are shown in red, blue, white and yellow colors respectively. Fe^{3+} ion is shown as orange sphere. Hydroxide ion is shown in ball-and-stick representation.

(A).

Enzyme	ML355 IC_{50} (μM)
wt12-LOX	0.36 ± 0.02
A417I/V418M	0.83 ± 0.18
A417I/V418M/S594T	>20 (45 % ^a)
L407G/A417I/V418M	>80 (19 % ^a)

(B).

Enzyme	Lox12Slug001 IC ₅₀ (μM)
wt12- LOX	0.05 ± 0.02
A417I/V418M	0.12 ± 0.04
A417I/V418M/S594T	>20 (44 % ^a)
L407G/A417I/V418M	>150 (10 % ^a)

Table 4. IC₅₀ values of **(A). ML355** and **(B). Lox12Slug001** with wt12-LOX and the mutants of Sloane determinants. ^aPercent inhibition at 20 μM inhibitor.

12-LOX Inhibitor	IC ₅₀ (μM)	XP Docking Score
ML355	0.36 ± 0.02	-10.37
Lox12Slug001	0.05 ± 0.02	-11.40

Table 5. IC₅₀ values and XP Scores of **ML355** and **Lox12Slug001** against wt12-LOX

π-π Interactions of ML355 and Lox12Slug001 with F352 and F414 12-LOX

The ML355 docking model predicts that the benzothiazole ring of **ML355** is buried in a hydrophobic pocket created by the aromatic side chains of F352 and F414, with closest distances to ML355 being 4.1 Å and 4.5 Å, respectively (**Figure 7**).

Considering that **Lox12Slug001** appears to have a similar binding mode to ML355 in

the 12-LOX active site, we hypothesized that these aromatic residues could participate in π - π interactions with the benzothiazole moieties of both **ML355** and **Lox12Slug001**. Therefore, the mutants, F352L and F414L, were generated, however for **ML355**, only a modest increase in IC_{50} was observed, compared to wt12-LOX (**Table 6A**). On the other hand, the IC_{50} values of **Lox12Slug001** against these mutants increased more significantly, with a 3.6-fold increase for F414L and a 9.8-fold increase for F352L (**Table 6B**). These results are intriguing because both mutations increase the active site cavity size, however they have a greater negative effect on the larger inhibitor, **Lox12Slug001**. This suggests that there is a specific interaction with **Lox12Slug001** that is not present in **ML355**, which is disrupted upon the decreased size and loss of aromaticity in the mutations. Since **Lox12Slug001** is not only larger but has a more extensive aromatic structure than **ML355**, the data is consistent with **Lox12Slug001** having a stronger π - π interaction with F352 and F414, which is lost upon mutation.

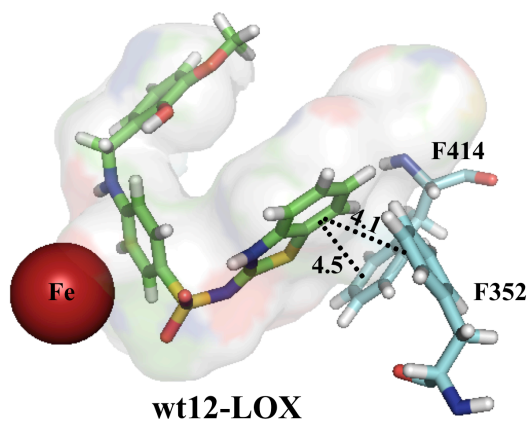


Figure 7. Predicted binding mode of ML355 in the active site of wt12-LOX showing the closest distances of benzothiazole ring to aromatic side chains of F352 and F414.

(A).

Enzyme	ML355 IC ₅₀ (μM)	Relative ML355 IC ₅₀
wt12-LOX	0.36 ± 0.02	1
F414L	0.49 ± 0.03	1.4
F352L	0.89 ± 0.08	2.5

(B).

Enzyme	Lox12Slug001 IC ₅₀ (μM)	Relative Lox12Slug001 IC ₅₀
wt12-LOX	0.05 ± 0.02	1
F414L	0.18 ± 0.01	3.6
F352L	0.49 ± 0.05	9.8

Table 6. (A). ML355 and (B). Lox12Slug001 IC₅₀ values and Relative IC₅₀ values of the wt12-LOX and its two mutants to determine the π - π interactions with the aromatic amino acids of 12-LOX

H596 binding Interaction with the p-methoxy Catechol Moiety of ML355

The role of R402 was previously determined unimportant with respect to substrate binding for h12-LOX,[26] however, computational prediction and subsequent experimental study showed that H596 could play a role in anchoring the carboxylate of AA during catalysis.[26] Considering this result and close proximity (3.6Å) of H596 epsilon nitrogen (NE) to the oxygen atom of the hydroxyl group of p-methoxy catechol moiety of **ML355 (Figure 8A)**, H596L was generated and displayed a 5-fold decrease in potency relative to wt12-LOX, $1.8 \pm 0.4 \mu\text{M}$ and $0.36 \pm 0.02 \mu\text{M}$, respectively (**Table 7**). These results suggest that H596 in h12-LOX may contribute to properly positioning **ML355** in the active site but not R402, possibly through the interaction with the p-methoxy catechol moiety of **ML355**, as observed in the docking model. This can be further supported by the observed lowest energy docking pose of ML355 against H596L mutant in which the p-methoxy catechol

moiety is 180° flipped from the pose observed for the wild-type (**Figure 8A and 8B**).

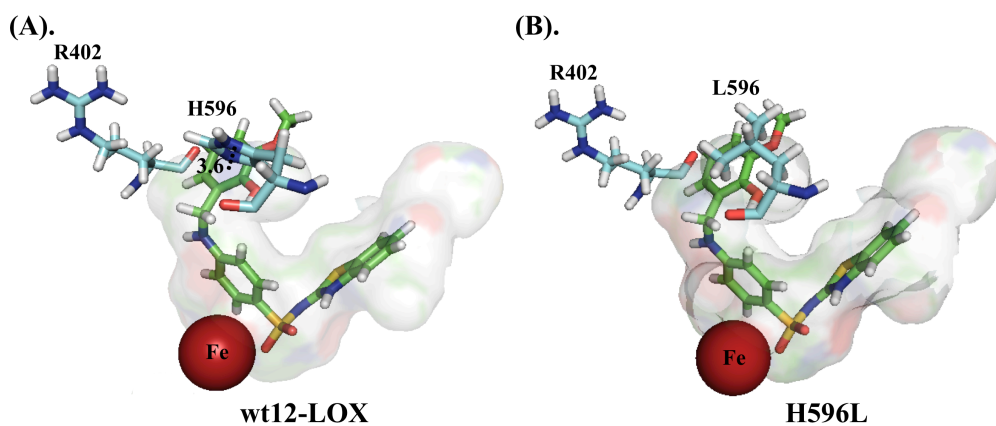


Figure 8. Predicted binding mode of ML355 in the active site of **(A)**. wt12-LOX showing the H bonding to H596 and **(B)**. H596L

Enzyme	ML355 IC ₅₀ (μM)	Relative ML355 IC ₅₀
wt12-LOX	0.36 ± 0.02	1
R402L	0.28 ± 0.06	0.8
H596L	1.80 ± 0.39	5

Table 7. ML355 IC₅₀ values and Relative IC₅₀ values of the wt12-LOX and its two mutants to determine the binding of p-methoxy catechol moiety of **ML355** with human 12-LOX

Islet Effect: Lox12Slug001 Improves GSIS and Increases Insulin Content of Human Islets Treated with PIC

Given the improved potency of **Lox12Slug001** against h12-LOX, its potency in islet cells was investigated. PIC exposure of human and mouse β cells upregulated the 12-LO pathway, and the inhibition of the 12-LO pathway was implicated in protecting the viability and function of human and mouse β cells after PIC exposure. Since **ML355** was previously shown to be a highly selective inhibitor of ALOX12 with a favorable ADME profile in protecting human islets against the impairment of GSIS by PIC [19], **Lox12Slug001** was also tested (**Figure 9**). PIC treatment at the dose and duration used predominantly increased basal insulin secretion at 3 mmol/L of glucose and led to the reduction of further increases in insulin secretion at 18 mmol/L of glucose. **Lox12Slug001** was also used at 10 μ M dose and showed similar effects (unpublished observation).

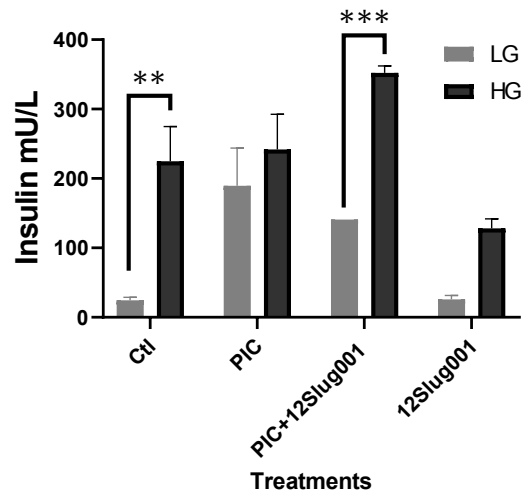


Figure 9. Batch incubation of human islets treated with PIC with or without 12-LO inhibitor. GSIS was compared between human islets that were untreated (Ctl), pretreated with PIC, or pretreated with PIC plus Lox12Slug001 for 24 hours. Each condition from a single donor was performed in triplicate, and data from three donors were combined (n = 8 to 9). *P < 0.05; **P < 0.01; ***P < 0.005; ****P < 0.001 by Two-way Anova's variance Sidak's multiple comparison test.

5.5 Conclusions

ML355 is a lead molecule targeting 12-LOX, a potential drug target to decrease platelet reactivity following vascular insult or injury.[20] Therefore, it is critical to investigate the binding mode of this promising lead molecule to its target in order to gain insights for further optimization. From the ML355 docking pose in the h12-LOX active site, we mutated residues with the potential of affecting ML355 binding, determined the ML355 binding affinity against the mutants and compared them to the calculated wt12-LOX/ ML355 binding affinity. The relationship between their docking score and inhibitor potency have a positive correlation lending confidence to the docking model of ML355 bound to the h12-LOX active site (**Figure 1**).

The docking model predicts a number of interactions between the active site and **ML355**. A key characteristic of the h12-LOX active site is its curved nature, which has been described as a “U” shape. L407 defines the “U” shape of the h12-LOX active site and has been shown to properly position the fatty acid, AA, for catalysis [26]. Appropriately, **ML355** conforms to the “U” shape of the h12-LOX

active site, having specific interactions with active site residues. L407 is at the bottom of the “U”, with **ML355** wrapping around the residue, with interaction to the phenyl linker region of **ML355**. Reducing the size of L407 progressively decreases **ML355** potency, manifesting a 7-fold decrease in the IC₅₀ value with L407G (**Figure 3**), supporting the hypothesis that **ML355** gains binding affinity from the curvature of the active site.

Beyond L407, the benzothiazole of **ML355** extends into the bottom of the active site cavity, pointing towards the Sloane determinants, residues A417 and V418. However, the docking model indicates limited interaction between **ML355** and these residues. This lack of interaction was confirmed by the lack of effect by the cavity reducing mutation, A417I/V418M. This indicated potential space to increase the volume of **ML355** and optimize van der Waals interactions in this portion of the cavity, such as by attaching substituents to the benzothiazole moiety. In order to test this hypothesis, a derivative of **ML355** with a larger naphthyl-benzothiazole, Lox12Slug001 (**Scheme 1**), was synthesized and found to have 7.2-fold greater

potency than **ML355** against 12-LOX, supporting our docking model. Unexpectedly, the double mutant, A417I/V418M, only had a 2.4-fold increase in the IC₅₀ with Lox12Slug001, suggesting additional cavity space even with **Lox12Slug001**. If, however, the cavity volume was decreased further, A417I/V418M/S594T, the IC₅₀ increased dramatically to greater than 20 μ M, for both **ML355** and **Lox12Slug001**. This result suggests that both the depth and width of the active site affect inhibitor binding. The specificity of the inhibitor/active site interaction was confirmed with additional loss of inhibitor potency with the triple mutant, L407G/A417I/V418M. The curious aspect of this mutation is that by increasing the size of the active site in the middle of the cavity, but reducing the size at the end abolishes inhibitor potency, suggesting that both **ML355** and **Lox12Slug001** interact with L407 in such a way to position them in a precise manner in the active site.

Another aspect of the active site of h12-LOX is the aromaticity on key residues, F414 and F352, which the model suggests interacts with the aromatic moieties of the inhibitors. However, loss of the aromaticity of F414 and F352 affected the potency of

Lox12Slug001 more so than **ML355**. This suggests a difference in their binding mode, with potentially having **Lox12Slug001** have more pi-pi interactions than **ML355**. This is a reasonable hypothesis since **Lox12Slug001** has a more extensive pi-system.

Computational prediction and subsequent experimental study showed that H596 could play a role in anchoring the carboxylate of AA during catalysis but not R402[26]. Therefore, both H596 and R402 were replaced with a nonpolar leucine and the inhibitory potency against **ML355** was tested. H596L showed a greater increase in the IC₅₀ than that of R402 relative to wt12-LOX (5-fold increase for H596L and 0.8-fold for R02L), suggesting that H596 in h12-LOX may contribute to properly positioning **ML355** binding in the active site but not R402, possibly through the interaction with the p-methoxy catechol moiety of **ML355**.

The gain in potency of **Lox12Slug001** supported our binding hypothesis however, its improved potency also suggested improved drug qualities. Gratifyingly, its selectivity against other LOX isozymes was maintained and more importantly, it

maintained its potency in human islet cells, comparable to that of **ML355** (**Figure 5**).

These results are supportive of **Lox12Slug001** being an improved drug candidate to **ML355**, however, its solubility in DMSO was observed to decrease. This is a negative drug quality for **Lox12Slug001** and therefore further studies are currently being pursued to derivatize **ML355** in order to optimize the additional space in the active site, while maintaining acceptable solubility.

References

1. Brash, A.R., *Lipoxygenases: Occurrence, Functions, Catalysis and Acquisition of Substrate*. J. Biol. Chem., 1999. **274**(34): p. 23679-23682.
2. Kuhn, H., et al., *Structural biology of mammalian lipoxygenases: enzymatic consequences of targeted alterations of the protein structure*. Biochem Biophys Res Commun, 2005. **338**(1): p. 93-101.
3. Pidgeon, G.P., et al., *Lipoxygenase metabolism: roles in tumor progression and survival*. Cancer Metastasis Rev, 2007. **26**(3-4): p. 503-24.
4. Burkhart, J.M., et al., *The first comprehensive and quantitative analysis of human platelet protein composition allows the comparative analysis of structural and functional pathways*. Blood, 2012. **120**(15): p. e73-82.
5. Yeung, J., et al., *12-lipoxygenase activity plays an important role in PAR4 and GPVI-mediated platelet reactivity*. Thromb Haemost, 2013. **110**(3): p. 569-81.
6. Ciko, Z., *[Circulating platelet aggregation in ischemic heart disease]*. Vojnosanitetski pregled. Military-medical and pharmaceutical review, 1981. **38**(1): p. 17-9.
7. Chen, S.H., *[Observations on platelet aggregation in patients with ischemic heart disease]*. Zhonghua yi xue za zhi, 1985. **65**(7): p. 414-7.
8. Dreyfuss, F. and J. Zahavi, *Adenosine diphosphate induced platelet aggregation in myocardial infarction and ischemic heart disease*. Atherosclerosis, 1973. **17**(1): p. 107-20.
9. Elwood, P.C., et al., *Ischemic heart disease and platelet aggregation. The Caerphilly Collaborative Heart Disease Study*. Circulation, 1991. **83**(1): p. 38-44.
10. Gormsen, J., et al., *ADP-induced platelet aggregation in vitro in patients with ischemic heart disease and peripheral thromboatherosclerosis*. Acta medica Scandinavica, 1977. **201**(6): p. 509-13.
11. Gryglik, J., *[Pharmacological inhibition of platelet aggregation in primary*

- and secondary prevention of ischemic heart disease*]. *Polski tygodnik lekarski*, 1979. **34**(13): p. 509-11.
12. Helo, O.H., J.K. Madsen, and J. Kastrup, [*Treatment of ischemic heart disease with the platelet aggregation inhibitor clopidogrel*]. *Ugeskrift for laeger*, 2004. **166**(18): p. 1659-62.
 13. Yeung, J. and M. Holinstat, *Newer agents in antiplatelet therapy: a review*. *J Blood Med*, 2012. **3**: p. 33-42.
 14. McMahan, G.S., et al., *Transient heparin-induced platelet activation linked to generation of platelet 12-lipoxygenase. Findings from a randomised controlled trial*. *Thromb Haemost*, 2013. **109**(6): p. 1099-107.
 15. Svensson Holm, A.C., et al., *Inhibition of 12-lipoxygenase reduces platelet activation and prevents their mitogenic function*. *Platelets*, 2014. **25**(2): p. 111-7.
 16. Luci, D.K., et al., *Synthesis and Structure-Activity Relationship Studies of 4-((2-Hydroxy-3-methoxybenzyl)amino)benzenesulfonamide Derivatives as Potent and Selective Inhibitors of 12-Lipoxygenase*. *J Med Chem*, 2014. **57**(2): p. 495-506.
 17. Yeung, J., et al., *Platelet 12-LOX is essential for FcγRIIa-mediated platelet activation*. *Blood*, 2014. **124**(14): p. 2271-9.
 18. Adili, R., et al., *First Selective 12-LOX Inhibitor, ML355, Impairs Thrombus Formation and Vessel Occlusion In Vivo With Minimal Effects on Hemostasis*. *Arterioscler Thromb Vasc Biol*, 2017. **37**(10): p. 1828-1839.
 19. Ma, K., et al., *12-Lipoxygenase Inhibitor Improves Functions of Cytokine-Treated Human Islets and Type 2 Diabetic Islets*. *J Clin Endocrinol Metab*, 2017. **102**(8): p. 2789-2797.
 20. Tourdot, B.E. and M. Holinstat, *Targeting 12-Lipoxygenase as a Potential Novel Antiplatelet Therapy*. *Trends Pharmacol Sci*, 2017. **38**(11): p. 1006-1015.
 21. Andreou, A. and I. Feussner, *Lipoxygenases - Structure and reaction mechanism*. *Phytochemistry*, 2009. **70**(13-14): p. 1504-10.

22. Amagata, T., et al., *Exploring sponge-derived terpenoids for their potency and selectivity against 12-human, 15-human, and 15-soybean lipoxygenases*. J Nat Prod, 2003. **66**(2): p. 230-5.
23. Robinson, S.J., et al., *Using enzyme assays to evaluate the structure and bioactivity of sponge-derived meroterpenes*. Journal of Natural Products, 2009. **72**(10): p. 1857-63.
24. Jameson, J.B., et al., *Discovery and characterization of potent and selective inhibitors to human epithelial 15-lipoxygenase-2*. Faseb Journal, 2014. **28**(1).
25. Smyrniotis, C.J., et al., *ATP Allosterically Activates the Human 5-Lipoxygenase Molecular Mechanism of Arachidonic Acid and 5(S)-Hydroperoxy-6(E),8(Z),11(Z),14(Z)-eicosatetraenoic Acid*. Biochemistry, 2014.
26. Aleem, A.M., et al., *Probing the Electrostatic and Steric Requirements for Substrate Binding in Human Platelet-Type 12-Lipoxygenase*. Biochemistry, 2019. **58**(6): p. 848-857.

Chapter 6

Kinetic and Structural Investigations of Novel Inhibitors of Human Epithelial

15-Lipoxygenase-2

6.1 Introduction

Lipoxygenases catalyze the peroxidation of fatty acids which contain bisallylic hydrogens between two cis double bonds, such as in linoleic acid (LA) and arachidonic acid (AA).[1][1] Lipoxygenases are named according to their product specificity with AA as the substrate because AA is the major precursor of many active lipid metabolites that are involved in a number of significant disease states.[2-4] The human genome contains six functional lipoxygenase (LOX) genes (ALOX5, ALOX12, ALOX12B, ALOX15, ALOX15B, eLOX3) encoding for six different LOX isoforms (h5-LOX, h12S-LOX, h12R-LOX, h15-LOX-1, h15-LOX-2, eLOX3, respectively).[3] The biological role in health and disease for each LOX isozyme varies dramatically, ranging from asthma (h5-LOX) to diabetes (h12-LOX) to stroke (h15-LOX-1). [2]

Interestingly, the role of epithelial h15-LOX-2 is not as clear as those of the other isozymes. h15-LOX-2 is expressed in macrophages, neutrophils, skin, hair roots and

prostate.[5-7] It is also highly expressed in atherosclerotic plaques and linked to the progression of macrophages to foam cells, which are present in atherosclerotic plaques.[2, 8-12] Recent data demonstrates that silencing the ALOX15B gene in human macrophages leads to decreased cellular lipid accumulation, a major factor in foam cell formation and thus plaque accumulation.[13, 14] Furthermore, h15-LOX-2 mRNA levels are highly elevated in human macrophages isolated from carotid atherosclerotic lesions of symptomatic rather than asymptomatic patients[13, 15] and its products have been shown to promote formation of atherosclerotic lesions in a mouse model.[16]

Additionally, h15-LOX-2 has been shown to play a central role in the “ class switch “ of eicosanoid mediator biosynthesis from leukotrienes (LTs) to lipoxins (LXs) in the airways. The Urbach lab observed that the reduced expression level of h15-LOX-2 in the lower airways associated with a depressed of LXA₄/LTB₄ ratio contributed to cystic fibrosis (CF) lung disease in children.[17]

Furthermore, the h15-LOX-2/PEBP1 complex has been demonstrated to be

regulator of ferroptosis, with PEBP1 acting as a rheostat by changing h15-LOX-2 substrate specificity from free PUFA to PUFA-PE, leading to generation of HpETE-PEs.[18] Accumulation of these hydroperoxy membrane phospholipids has been shown to cause ferroptotic cell death, which implicates h15-LOX-2 in neurodegenerative diseases, such as Alzheimer's, Parkinson's and Huntington's diseases.[19]

The role of h15-LOX-2 in atherosclerosis, cystic fibrosis (CF) lung disease and ferroptosis implicates h15-LOX-2 as a potential therapeutic target for drug discovery. Currently, only a few published inhibitors targeting h15-LOX-2 have been reported to date (**Figure 1**). Nordihydroguaiaretic acid (NDGA), a redox inhibitor, has a potency of 11 μM ,[20] while a 6,7-dihydroxyisoflavan (27d) has an $\text{IC}_{50} = 8 \mu\text{M}$,[20] but neither molecule is selective towards h15-LOX-2. Two molecules previously discovered by our laboratory, MLS000545091 (**545091**) and MLS000536924 (**536924**), do exhibit strong potency, as well as selectivity for h15-LOX-2, with IC_{50} values of 2.6 and 3.1 μM , respectively.[21] The observed micromolar potencies of

these inhibitors constitute acceptable probe molecule properties for h15-LOX-2 inhibition, however, it is unknown if these molecules are potent in cellular h15-LOX-2 assays, which would increase their usefulness considerably. This lack of cellular activity investigations, as well as the dearth of h15-LOX-2 inhibitor chemotypes, underscore the importance of discovering additional inhibitors and determining their *ex vivo* activity so they could be used to probe the role of h15-LOX-2 in atherosclerosis, cystic fibrosis (CF) lung disease and ferroptosis, to name a few. Herein, we report the discovery and characterization of a novel pharmacophore which is both potent and selective against h15-LOX-2. In addition, we identify the pharmacophore binding mode with computer docking models, a crystallographic co-structure and hydrogen/deuterium exchange (HDX) investigations, which provide proof-of-principle for future SAR/Drug design efforts to target h15-LOX-2 in more detail.

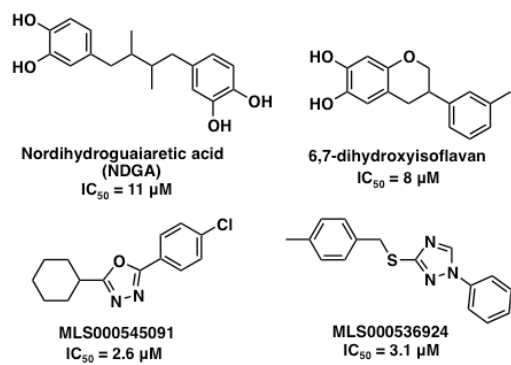


Figure 1. Structures of known h15-LOX-2 Inhibitors.

6.2 Materials and Methods

Materials

All commercial fatty acids were purchased from Nu Chek Prep, Inc. (MN, USA). BWb70c was purchased from Sigma/Aldrich Chemicals. Unless specifically mentioned, the inhibitors were obtained from the NIH Molecular Libraries Small Molecule Repository (MLSMR): (<https://mli.nih.gov/mli/compound-repository/>). All other chemicals were reagent grade or better and were used without further purification.

Inhibitor Synthesis

General Methods for Chemistry

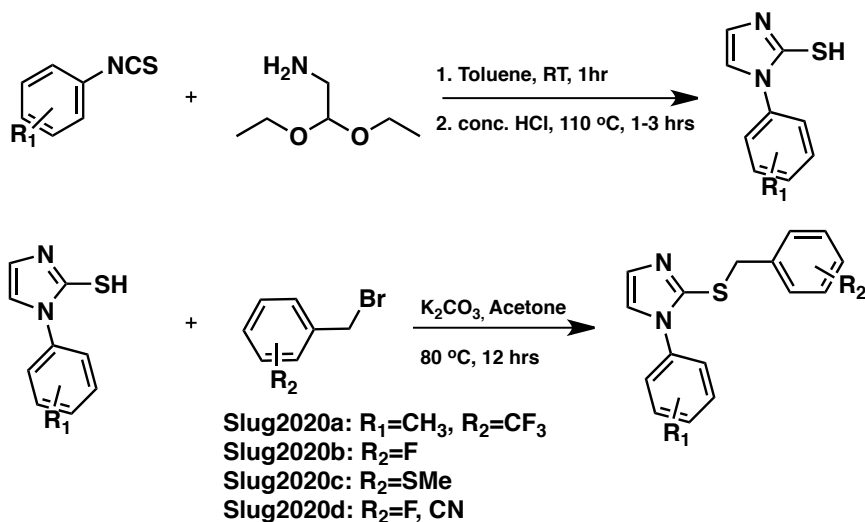
All air or moisture sensitive reactions were performed under positive pressure of nitrogen with oven-dried glassware. Chemical reagents and anhydrous solvents were obtained from commercial sources and used as-is. The analog for assay has purity greater than 95% and ¹H and ¹³C NMR spectra were recorded on a Bruker

Avance III HD 500MHz NMR spectrometer. The novel inhibitors were synthesized via the following steps (**Scheme 1**).

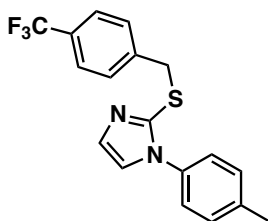
Step 1. A mixture of required phenyl isothiocyanate (5 mmol) and aminoacetaldehyde diethyl acetal (5 mmol) in toluene (10 mL) was stirred at room temperature for 1 hr. To the reaction mixture, conc. HCl (37 wt. % in water, 2.5 mmol) was added, followed by heating to reflux (bath temp. = 110° C) for 1-3 hrs. After evaporating the solvents, the residue was treated with water and 1N NaOH (the pH was set to 8). The precipitates were collected by filtration, washed with water and hexane/ether, and dried in vacuum to give the desired imidazole-2-thiol products, which were recrystallized from an appropriate solvent (acetonitrile, methanol, or benzene) (yield: 43-53%).

Step 2. Imidazole-2-thiol product from step 1 (5 mmol) in acetone was placed in the flask and potassium carbonate (15 mmol) was slowly added. The reaction was stirred under nitrogen for 1 hr and then benzyl bromide (7.5 mmol) in ethanol (10 mL) was added. The reaction was heated to 80° C for 12 hrs. After removal of the solvent, the

residue was purified by normal phase silica chromatography to get desired final product. (yield: 60-69%)



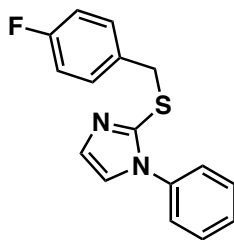
Scheme 1. Synthesis of h15-LOX-2 Inhibitor derivatives, Slug2020a-d



1-(*p*-tolyl)-2-((4-(trifluoromethyl)benzyl)thio)-1*H*-imidazole (Slug2020a)

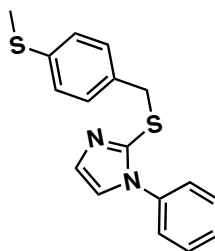
^1H NMR (500 MHz, CD_3OD) δ 7.48-7.46 (m, 2H), 7.26-7.19 (m, 6H), 6.94-6.92 (m, 2H), 4.13 (s, 2H), 2.39 (s, 3H). ^{13}C NMR (500 MHz, CD_3OD) δ 143.80, 141.60,

140.19, 135.86, 130.82, 130.69, 130.47, 130.44, 126.94, 126.83, 126.49, 126.46, 126.43, 126.40, 125.04, 124.67, 40.07, 21.23. HRMS: m/z (M + H)⁺ = calculated for C₁₈H₁₅F₃N₂S, 348.0908; found, 348.0909.



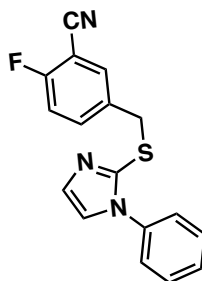
2-((4-fluorobenzyl)thio)-1-phenyl-1H-imidazole (Slug2020b)

¹H NMR (500 MHz, CDCl₃) δ 7.39-7.37 (m, 3H), 7.19-7.12 (m, 6H), 6.89-6.86 (m, 2H), 4.23 (s, 2H). ¹³C NMR (500 MHz, CDCl₃) δ 161.33, 141.64, 137.23, 133.19, 133.16, 130.78, 130.72, 129.74, 129.40, 128.63, 125.77, 122.68, 115.59, 115.42, 38.17. HRMS: m/z (M + H)⁺ = calculated for C₁₆H₁₃FN₂S, 284.0783; found, 284.0780.



2-((4-(methylthio)benzyl)thio)-1-phenyl-1H-imidazole (Slug2020c)

^1H NMR (500 MHz, CDCl_3) δ 7.55-7.51 (m, 4H), 7.40-7.33 (m, 4H), 7.30-7.27 (m, 3H), 4.37 (s, 2H), 2.58 (s, 3H). ^{13}C NMR (500 MHz, CDCl_3) δ 141.73, 137.77, 137.27, 134.15, 129.82, 129.56, 129.31, 128.80, 128.50, 126.80, 125.77, 122.62, 121.73, 121.69, 38.59, 16.04. HRMS: m/z ($M + H$) $^+$ = calculated for $\text{C}_{17}\text{H}_{16}\text{N}_2\text{S}_2$, 312.0755; found, 312.0753.



2-fluoro-5-(((1-phenyl-1H-imidazol-2-yl)thio)methyl)benzonitrile (Slug2020d)

^1H NMR (500 MHz, CDCl_3) δ 7.45-7.40 (m, 5H), 7.17-7.14 (m, 3H), 7.09-7.01 (m, 2H), 4.20 (s, 2H). ^{13}C NMR (500 MHz, CDCl_3) δ 161.38, 140.49, 136.98, 135.78, 135.71, 135.31, 135.28, 133.83, 130.06, 129.52, 128.83, 125.59, 122.98, 116.61,

116.45, 113.82, 37.01. HRMS: m/z (M + H)⁺ = calculated for C₁₇H₁₂FN₃S, 309.0736; found, 309.0737.

Protein Expression

All the LOX isozymes used in this publication were expressed and purified as previously reported (h5-LOX [22], h12-LOX [23], h15-LOX-1 [23] and h15-LOX-2 [24]). Human leukocyte 5-lipoxygenase was expressed as a non-tagged protein and used as a crude ammonium sulfate precipitated protein. The remaining enzymes: h15-LOX-1, h15-LOX-2 and h12-LOX were expressed as N-terminal His6-tagged proteins and purified via immobilized metal affinity chromatography (IMAC) using Ni-NTA resin. The purity of each protein was analyzed by SDS-PAGE and found to be greater than 90%.

Lipoxygenase UV-Vis-based IC₅₀ Assay

The initial one-point inhibition percentages were determined by following the formation of the conjugated diene product at 234 nm ($\epsilon = 25,000 \text{ M}^{-1}\text{cm}^{-1}$) with a Perkin-Elmer Lambda 40 UV/Vis spectrophotometer at 25 μM inhibitor

concentration. All inhibitors that showed greater than 70% inhibition were investigated further to determine their IC₅₀ values. The full IC₅₀ experiments were done with at least five different inhibitor concentrations. All reaction mixtures were 2 mL in volume and constantly stirred using a magnetic stir bar at room temperature (23°C) with the appropriate amount of LOX isozyme (h5-LOX (~ 200 nM); h12-LOX (~ 50 nM); h15-LOX-1 (~ 60 nM); h15-LOX-2 (~ 200 nM)). The protein concentrations are the total protein concentration; however, active protein concentration will be significantly less due to incomplete metallation. Reactions with h12-LOX were carried out in 25 mM HEPES (pH 8.0) 0.01% Triton X-100 and 10 μM AA. Reactions with the crude, ammonium sulfate precipitated h5-LOX were carried out in 25 mM HEPES (pH 7.3), 0.3 mM CaCl₂, 0.1 mM EDTA, 0.2 mM ATP, 0.01% Triton X100 and 10 μM AA. Reactions with h15-LOX-1 and h15-LOX-2 were carried out in 25 mM HEPES buffer (pH 7.5), 0.01% Triton X-100 and 10 μM AA. The concentration of AA was quantitated by allowing the enzymatic reaction to proceed to completion in the presence of soybean 15-LOX-1 (s15-LOX-1). IC₅₀

values were obtained by determining the percent inhibition at various inhibitor concentrations and plotting against inhibitor concentration, followed by a hyperbolic saturation curve fit. The percent inhibition was calculated by comparing the enzymatic rate of the control (DMSO) to the enzymatic rate with the respective inhibitor present. The experiments used for generating the saturation curves were performed in duplicate or triplicate, depending on the quality of the data. All inhibitors were stored at -20 °C in DMSO.

Steady-State Inhibition Kinetics of h15-LOX-2

The steady-state equilibrium constants of dissociation for MLS000327069 (**327069**), MLS000327186 (**327186**), MLS000327206 (**327206**) were determined by monitoring the formation of the conjugated product, 15-HpETE, at 234 nm ($\epsilon = 25,000 \text{ M}^{-1}\text{cm}^{-1}$) with a Perkin Elmer Lambda 40 UV/Vis spectrophotometer. Reactions were initiated by adding h15-LOX-2 to a constantly stirring 2 mL reaction mixture containing 0.7 μM – 20 μM AA in 25 mM HEPES buffer (pH 7.5), in the presence of 0.01% Triton X-100. Kinetic data were obtained by recording initial

enzymatic rates, at varied inhibitor concentrations, and subsequently fitting the data to the Henri-Michaelis-Menten equation using KaleidaGraph (Synergy) to determine V_{\max} ($\mu\text{mol}/\text{min}$) and K_m (μM). The primary data were then plotted in Dixon format using Microsoft Excel by graphing $1/v$ vs. $[I]$ μM at the chosen substrate concentrations. From the Dixon plots, the slope at each substrate concentration was extracted and plotted against $1/[S]$ μM to produce the Dixon replots. The K_{ic} equilibrium constant of dissociation was calculated by dividing K_m/V_{\max} by the slope of the replot. To obtain K_{iu} , $1/V_{\max}$ was divided by the y-intercept of the replot. K_{ic} and K_{iu} are defined as the equilibrium constant of dissociation from the catalytic and secondary sites, respectively.

Pseudo-peroxidase Assay

The pseudo-peroxidase activity of **327069**, **327186**, **327206** was determined with h15-LOX-2 on a Perkin-Elmer Lambda 40 UV/Vis spectrophotometer as described previously [25]. 13-HpODE was used as the oxidant and BWb70c as the positive control. The reaction was initiated by addition of 20 μM 13-HpODE to 2 mL

buffer (50 mM sodium phosphate (pH 7.4), 0.3 mM CaCl₂, 0.1 mM EDTA, 0.01% Triton X-100) containing 20 μM **327069**, **327186**, or **327206** and 200 nM h15-LOX-2. The reaction mixtures were constantly stirred at 23 °C. Activity was determined by monitoring the decrease at 234 nm (product degradation) and the percent consumption of 13-HpODE was recorded. More than 25% 13-HpODE degradation indicates redox activity of that particular inhibitor. The negative controls used were: enzyme alone with product, enzyme alone with inhibitor, as well as inhibitor alone with product. These formed a baseline for the assay, reflecting non-pseudo-peroxidase dependent hydroperoxide product decomposition. To rule out the auto-inactivation of the enzyme from pseudo-peroxidase cycling, the h15-LOX-2 residual activity was determined by the addition of 20 μM AA at the end of each reaction. The initial rates of the inhibitor and 13-HpODE were compared to initial rates of inhibitor alone because the inhibitor by itself inherently lowers the rate of oxygenation. Activity is characterized by direct measurement of the product formation with the increase of absorbance at 234 nm.

Cyclooxygenase Selectivity Assay

Cyclooxygenase selectivity assay was performed as previously described. [26]

Approximately 3 μg of either ovine COX-1 (COX-1) or human recombinant COX-2 (COX-2) (Cayman Chemical) were added to buffer containing 0.1 M Tris-HCl buffer (pH 8.0), 5 mM EDTA, 2 mM phenol and 1 μM hemin at 37 $^{\circ}\text{C}$. The selected inhibitors, **327069**, **327186**, or **327206**, were added to the reaction cell, followed by a 5 minutes incubation with either of the COX isozymes. The reaction was then initiated by adding approximately 100 μM AA in the reaction cell, as indicated in the enzymatic protocol (Cayman Chemicals). A Hansatech DWI oxygen electrode was utilized for data collection and the consumption of oxygen was recorded. Indomethacin and the vehicle of inhibitor (DMSO) were the positive and negative controls, respectively. The percent inhibition of the enzyme was calculated by comparing the rates of O_2 consumption for experimental samples (with inhibitor) to the rates of control samples (with DMSO).

Study of Inhibitors as Substrates

The inhibitors **327069**, **327186**, or **327206** were reacted with h15-LOX-2 to determine if they act as substrates. All buffer conditions and the determination of each rate are identical to the UV-Vis assay mentioned above (Methods section 2.4). 20 μ M of each inhibitor was reacted with h15-LOX-2 in 2 mL reaction mixtures in the absence of AA. Controls consisted of DMSO (vehicle), 10 μ M AA and enzyme. All reactions were conducted on a Perkin Elmer Lambda 40 UV/Vis spectrophotometer. No change of absorbance at 234 nm or at 280 nm was observed for each reaction. Each reaction mixture was subsequently extracted and analyzed via RP-HPLC using a Higgins HAsiL analytical column. Solution A was 99.9% ACN and 0.1% acetic acid; solution B was 99.9% H₂O and 0.1% acetic acid. An isocratic elution of 55%A:45%B was used in the HPLC analysis. Retention times and absorbance spectra of each of the reactions were compared to spectra of the controls. Collectively, the data from the UV-Vis experiments as well as the HPLC analysis confirm that these inhibitors do not act as substrates to h15-LOX-2.

Inhibition of h15-LOX-2 in HEK293T cells

HEK293T cells over-expressing h15-LOX-2 were grown in MEM (Gibco) with 10% FBS (Gibco), 2mM glutamine (Sigma), 100U/mL of penicillin/streptomycin (Gibco) and 640 ug/ml G418 sulfate (Fisher) as a selection agent (REF). Cells were harvested at 90% confluence with trypsin-EDTA (Gibco), and washed once with MEM with 10% FBS. Cells were then washed with 0.1% glucose (Fisher) in PBS (Gibco). Cells were then diluted in 0.1% glucose in PBS to a concentration of 1 million cells/mL. Cells were treated with DMSO (0.2%) or inhibitor in DMSO and incubated at 37 °C for 20 min. Cells were then stimulated with 100uM CaCl₂ (Sigma), 5 μM Ca Ionophore A23187 (Sigma) and 1 μM arachidonic acid (NuCheck) for 10 min at 37 °C. Cells were then acidified to 40uM HCl and snap-frozen in liquid nitrogen. Analysis of 15-HETE was performed as described previously (Cite Jen's paper), with the addition that m/z transition 319.2→219 was used to measure 15-HETE. Leftover cells from the inhibition assay were used to seed flasks and grew as well as untreated cells. Additionally, a cell survival assay was performed, in which cells were treated with 0.2% DMSO, 10 μM

inhibitor, or 20 μ M inhibitor for 1hr. After incubation, the media was replaced and the cells were monitored daily.

Virtual Screening of Novel h15-LOX-2 Inhibitors

In order to approximate the binding mode of the ligands **327069**, **327186** and **327206**, We used virtual screening software, Glide (version 8.7, Schrodinger Suite 2020 release 2), to identify binding modes of inhibitors discovered in this study. The crystal structure of h15-LOX2 co-crystallized with a substrate mimic inhibitor (hydroxyethyloxy)-tri(ethyloxy)octane) was used in docking (pdb id: 4NRE). Prior to docking, the protein structure was subjected to a protein-preparation step (Schrodinger Inc). During this step appropriate bond-orders and atom types were set, hydrogen atoms were added, protonation states of titratable residues such as His, Asp and Glu were adjusted, side chains of Asn, Gln, Thr and Tyr residues were optimized to make hydrogen bond interactions and finally a short minimization of the whole protein structure was performed such that the heavy atoms did not move beyond 0.3 Å from their starting positions. During the protein preparation step, we

retained the co-crystallized ligand, the metal ion (Fe^{2+}) and a water molecule that coordinates to the metal ion. The structures of the ligands identified in this study were built using Edit/Built panel of Maestro software (version 12.4, Schrodinger Inc). They were subsequently energy minimized using LigPrep software (Schrodinger Inc). The docking process consisted of grid preparation and ligand-docking steps. From the protein structure, we performed the following the protein-preparation step, we removed the co-crystallized ligand and used its co-ordinates to define the grid-box center. Inhibitors were docked using the standard-precision (SP) docking scoring function. During docking, the protein was held rigid, however, inhibitor conformations were sampled extensively. Since the structure of the co-crystallized inhibitor was a mimetic of the fatty acid substrate (i.e. a linear aliphatic chain), residues in the active site block inhibitors having aromatic rings from binding in the active site. Therefore, we decided to open the active site by means of InducedFit docking. In our earlier calculation, we successfully docked the h15-LOX-2 inhibitors, MLS000545091 (**545091**) and MLS000536924 (**536924**), after opening the active site

by means of induced fit docking (using the software InducedFit Dock, Schrodinger Inc).[27] Following this approach, we docked the most-potent inhibitor, Slug2020a, using InducedFit docking. During InducedFit docking all residues in the active site, except the Fe^{3+} , the water molecule, His373, His378 and His553 were treated flexibly. This flexible-receptor flexible-ligand docking approach opened the active site. We took the protein model from the top ranking InducedFit docking pose and docked all inhibitors using standard rigid-receptor flexible ligand docking (Glide) with the standard-precision (SP) scoring function.

Co-Structure of h15-LOX-2 and Inhibitor

The loop mutant (LM) of h15-LOX-2 has amino acids 73-79 deleted (PPVLPLL) and was previously cloned and described.[28] Briefly, 15-LOX-2 LM is overexpressed in Rosetta 2 (DE3) cells in the pET Duet-1 vector with the *E. coli yijgD* gene after promoter 2. For Mn^{2+} -substituted h15-LOX-2, the enzyme is grown in M9 minimal media containing 0.4% (w/v) glucose, 1 mM MgSO_4 , 0.1 mM CaCl_2 , 100 $\mu\text{g mL}^{-1}$ thiamine, 150 μM $\text{Mn(II)(SO}_4)_2$, and 0.2% (w/v) casamino acids.

Enzymes are purified on 5 mL HisTrap HP columns loaded with Co^{2+} attached to an AKTA FPLC (Cytiva, formerly GE Healthcare Life Sciences). After protein is bound, the column is washed with 20 column volumes (CV) of buffer A (20 mM Tris, 500 mM NaCl, 20 mM imidazole, pH 8.0) and eluted with a 20 CV gradient with buffer B (20 mM Tris, 500 mM NaCl, 200 mM imidazole, pH 8.0). Fractions are concentrated in Amicon Ultra-15 centrifugal filter units with a 30 kDa cutoff. Protein is applied to a Superdex 200 Increase 10/300 GL column; monomer and dimer peaks are collected and used separately for crystallization studies.

h15-LOX-2 LM Mn^{2+} -substituted at 10 mg/mL with a cocktail of 500 μM of both inhibitors **545091** and **536924** was screened with sparse matrix screens from Hampton Research, Rigaku Reagents, Qiagen, and Molecular Dimensions on a Gryphon liquid dispenser (ARI). The condition of 20% Jeffamine M-2070 and 20% DMSO resulted in rod like crystals directly from the HTS conditions. Attempts at repeating conditions by hand were unsuccessful. Jeffamine M-2070 is an industrial-grade reagent that was sold by Molecular Dimensions and is no longer

available for purchase.

The h15-LOX-2 LM crystals were directly looped from the HTS condition and plunged into liq. N₂ for shipping. X-ray data was collected at the 24ID-E beamline of the Northeastern Collaborative Access Team at the Advanced Photon Source (Argonne National Laboratory). XDS, pointless, and Scala were used via the RAPD processing suite of the Northeastern Collaborative Access team. RAPD applies a resolution cutoff at $CC_{1/2} > 0.35$.^[29] Molecular replacement with h15-LOX-2 (4NRE) was performed in the Phenix program suite and two molecules were placed in the asymmetric unit.^[30] Phenix.refine and coot were used for refinement and manual model building. Phenix.elbow was used to generate restraints for the small molecule inhibitors. Density consistent with an inhibitor is clearly present in the active site of both protomers in the asymmetric unit. However, given the similarity of the structures of the two compounds, it is not possible to determine if there is a mixture of occupancy for the inhibitors or a single inhibitor, and which orientation each inhibitor binds in the active sites. Final refinements for each inhibitor

positioned in the two possible binding modes in the electron density for each chain are included in the table below. The electron density clearly suggests that the inhibitor does not occupy a position in the metal coordination sphere. A water molecule mediates an interaction in chain A between the ligand and the metal. Real-space correlation coefficients and occupancies are provided in the final parallel refinements for both inhibitors in each chain and each orientation (table below).

Ligand	Real-space correlation coefficients	Occupancy
536924	(chain A) 0.89 (chain B) 0.89	(chain A) 0.65 (chain B) 0.70
536924 (flipped)	(chain A) 0.83 (chain B) 0.89	(chain A) 0.68 (chain B) 0.75
545091	(chain A) 0.79 (chain B) 0.82	(chain A) 0.68 (chain B) 0.73
545091 (flipped)	(chain A) 0.75 (chain B) 0.78	(chain A) 0.66 (chain B) 0.70

Hydrogen/Deuterium Exchange h15-LOX-2 Preparation

Aliquots of 15-LOX-2, purified from *E. coli* cultures as described previously,[31] were thawed and were diluted 10-fold (5 μ L into 45 μ L) in 10 mM HEPES, 150 mM NaCl, pD 7.4 D₂O (99%D, Cambridge Isotopes) buffer (corrected; pD = pH_{read} + 0.4). Samples were incubated randomly at 10 time points (0, 10, 20, 45, 60, 180, 600, 1800, 3600, and 7200 s) at 25 °C using a water bath. For each given temperature and mutant, the time points (samples) were collected over the course of

three to four days and randomized to reduce systematic error. Each sample (from a unique time point) was prepared and processed once. For the samples containing inhibitors, the inhibitor was added (20 μ M final concentration) to the protein stock solution (at least one minute) *prior* to D₂O addition. The specific inhibitor was also added to the D₂O buffer at a final concentration of 20 μ M prior to the exchange experiment.

Upon completion of the designated incubation time, all samples were then treated identically; the samples were rapidly cooled (5-6 seconds in a -20 °C bath) and acid quenched (to pH 2.4, confirmed with pH electrode, with 0.32 M citric acid stock solution [90 mM final concentration] at 0 °C). Procedures from this point were conducted near 4 °C. Prior to pepsin digestion, guanidine HCl (in citric acid, pH 2.4) was mixed with the samples to a final concentration of ca. 0.5 M. This solution contained DTT to the final concentration of 5 mM. Addition of the reducing and chaotropic agents were necessary for obtaining high coverage of the primary sequence (90-94%). 15-LOX-2 samples were digested with pre-equilibrated (10 mM

citrate buffer, pH 2.4), immobilized pepsin for 2.5 min. The peptide fragments were filtered, removing the pepsin, using spin cups (cellulose acetate) and by centrifugation for 10 seconds at 4 °C. Samples were flash frozen immediately in liquid nitrogen and stored at -80 °C until data collection.

Liquid chromatography-tandem mass spectrometry for peptide identification

To identify peptide fragments of human 15-LOX-2 resulting from pepsin digestion, samples of pepsin-digested h15-LOX-2 at time = 0s (H₂O buffer) were analyzed using a Thermo Dionex UltiMate3000 RSLCnano liquid chromatograph (LC) that was connected in-line with an LTQ Orbitrap XL mass spectrometer equipped with an electrospray ionization (ESI) source (Thermo Fisher Scientific, Waltham, MA). The LC was equipped with a C18 analytical column (Acclaim® PepMap 100, 150 mm length × 0.075 mm inner diameter, 3 μm particles, Thermo). Solvent A was 99.9% water/0.1% formic acid and solvent B was 99.9% acetonitrile/0.1% formic acid (v/v). The elution program consisted of isocratic flow at 2% B for 4 min, a linear gradient to 30% B over 38 min, isocratic flow at 95% B for 6

min, and isocratic flow at 2% B for 12 min, at a flow rate of 300 nL/min. The column exit was connected to the ESI source of the mass spectrometer using polyimide-coated, fused-silica tubing (20 μm inner diameter \times 280 μm outer diameter, Thermo). Full scan mass spectra were acquired in the positive ion mode over the range $m/z = 350$ to 1800 using the Orbitrap mass analyzer, in profile format, with a mass resolution setting of 60,000 (at $m/z = 400$, measured at full width at half-maximum peak height).

In the data-dependent mode, the eight most intense ions exceeding an intensity threshold of 30,000 counts were selected from each full-scan mass spectrum for tandem mass spectrometry (MS/MS) analysis using collision-induced dissociation (CID). Real-time dynamic exclusion was enabled to preclude re-selection of previously analyzed precursor ions. Data acquisition was controlled using Xcalibur software (version 2.0.7, Thermo). Raw data were searched against the amino acid sequence of 15-LOX-2 using Proteome Discoverer software (version 1.3, SEQUEST, Thermo) to identify peptides from MS/MS spectra.

Liquid chromatography-mass spectrometry for hydrogen/deuterium exchange measurements

Deuterated, pepsin-digested samples of 15-LOX-2 (see details above) were analyzed using an Agilent 1200 LC (Santa Clara, CA) that was connected in-line with the LTQ Orbitrap XL mass spectrometer (Thermo). The LC was equipped with a reversed-phase analytical column (Viva C8, 30 mm length \times 1.0 mm inner diameter, 5 μ m particles, Restek, Bellefonte, PA) and guard pre-column (C8, Restek). Solvent A was 99.9% water/0.1% formic acid and solvent B was 99.9% acetonitrile/0.1% formic acid (v/v). Each sample was thawed immediately prior to injection onto the column. The elution program consisted of a linear gradient from 5% to 10% B over 1 min, a linear gradient to 40% B over 5 min, a linear gradient to 100% B over 4 min, isocratic conditions at 100% B for 3 min, a linear gradient to 5% B over 0.5 min, and isocratic conditions at 5% B for 5.5 min, at a flow rate of 300 μ L/min. The column compartment was maintained at 4 °C and lined with towels to absorb atmospheric moisture condensation. The column exit was connected to the ESI source of the mass

spectrometer using PEEK tubing (0.005" inner diameter × 1/16" outer diameter, Agilent). Mass spectra were acquired in the positive ion mode over the range $m/z = 350$ to 1800 using the Orbitrap mass analyzer, in profile format, with a mass resolution setting of 100,000 (at $m/z = 400$). Data acquisition was controlled using Xcalibur software (version 2.0.7, Thermo).

Mass spectral data acquired for HDX measurements were analyzed using the software, HDX WorkBench.[32] The percent deuterium incorporation was calculated for each of these peptides, taking into account the number of amide linkages (excluding proline residues) and the calculated number of deuterons incorporated. The values were normalized for 100% D₂O and corrected for peptide-specific back-exchange, $\text{HDX\%} = (\text{observed, normalized extent of deuterium incorporation \{in percent\}}) / (1 - \{\text{BE}/100\})$. [33, 34]

Peptide-specific back-exchange was determined by fully exchanging the 15-LOX-2-derived peptides in 100% D₂O, quench with deuterated acid and HDX measured to examine the extent of the reverse exchange (N-D→N-H). Peptides of

15-LOX-2 were generated from pepsin digestion as described above, but in H₂O buffer. Water was subsequently removed by lyophilization. The peptide mixture was dissolved in buffered D₂O, pD 9 and incubated at 90°C for 2 hrs in a sealed microcentrifuge tube and then quenched to pD 2.5 using dilute DCl (Cambridge Isotopes). The sample was frozen in liquid nitrogen and stored at -80°C until HDX analysis. The extent of deuterium incorporation in this sample was analyzed via LC-MS as described above for HDX. Back-exchange values ranged from 17 to 60%, for an average value of 36% (**Supporting Information, HDX Table**). The resulting data were plotted as deuterium exchange versus time using Igor Pro software (See SI HDX traces).

6.3 Results and Discussion

Compound Identification and Inhibitor Potency

Previously, our laboratory reported the identity of two novel and specific h15-LOX-2 inhibitors, **545091** and **536924**, from our High Throughput Screening (HTS) of a 107,261 compound library.[27] Structurally, **545091** contains a 1,3,4-oxadiazole heterocycle, while **536924** contains a 1,2,4-triazole ring. These two inhibitors were discovered from manually screening the top 300 molecules of the HTS which displayed micromolar potencies (**Table 1**). In this publication, the next top 600 molecules were manually screened and three additional inhibitors were discovered, **327069**, **327186**, and **327206**. The newly discovered molecules are structurally different from **545091** and **536924** in that they contain a central imidazole ring, which is substituted at the one position with a phenyl moiety and the two position with a thiol ether phenyl moiety (**Table 1**). Inspection of the three chemotypes, it is observed that the central 5-membered ring heterocycle with a phenyl substituent is a common feature among them all. Upon further investigation,

327069 inhibited h15-LOX-2 with an IC_{50} equaling $0.34 \pm 0.05 \mu\text{M}$, while **327186** had a potency of $0.53 \pm 0.04 \mu\text{M}$ and finally **327206** showed a similar potency with a value of $0.87 \pm 0.06 \mu\text{M}$.

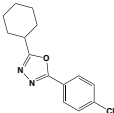
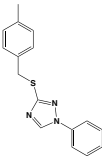
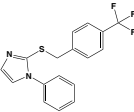
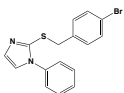
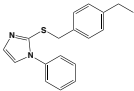
Inhibitors	Structure	IC_{50} (μM) (\pm SD (μM))
545091		2.6 (0.4)
536924		3.1 (0.4)
327069		0.34 (0.05)
327186		0.53 (0.04)
327206		0.87 (0.06)

Table 1. IC_{50} values for the newly discovered inhibitors targeting h15-LOX-2 with error in parentheses. All experiments were conducted in duplicate and with 10 μM AA.

Steady-State Inhibition Kinetics

Given that **327069**, **327186**, and **327206** exhibit the greatest potency against h15-LOX-2 of our modest SAR library, their modes of inhibition were probed

utilizing steady-state inhibition kinetics. The formation of 15-HpETE was monitored as a function of substrate and inhibitor concentration in the presence of 0.01% Triton-X-100. Fitting the data for **327186** yielded a K_{ic} of $0.80 \pm 0.05 \mu\text{M}$ and a K_{iu} of $4.0 \pm 3 \mu\text{M}$, which are defined as the equilibrium constants of inhibitor dissociation from the enzyme and enzyme substrate complex, respectively (**Supporting Information, Figure S2**). The steady-state inhibition kinetic experiments were also performed for **327069** and **327206** (**Table 2**), with the inhibition constants of all three molecules being comparable, as determined from their Dixon plots and Dixon replots. The data demonstrate that all three inhibitors exhibit mixed inhibition against h15-LOX-2, with the numbers being consistent with the IC_{50} values (**Table 1**).

Table 2. Data from the Dixon Plots		
Inhibitor	K_{ic} (μM)	K_{iu} (μM)
545091 [^]	0.90 (0.4)	9.9 (0.7)
536924 [^]	2.5 (0.5)*	N/A
327069	0.70 (0.07)	1.2 (0.9)
327186	0.80 (0.05)	4.0 (3)
327206	0.90 (0.04)	3.4 (2)

Table 2. The equilibrium constant of dissociation from the catalytic (K_{ic}) and secondary (K_{iu}) sites extracted from Dixon plots and Dixon replots of h15-LOX-2 and **545091**, **536924**, **327069**, **327186**, and **327206**.[^] Previously published[27]. * **536924** displayed competitive inhibition.

Selectivity Assays

Once the potencies of the three small molecule inhibitors against h15-LOX-2 had been determined, their selectivity against h5-LOX, h15-LOX-1, h12-LOX, COX-1 and COX-2 were investigated. All three molecules displayed extremely high selectivity for h15-LOX-2 against all enzymes tested (**Table 3**), with approximately 100-fold selectivity against h5-LOX, h12-LOX, COX-1 and COX-2. Against h15-LOX-1, the three molecules displayed slightly less selectivity, approximately 50-fold.

Potencies of Inhibitors Against Selected Oxygenases (μM)							
Inhibitors	h15- LOX-2	h15-hLO-1	h12-LOX	h5-LOX	COX-1	COX-2	Redox
327069	0.71 (0.06)	> 50	> 100	> 100	> 100	> 100	No
327186	0.9 (0.1)	> 50	> 100	> 100	> 100	> 100	No
327206	1.1 (0.1)	> 50	> 100	> 100	> 100	> 100	No

Table 3. Full IC_{50} experiments were performed with h15-LOX-2, while for the other oxygenases the IC_{50} values were estimated at 25 μM inhibitor concentration. Inhibition that was less than 15% and less than 30% at 25 μM are estimated to have IC_{50} values of > 100 μM and > 50 μM , respectively. All experiments were done in duplicate and all assays were performed with 10 μM AA except for the cyclooxygenases which were conducted at 100 μM AA. The values are in units of micromolar with error displayed in the parentheses.

3.5 Pseudo-peroxidase Activity Assay

To better understand the mechanism of inhibition between **327069**, **327186**, and **327206** and h15-LOX-2, the redox capability of the three molecules was investigated in a pseudo-peroxidase activity assay. Although many LOX inhibitors in the literature exhibit redox activity, they are not regarded as good therapeutics due to their tendencies for off-target redox reactions. [3,6] All three inhibitors were tested using the UV-Vis pseudo-peroxidase assay, with the lack of degradation of 13-HpODE at 234 nm confirming that the inhibitors are not redox active (**Table 3**).

3.6 Substrate Activity of Inhibitor

To determine whether h15-LOX-2 has the capability of catalytically modifying the inhibitors, 20 μM of each inhibitor was reacted with h15-LOX-2 and the reaction monitored at 205 nm, 234 nm and 280 nm. An increase in absorbance at each wavelength was not detected indicating no chemical reaction. To confirm these results, the reactions were extracted, dried under N_2 and brought up in methanol for RP-HPLC analysis. No significant difference in spectra or retention time was observed at 212 nm (λ_{max} of inhibitor), 234 nm or 280 nm, confirming that **327069**, **327186**, and **327206** are not substrates to h15-LOX-2.

Structure/Activity Relationship (SAR) Study

Following the discovery of the new chemotype, a limited SAR utilizing both synthesized and public domain molecules was performed (**Figure S1**). The three lead molecules, **327069**, **327186**, and **327206** possess an imidazole ring substituted at the one and two positions. The one position of the imidazole heterocycle contains a phenyl and the two position contains a thiol ether phenyl moiety. The three

compounds have a variety of substituents at the para position of the thiol ether phenyl ring, a trifluoromethyl (**327069**), a bromo (**327186**) and an ethyl (**327206**) moiety, which all demonstrated comparable potency (**Table 1**). To probe this further, a thio-ether was substituted into the para position (**3**), lowering the potency slightly ($IC_{50} = 2.3 \mu\text{M}$), however, a fluoro in the para position (**2**) abolished all activity ($IC_{50} > 100 \mu\text{M}$), indicating possible electronic considerations. If a para-methyl was added to the one position phenyl of **327069**, (**1**), no change in potency was observed ($IC_{50} = 0.27 \mu\text{M}$). Substitutions of the ortho position of the thiol ether phenyl with a methyl (**A**) and the meta position with a chloro (**B**), lowers the inhibition dramatically to 31% and 39% at $20 \mu\text{M}$, respectively. A double substitution of a para-fluoro and meta-cyano (**4**) also lowered activity ($IC_{50} > 100 \mu\text{M}$), indicating the importance of the para-benzyl substitution. Addition of a methylene carbon in between the sulfur and benzylic carbon, with no para-substitution, also lowers inhibition (**C**) to 68% at $20 \mu\text{M}$, indicating a spatial importance of the benzyl ring. Replacement of the para-substituted benzyl with a hydroxamic acid (**D**), carboxylic acid (**E**), or amide

(**I-K**) completely abolishes inhibitor potency with only 0-18% inhibition at 20 μ M. When a ketone (**F-H**) is inserted on the benzylic carbon, poor inhibition is also seen (51-62% at 20 μ M). Modifications to the substitution patterns on the phenyl ring at position one of the imidazole (**L-R**), while retaining the carboxylic acid replacement of benzyl substituent near the sulphur, decreases the potency dramatically (4-16% at 20 μ M). Finally, amide substitutions of the benzyl moiety with a meta-methylphenyl (**S-T**) also lost potency (4-13% at 20 μ M). In summary, the majority of the substitutions in this small SAR study were not tolerated well and their potency was lost. A few molecules retained their sub-micromolar potency, but none improved the potency greater than the original three inhibitors (**327069**, **327186**, **327206**).

Computational Docking of h15-LOX-2 Inhibitors

In our previous publication, we docked **536924** and **545091** using both Glide XP and MM-GBSA scoring.[REF] The Glide XP score did not correlate well with inhibitor potency, however the MM-GBSA score did. The low energy binding poses and docking scores were therefore determined for **327069**, **327206**, **327186**, **545091**

and **536924**, as shown in **Figure 2** and **Table 5**. The inhibitors bind in the U-shaped active site, with the heterocyclic ring occupying the pocket near the metal ion and both aromatic rings filling the hydrophobic pockets on either side of the heterocycle.

For all inhibitors but **536924** and **545091**, the heterocyclic ring in the middle

Compound	Docking Score	h15-LOX-2 IC₅₀ (μM)
327069	-8.1	0.34
327186	-7.8	0.53
327206	-8.2	0.87
545091	-7.0	2.6
536924	-7.7	3.1

Table 4. Docking scores of h15-LOX-2 ligands docked to h15-LOX-2 crystal structure (pdb id: 4nre).

makes a pi-stacking interaction with His373 residue located right below the

heterocyclic ring (**Figure 2**). Although, the binding affinities predicted by the docking score (Glide SP) (**Table 4**) do not correlate well with the experimental IC_{50} values, the inhibitors **327069**, **327206** and **327186** ranked marginally better than **545091** and **536924**. Based on these poses, the heterocyclic ring and positions of the substituents attached to the heterocyclic ring are different among these compounds. Substituents attached at these carbon and nitrogen atoms as found in **327069**, **327206** and **327186** might facilitate the favorable pi-stacking interaction for these compounds.

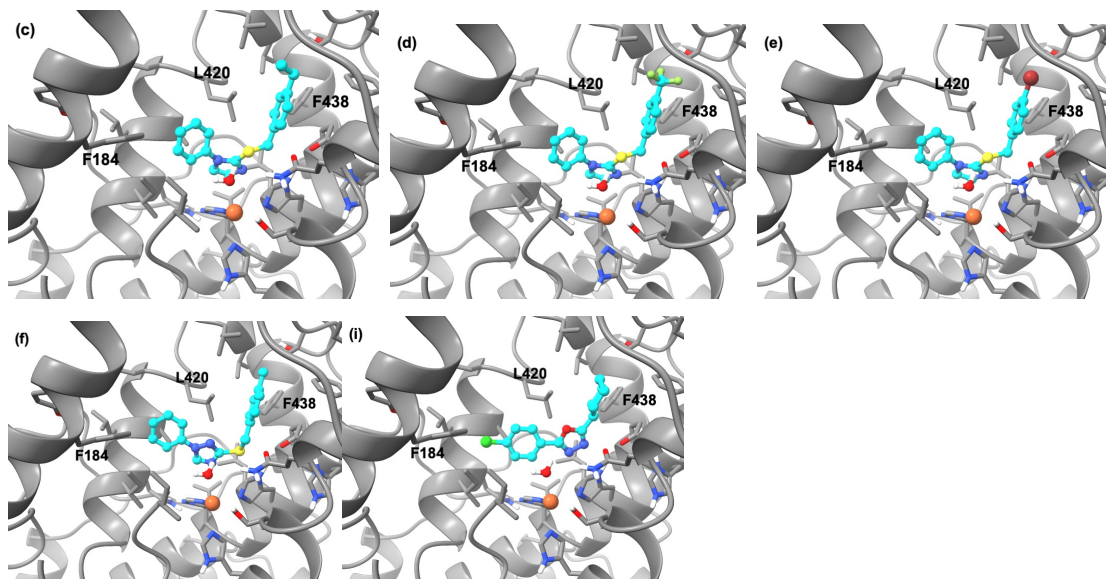


Figure 2. Docking pose of ligands bound to h15-LOX-2 (a) **327206**, (b) **327069**, (c) **327186**, (d) **536924**, (e) **545091**. Carbon atoms of the ligands are shown in cyan color and the protein are shown in grey color. Nitrogen, oxygen, sulfur, fluorine and

bromine and hydrogen atoms are shown in blue, red, yellow, green, brown and white colors respectively and the metal ion is shown in orange color.

Co-Structure of h15-LOX-2 and Inhibitor

The original crystallization condition of h15-LOX-2 required a detergent for high-resolution structure determination.[31] The substrate-mimicking, competitive-inhibitor detergent, octyltetraethylene glycol ether (C8E4), was bound in the active site described as a U-shaped channel.[35] An additional detergent molecule was revealed next to the catalytic domain near helix- α 2 ($H\alpha$ 2) which mediates crystal contacts. Attempts at utilizing these conditions for co-inhibitor structural studies were fruitless due to the requirement of the C8E4 detergent. New crystallization conditions were screened for a loop mutant of 15-lipoxygenase-2 (h15-LOX-2 LM), with amino acids 73-79 deleted (PPVLPLL).[36] In the structure of the wildtype enzyme the hydrophobic loop projects from the β -barrel domain and hinders access to the active site of a neighboring promoter in the crystal lattice. Data suggest that peripheral insertion of this loop into the bilayer is the primary membrane-binding determinant for Ca^{2+} -signaling and targeting.[36] A cocktail of inhibitors **545091** and **536924** was

used in the crystallization trials of h15-LOX-2 LM substituted with Mn^{2+} . Crystals grew in our high-throughput screening (HTS) effort in conditions of 20% DMSO and 20% Jeffamine M-2070. Rod-shaped crystals directly from the HTS condition were flash frozen and x-ray diffraction data were collected. The protein crystallized in spacegroup C2 and data was collected to 2.4 Å resolution (**Supporting Information, Table S1**). Two monomers were positioned in the asymmetric unit of the search model h15-LOX-2 WT (4nre.pdb). According to macromolecular interface tool PISA (Proteins, Interfaces, Structures and Assemblies) this interface is significant and could represent the dimer observed in size-exclusion chromatography.[37]

Additional electron density $|Fo-Fc|$ near the active site metal was resolved after subsequent refinement (**Supporting Information, Figure S4**). The different inhibitors were modeled and refined in parallel refinements in the density near the active site metal. However, we are unable to unambiguously identify which inhibitor(s) is(are) present. Real-space correlation coefficients for inhibitor **536924** (0.88 CC and 0.89 CC) in both chains correlates to a higher degree versus inhibitor

545091 (0.79 CC and 0.82 CC). We can, however, unambiguously state that the inhibitors bind in the U-shaped channel and do not directly interact with the active-site metal (**Figure 3**). Additionally, a water molecule that occupies the open sixth position of the octahedral-coordinated Fe^{2+} in the wildtype structure was observed in chain A of the crystal structure of the Mn^{2+} -substituted h15-LOX-2 LM (**Supporting Information, Figure S5**). When inhibitor **536924** is placed in the electron density near the metal, the sulfur of the inhibitor forms an H-bond with the Mn^{2+} -coordinated water and His 373. All other potential interactions of inhibitors in the crystal structures share only van der Waal contacts in the U-shaped pocket defined by Ile 412, Phe 365, Thr 431, and Leu 420, which positions the targeted pentadiene of AA for attack. The crystal structure validates many key findings of the docking experiments including water-mediated binding of the inhibitor to the metal coordination sphere near the imidazole heterocycle, and the aromatic structures of the inhibitors positioned on opposite ends of the U-shaped channel. The minimal differences of the atomic positions of amino acids in the original wild type structure

of h15-LOX-2 bound to the detergent C8E4 and our new structure of h15-LOX-2 LM co-crystallized with a cocktail of inhibitors (7laf.pdb) further validates and justifies the *in silico* rigid body docking strategy performed.

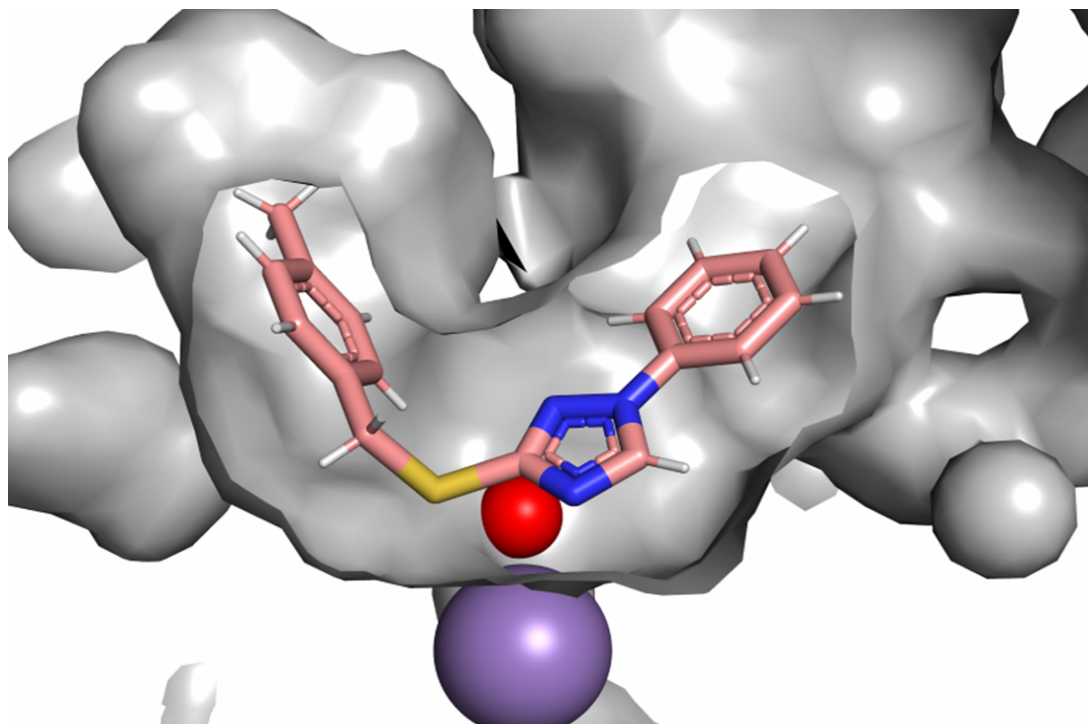


Figure 3. Inhibitor 536924 in the U-shaped channel. Surface rendering in the cavities and pockets only mode from Pymol of chain A of the 15-LOX-2 LM structure (7laf.pdb) is shown as grey. The Mn²⁺ is shown as purple sphere and water molecule as red sphere. Inhibitor 536924 (C, pink) binds in the U-shaped channel and interacts with the water that coordinates the 6th position of the metal.

Hydrogen/Deuterium Exchange Mass Spectrometry of h15-LOX-2

Hydrogen deuterium exchange mass spectrometry (HDX-MS) has been utilized to assess the effects of binding small molecule effectors, regulators, and inhibitors on protein conformational flexibility. [33, 38-42] Therefore, it offers an incisive high-throughput technique, complementary to the high-resolution X-ray crystal structures solved with inhibitors bound, to screen inhibitors and to resolve their impact on protein structure and flexibility. In the specific case of lipoxygenases, allosteric effectors and substrates have been shown to influence the HDX properties of both soybean lipoxygenase-1.[43] and human 15-LOX-2.[44]

Herein, we set to examine the impact of the isozyme selective inhibitors, **536924** that was characterized previously,[45] and **327069** that is described in this report. Tandem MS analysis of pepsin-generated peptides of 15-LOX-2 identified 242 peptides corresponding to 94% coverage of the primary sequence.

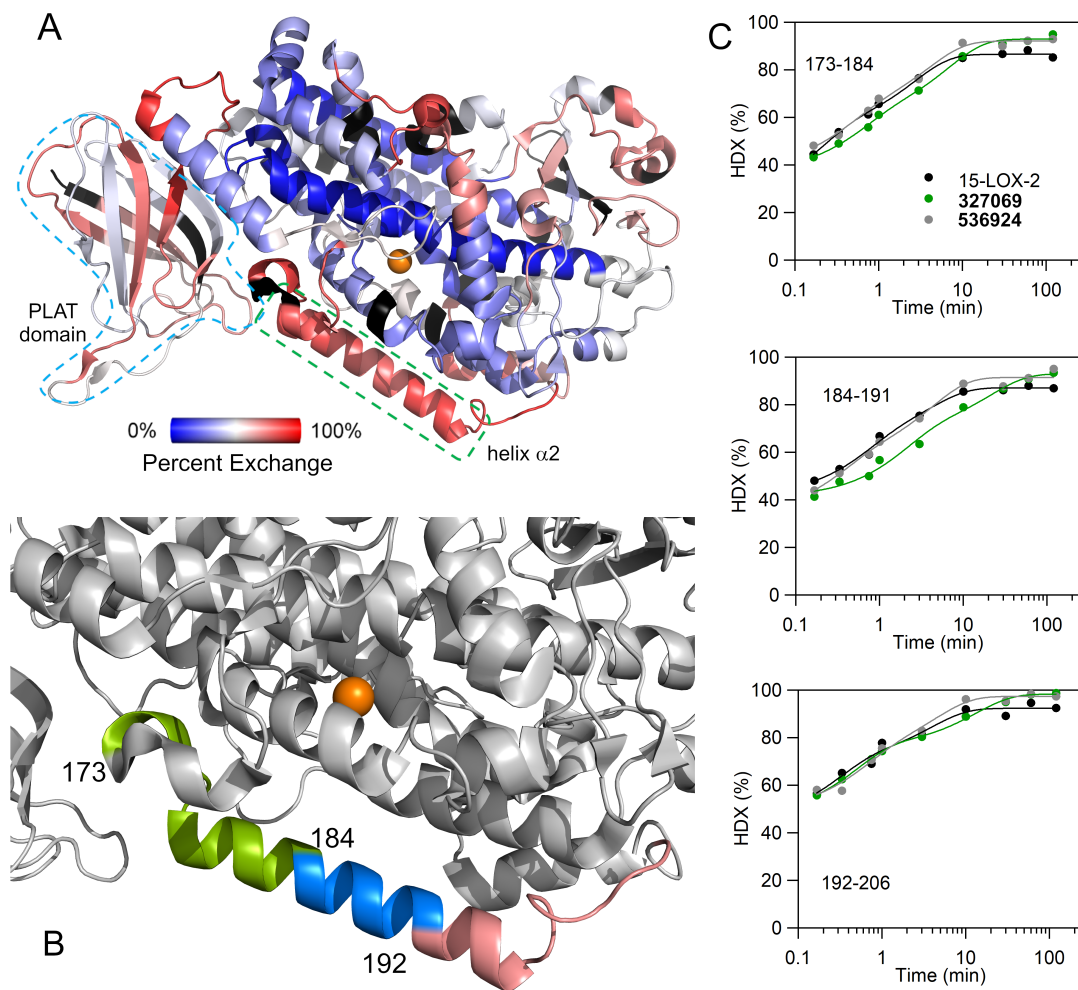


Figure 4. HDX-MS properties of 15-LOX-2 isozyme specific inhibitors. (A) HDX-MS behavior at 2 h and 25°C of h15-LOX-2 peptides in the absence of any inhibitor is mapped onto the crystal structure (PDB entry, 4NRE). The coloring is defined by the spectrum bar. Black coloring represents uncovered regions. The PLAT domain is highlighted by cyan outline and the helix $\alpha 2$ is highlighted by the green box. (B, C) presents the impact of isozyme selective inhibitors, **536924**[27] and **327069**, on the HDX-MS properties of 15-LOX-2. The effect is localized to the helix $\alpha 2$ of 15-LOX-2 and the peptides are colored as follows: chartreuse, 173-184; marine, 184-191; and salmon, 192-206. Additional, overlapping peptides are presented in the SI HDX traces pdf.

This represents a significant increase in primary sequence coverage from the previous report of 72%.[44] For data reduction purposes, 44 non-overlapping peptides, ranging from 5 to 25 amino acids (average length, 12), were selected for HDX-MS analysis. The peptide list was well covered over all 10 time points, ranging from 10 s to 2 h, and identical for samples prepared with inhibitors.

The percent exchange at 2 h for samples of h15-LOX-2 alone is mapped onto the crystal structure of 15-LOX-2[31] (**Figure 4A**) that was solved with a substrate mimic, C8E4, in the active site. The general trend in this HDX heat map is comparable to that reported from the Armstrong lab.[44] Of note is the exchange behavior of helix- α 2, a peptide which restricts the substrate entrance portal and whose flexibility has been implicated to play an important regulatory role in substrate binding in LOXs.[43, 45-47]

Peptide 184-191 (and its overlapping counterparts) is located in the central region of helix α 2 and flanked by peptides 173-184 (**Figure 4B**, chartreuse) and 192-206 (**Figure 4B**, salmon). All three peptides are highly exchanged ($\geq 80\%$) at 2 h

(**Figure 4A** and **4B**). Considering the variability in protein handling, mass spec instrumentation used, and potential differences in buffer preparation, the exchange properties of this helix $\alpha 2$ reported in Droege *et al.*[48] and herein are nearly identical (see **Figure S6A**). Further, to corroborate our h15-LOX-2 HDX properties, we conducted HDX-MS of h15-LOX-2 isolated from insect cell (SF9) cultures. Exchange properties are nearly superimposable including helix $\alpha 2$ (**Figure S6B**). This enhanced exchange behavior for a crystallographically resolved alpha helical peptide is comparable to that described for the model 15-lipoxygenase from plants, SLO-1 (**Figure S7**).[34, 43]

One notable distinction between h15-LOX-2 and SLO-1 is the general increase in exchange of the N-terminal PLAT domain with an average 10% higher overall extent of exchange for 15-LOX-2 (**Figure S8**). In addition, the linker peptide between the PLAT and catalytic domains, 117-134, in h15-LOX-2 exhibits a significantly higher exchange (87 % at 2 h) compared to the corresponding peptide in SLO-1 of *ca.* 45 % (residues 137-160). The trend in these HDX properties of the

PLAT domain is consistent with the previously reported small angle X-ray scattering (SAXS) experiments. SAXS data of rabbit 15-LOX-1 suggested high mobility of the PLAT domain, supporting a ‘rocking’ motion that has been proposed to play a role in membrane binding.[49, 50] Conversely, SAXS analysis of SLO-1 indicates no significant mobility of the PLAT domain.[51]

Impact of isozyme-selective inhibitors on h15-LOX-2 Hydrogen/Deuterium Exchange properties

Addition of substrate arachidonic acid (AA) to h15-LOX-2 was previously found to decrease the exchange behavior of peptide 185-191 (helix $\alpha 2$) at early time points (15-120 s) by as much as 20%.[44] This was accompanied by a modest impact on the exchange percentage at the arched helix that runs nearly parallel to helix $\alpha 2$ and lines the substrate binding site. This leads to the question if the inhibitors described herein might influence the protein flexibility of 15-LOX-2 and if so, to what extent.

For the current HDX study of h15-LOX-2, two inhibitors were selected,

536924 and **327069**, that represented the two different chemotypes of this study. In the presence of saturating concentration (20 μ M) of **327069**, two non-overlapping h15-LOX-2 peptides (173-184 and 184-191) were associated with significant reduction in exchange by as much as 20% at short time scales (< 10 min). From the bi-exponential fits of the time-dependent HDX traces (**Figure 4C**), the average rate constants for these peptides were found to be 2- and 4-times slower in the presence of **327069**. This behavior is consistent with a rigidification of regional protein motions and is the canonical HDX behavior reported for protein inhibitors (see refs[52-55] for examples). The rigidification of helix α 2 in the presence of **327069** was also similar to the HDX behavior previously characterized at short time scales for the presence of AA.[44] Conversely, within the dynamic range of the experiment employed, HDX samples of h15-LOX-2 prepared with **536924** showed no significant exchange differences to samples with 15-LOX-2 alone (*cf.* **Figure 4C**, black and gray traces). The difference in HDX behavior observed here for the two different h15-LOX-2 inhibitors can be attributed to the near 10-fold enhanced inhibition of **327069** (IC_{50} =

0.34) over **536924** ($IC_{50} = 3.1 \mu\text{M}$). The observation that the ‘better’ inhibitor resulted in the structural rigidification of h15-LOX-2 helix $\alpha 2$ underscores the utility of HDX-MS as a powerful, high-throughput method for screening h15-LOX-2 inhibitors.

Droege *et al.* previously reported notable decreased HDX-MS behavior for h15-LOX-2 peptides in the PLAT domain, namely 45-52, 54-66, and 67-86 with the addition of the AA substrate.[44] However, from our data even under saturating inhibitor concentrations, there is no significant effect on the apparent HDX rate in this region between the samples in the presence and absence of either inhibitor (**Supporting Information, HDX traces**). Note that at long time points, the inhibitors cause a slight increase in the extent of exchange, including peptide 45-53. Because this is only observed at longer time points, we attribute this effect to a possible regional dependent destabilization of the protein structure in the presence of the inhibitors.

This distinction between the exchange behavior reported for AA and that

described for the inhibitors described herein could be catalytically significant. Note that during the 15-120 second exchange experiment with AA,[44] the substrate will be converted to 15-HpETE. While not fully resolved for h15-LOX-2, conformational changes are expected to accompany substrate binding, turnover, and product release.[56] Further, AA could potentially bind at an allosteric site in h15-LOX-2 and elicit altered protein conformational ensembles. The substrate selectivity of h15-LOX-2 has been shown to be influenced by allosteric effectors, including 13S-HODE, an enzymatic product from the reaction of h15-LOX-1 with linoleic acid.[57] Allosteric effects in the HDX behavior have also been detected in the PLAT domain of SLO-1 when using the SLO-1 allosteric effector, oleyl sulfate.[43] Future HDX-MS studies will be aimed at resolving the effects from the interactions of selective allosteric modulators that target h15-LOX-2.

Inhibition of h15-LOX-2 in HEK293T cells

A key aspect of any inhibitor that will be used as a tool to investigate the biological relevancy of h15-LOX-2 is its efficacy in a cellular model. Currently, there

are no potent/specific inhibitors against h15-LOX-2 which are effective in the cellular milieu. Our h15-LOX-2 inhibitors of this work and our previous work,[REF] were therefore tested in HEK293T cells expressing h15-LOX-2 to inhibit LOX activity and reduce 15-HETE production. The majority of these inhibitors, **327069**, **327206** and **536924**, demonstrated EC₅₀ values of approximately 1 μ M (**Table 5, Supporting Information, Figure S3**), which is consistent with their *in vitro* IC₅₀ values (**Table 1**). **327186**, however, manifested weaker potency, with an approximate IC₅₀ of 30 μ M. It is unclear why **327186** is less potent, but it could be due to increased cellular inactivation or decreased cell penetration. Nonetheless, these data demonstrate that this class of inhibitors are capable of penetrating the cell and inhibiting the oxygenation of free, exogenous AA. Additionally, these inhibitors were non-toxic, since cells continued to grow at the same rate as their DMSO controls after treatment with 10 μ M of all four inhibitors, confirming them as viable *ex vivo* tools for examining the activity of h15-LOX-2.

Table 5. EC₅₀ values determined in h15-LOX-2/HEK293T cells	
Inhibitor	EC₅₀ (μM)
536924	0.60 (0.1)
327069	0.75 (0.2)
327186	31 (6)
327206	1.3 (0.3)

6.4 Conclusions

In summary, we have discovered three potent inhibitors of h15-LOX-2, **327069**, **327186**, and **327206**, that are potent and highly selective over other oxygenases. They are mixed type inhibitors and similar to our previously published h15-LOX-2 inhibitors, **545091** and **536924**, they are non-reductive inhibitors. Importantly, they all are active in our HEK293 cell assay indicating their biological activity and are important tools in gaining a better understanding of h15-LOX-2's role in biology. With respect to their mode of action, all five inhibitors have similar binding poses according to the computational docking data, which was confirmed in our crystallographic co-structure. The HDX results also indicate a similar binding between **536924** and **327069**, however the later restricts protein motion of helix- α 2 more. These results along with the poor potency of the purchased derivatives, suggest that these pharmacophores bind in a similar manner but have a confined SAR. Given these results, we designed, docked and synthesized novel inhibitors and

confirmed our binding mode hypothesis. In total, we have discovered a suite of similar pharmacophores which target h15-LOX-2 and determined their binding mode. With this information we are now designing and synthesizing novel inhibitors to target h15-LOX-2 as a therapeutic target.

References

1. Klinman, J.P., *How Do Enzymes Activate Oxygen without Inactivating Themselves*. Accounts of Chemical Research, 2007. **40**(5): p. 325-333.
2. Anca D. Dobriana, D.C.L., Banumathi K. Coleb, David A. Taylor-Fishwickb, and a.J.L.N. Swarup K. Chakrabartib, *Functional and Pathological Roles of the 12- and 15-lipoxygenases*. Prog Lipid Res, 2011. **50**(1): p. 115-131.
3. Funk CD1, C.X., Johnson EN, Zhao L, *Lipoxygenase genes and their targeted disruption*. Prostaglandins Other Lipid Mediat., 2002. **68-69**: p. 303-312.
4. Funk, C.D., *Lipoxygenase pathways as mediators of early inflammatory events in atherosclerosis*. Thromb. Vasc. Biol., 2006. **26**: p. 1204-1206.
5. Brash, A.R., W.E. Boeglin, and M.S. Chang, *Discovery of a second 15S-lipoxygenase in humans*. Proc Natl Acad Sci U S A, 1997. **94**(12): p. 6148-52.
6. Jisaka, M., et al., *Molecular cloning and functional expression of a phorbol ester-inducible 8S-lipoxygenase from mouse skin*. J Biol Chem, 1997. **272**(39): p. 24410-6.
7. Hulten, L.M., et al., *15-Lipoxygenase-2 is expressed in macrophages in human carotid plaques and regulated by hypoxia-inducible factor-1alpha*. Eur J Clin Invest, 2010. **40**(1): p. 11-7.
8. Matthew J. Kobe, D.B.N., Caitlin E. Mitchell, Sue G. Bartlett, Marcia E. Newcomer, *The Structure of Human 15-Lipoxygenase-2 with a Substrate Mimic*. The Journal of Biological Chemistry, 2014. **289**: p. 8562-8569.
9. Danielsson, K.N., Rydberg, E. K., Ingelsten, M., Akyu`rek, L. M., Jirholt, P., and C. Ullstro`m, Forsberg, G. B., Bore`n, J., Wiklund, O., and Hulte`n, L. M., *15-Lipoxygenase-2 expression in human macrophages induces chemokine secretion and T cell migration*. Atherosclerosis, 2008. **199**: p. 34-40.
10. Ellen Knutsen Rydberg, A.K., Christina Ullstro, et al., *Hypoxia Increases LDL Oxidation and Expression of 15-Lipoxygenase-2 in Human Macrophages*. rterioscler Thromb Vasc Biol., 2004. **24**: p. 2040-2045.

11. Hersberger, M., *Potential role of the lipoxygenase derived lipid mediators in atherosclerosis*: Clin Chem Lab Med, 2010. **48**: p. 1063e73.
12. Hultén, L.M., Olson, F. J., Aberg, H., Carlsson, J., Karlström, L., Bore´n, J., and B. Fagerberg, and Wiklund, O., *15-Lipoxygenase-2 is expressed in macrophages in human carotid plaques and regulated by hypoxia-inducible factor-1*. Eur. J. Clin. Invest., 2010. **40**: p. 11-17.
13. Gertow, K., Nobili, E., Folkersen, L., Newman, J. W., Pedersen, T. L., Ekstrand, S. J., Kühn, H., Wheelock, C. E., Hansson, G. K., and U. Hedin, Haeggström, J. Z., and Gabrielsen, A., *12- and 15-lipoxygenases in human carotid atherosclerotic lesions: associations with cerebrovascular symptoms*. Atherosclerosis, 2011. **215**: p. 411-416.
14. Magnusson, L.U., Lundqvist, A., Carlsson, M. N., Skåle´n, K., Levin, M., and O. Wiklund, Bore´n, J., and Hultén, L. M., *Arachidonate 15-lipoxygenase type B knockdown leads to reduced lipid accumulation and inflammation in atherosclerosis*. PLOS One, 2012. **7**(8): p. e43142.
15. Wuest, S.J., Crucet, M., Gemperle, C., Loretz, C., and Hersberger, M. *Expression and regulation of 12/15-lipoxygenases in human primary macrophages*. Atherosclerosis, 2012. **225**: p. 121-127.
16. Kotla, S., Singh, N. K., Heckle, M. R., Tigyi, G. J., and Rao, G. N., *The transcription factor CREB enhances interleukin-17A production and inflammation in a mouse model of atherosclerosis*. Science Signaling, 2013. **6**(293): p. ra83.
17. Ringholz, F.C., et al., *Reduced 15-lipoxygenase 2 and lipoxin A4/leukotriene B4 ratio in children with cystic fibrosis*. Eur Respir J, 2014. **44**(2): p. 394-404.
18. Wenzel, S.E., et al., *PEBP1 Wardens Ferroptosis by Enabling Lipoxygenase Generation of Lipid Death Signals*. Cell, 2017. **171**(3): p. 628-641 e26.
19. Reichert, C.O., et al., *Ferroptosis Mechanisms Involved in Neurodegenerative Diseases*. Int J Mol Sci, 2020. **21**(22).
20. Vasquez-Martinez, Y., et al., *Structure-activity relationship studies of flavonoids as potent inhibitors of human platelet 12-hLO, reticulocyte*

- 15-hLO-1, and prostate epithelial 15-hLO-2*. Bioorganic & Medicinal Chemistry, 2007. **15**(23): p. 7408-25.
21. J. Brian Jameson II¹, A.K., Lena Schultz², Chakrapani Kalyanaraman³, Matthew P. Jacobson³, and A.J. David J. Maloney², Anton Simeonov^{2*}, Theodore R. Holman^{1*}, *A High Throughput Screen Identifies Potent and Selective Inhibitors to Human Epithelial 15-Lipoxygenase-2*. PLOS One, 2014. **9**(8): p. e104094.
 22. Sarah J. Robinson, E.K.H., † Michelle Riener,† Steven T. Loveridge,† Karen Tenney,† Frederick A. Valeriote,‡ Theodore R. Holman,† and Phillip Crews†, *Using Enzyme Assays to Evaluate the Structure and Bioactivity of Sponge-derived Meroterpenes*. J. Nat. Prod, 2009. **72**(10): p. 1857-1863.
 23. Amagata, T.W., S.; Johnson, T.A.; Stessman, C.C.; Loo, C.P.; Lobkovsky, E.; Clardy, J.; Crews, P.; Holman, T.R., *Exploring Sponge-Derived Terpenoids for Their Potency and Selectivity Against 12-Human, 15-Human, and 15-Soybean Lipoxygenases*. J. Nat. Prod, 2003. **66**: p. 230-235.
 24. Vasquez-Martinez Y, O.R., Kenyon V, Holman TR, Sepu'lveda-Boza S, *Structure-activity relationship studies of flavonoids as potent inhibitors of human platelet 12-hLO, reticulocyte 15-hLO-1, and prostate epithelial 15-hLO-2*. Bioorg Med Chem, 2007. **15**: p. 7408-7425.
 25. Hoobler, E.K.H., C.; Holman, T.R. , *Pseudoperoxidase Investigations of Hydroperoxides and Inhibitors with Human Lipoxygenases*. Bioorg Med Chem, 2013. **21**: p. 3894-3899.
 26. Rai, G.K., V.; Jadhav, A.; Schultz, L.; Armstrong, M.; Jameson, B.; Hoobler, E.; Leister, W.; Simeonov, A.; Holman, T.R.; Maloney, D.J. , *Discovery of Potent and Selective Inhibitors of Human Reticulocyte 15-Lipoxygenase-1*. J. Med. Chem, 2010. **53**: p. 7392-7404.
 27. Jameson, J.B., et al., *A High Throughput Screen Identifies Potent and Selective Inhibitors to Human Epithelial 15-Lipoxygenase-2*. Plos One, 2014. **9**(8).
 28. Bender, G., et al., *Membrane-dependent Activities of Human 15-LOX-2 and*

- Its Murine Counterpart: IMPLICATIONS FOR MURINE MODELS OF ATHEROSCLEROSIS*. J Biol Chem, 2016. **291**(37): p. 19413-24.
29. Karplus, P.A. and K. Diederichs, *Assessing and maximizing data quality in macromolecular crystallography*. Curr Opin Struct Biol, 2015. **34**: p. 60-8.
 30. Adams, P.D., et al., *The Phenix software for automated determination of macromolecular structures*. Methods, 2011. **55**(1): p. 94-106.
 31. Kobe, M.J., et al., *The structure of human 15-lipoxygenase-2 with a substrate mimic*. J Biol Chem, 2014. **289**(12): p. 8562-9.
 32. Pascal, B.D., et al., *HDX Workbench: software for the analysis of H/D exchange MS data*. J. Am. Soc. Mass Spectrom., 2012. **23**: p. 1512-1521.
 33. Hoofnagle, A.N., K.A. Resing, and N.G. Ahn, *Protein analysis by hydrogen exchange mass spectrometry*. Annu. Rev. Biophys. Biomol. Struct., 2003. **32**: p. 1-25.
 34. Offenbacher, A.R., et al., *Hydrogen-deuterium exchange of lipoxygenase uncovers a relationship between distal, solvent exposed protein motions and the thermal activation barrier for catalytic proton-coupled electron tunneling*. ACS Cent. Sci., 2017. **3**: p. 570-579.
 35. Newcomer, M.E. and A.R. Brash, *The structural basis for specificity in lipoxygenase catalysis*. Protein Sci, 2015. **24**(3): p. 298-309.
 36. Neau, D.B., et al., *The 1.85 Å structure of an 8R-lipoxygenase suggests a general model for lipoxygenase product specificity*. Biochemistry, 2009. **48**(33): p. 7906-15.
 37. Schlee, S., et al., *Prediction of quaternary structure by analysis of hot spot residues in protein-protein interfaces: the case of anthranilate phosphoribosyltransferases*. Proteins, 2019. **87**(10): p. 815-825.
 38. Marcsisin, S.R. and J.R. Engen, *Hydrogen exchange mass spectrometry: what is it and what can it tell us?* Anal. Bioanal. Chem., 2010. **397**: p. 967-972.
 39. Chalmers, M.J., et al., *Differential hydrogen/deuterium exchange mass spectrometry analysis of protein-ligand interactions*. Expert Rev. Proteomics, 2014. **8**: p. 43-59.

40. Wei, H., et al., *Hydrogen/deuterium exchange mass spectrometry for probing higher order therapeutics: methodology and applications*. Drug Discov. Today, 2014. **19**: p. 95-102.
41. Pirrone, G.F., R.E. Iacob, and J.R. Engen, *Applications of hydrogen/deuterium exchange MS from 2012 to 2014*. Anal. Chem., 2015. **87**: p. 99-118.
42. Masson, G.R., M.L. Jenkins, and J.E. Burke, *An overview of hydrogen deuterium exchange mass spectrometry (HDX-MS) in drug discovery*. Expert Opin. Drug Discov., 2017. **12**: p. 981-994.
43. Offenbacher, A.R., A.T. Iavarone, and J.P. Klinman, *Hydrogen-deuterium exchange reveals long-range dynamical allostery in soybean lipoxygenase*. J. Biol. Chem., 2018. **293**: p. 1138-1148.
44. Droege, K.D., et al., *Structural dynamics of 15-lipoxygenase-2 via hydrogen-deuterium exchange*. Biochemistry, 2017. **56**: p. 5065-5074.
45. Jameson, J.B., 2nd, et al., *A high throughput screen identifies potent and selective inhibitors to human epithelial 15-lipoxygenase-2*. PLoS One, 2014. **9**(8): p. e104094.
46. Gilbert, N.C., et al., *Structural and mechanistic insights into 5-lipoxygenase inhibition by natural products*. Nat. Chem. Biol., 2020. **16**: p. 783-790.
47. Offenbacher, A.R. and T.R. Holman, *Fatty acid allosteric regulation of C-H activation in plant and animal lipoxygenases*. Molecules, 2020. **25**: p. 3374.
48. Droege, K.D., et al., *Structural Dynamics of 15-Lipoxygenase-2 via Hydrogen-Deuterium Exchange*. Biochemistry, 2017. **56**(38): p. 5065-5074.
49. Hammel, M., et al., *Structural flexibility of the N-terminal b-barrel domain of 15-lipoxygenase-1 probed by small angle X-ray scattering. Functional consequences for activity regulation and membrane binding*. J. Mol. Biol., 2004. **343**: p. 917-929.
50. Shang, W., et al., *Probing dimerization and structural flexibility of mammalian lipoxygenases by small-angle X-ray scattering*. J. Mol. Biol., 2011. **409**: p. 654-668.
51. Dainese, E., et al., *Structural stability of soybean lipoxygenase-1 in solution*

- as probed by small angle X-ray scattering.* J. Mol. Biol., 2005. **349**: p. 143-152.
52. Cao, J., J.E. Burke, and E.A. Dennis, *Using hydrogen/deuterium exchange mass spectrometry to define the specific interactions of the phospholipase A2 superfamily with lipid substrates, inhibitors, and membranes.* J. Biol. Chem., 2013. **288**: p. 1806-1813.
 53. Konermann, L., J. Pan, and Y.-H. Liu, *Hydrogen exchange mass spectrometry for studying protein structure and dynamics.* Chem. Soc. Rev., 2011. **40**: p. 1224-1234.
 54. Sherry, K., et al., *Hydrogen-deuterium exchange and hydroxyl radical footprinting for mapping hydrophobic interactions of human bromodomain with a small molecule inhibitor.* J. Am. Soc. Mass Spectrom., 2019. **30**: p. 2795-2804.
 55. Pegram, L.M., et al., *Activation loop dynamics are controlled by conformation-selective inhibitors of ERK2.* Proc. Natl. Acad. Sci. U.S.A., 2019. **116**: p. 15463-15468.
 56. Ramachandran, S., et al., *Catalysis sensitive conformational changes in soybean lipoxygenase revealed by limited proteolysis and monoclonal antibody experiments.* Biochemistry, 1995. **34**: p. 14868-14873.
 57. Joshi, N., et al., *Kinetic and structural investigations into the allosteric and pH effect on the substrate specificity of human epithelial 15-lipoxygenase-2.* Biochemistry, 2013. **52**(45): p. 8026-35.

